MODEL PREDICTIVE CONTROL OF ELECTROMAGNETIC TORQUE IN PERMANENT MAGNET SYNCHRONOUS MACHINES

by

Tianshi WANG, B.Eng. (Elec.)

Submitted for the Degree of Master of Engineering

at

University of Technology, Sydney

2013

CERTIFICATE OF AUTHORSHIP/ORIGINALITY

I certify that the work in this thesis has not previously been submitted for a degree nor has it been submitted as part of requirements for a degree except as fully acknowledged within the text.

I also certify that the thesis has been written by me. Any help that I have received in my research work and the preparation of the thesis itself has been acknowledged. In addition, I certify that all information sources and literature used are indicated in the thesis.

Signature of Student

ACKNOWLEDGEMENTS

This work was carried out at the Centre for Electrical Machines and Power Electronics (CEMPE), School of Electrical, Mechanical & Mechatronic Systems, Faculty of Engineering and Information Technology, University of Technology, Sydney.

I wish to express my sincerest appreciation to my supervisor, Prof. Jianguo Zhu, Director of CEMPE and Head of School, for his invaluable expert technical guidance and advice throughout my study and research. Great gratitude goes to my previous supervisor Prof. Dianguo Xu for his guidance and recommendation.

I also wish to express my deep appreciation to Dr. Yongchang Zhang for his expert advice. Great gratitude also goes to Dr. Youguang Guo for his suggestion and kind help. Special gratitude goes to Dr. Greg Hunter and Mr. Jiang Chen for their technical support.

Acknowledgments go to Dr. Jack Lin and A/Prof. Hong Guang for his kind support when I met difficulties in my personal life and Dr. Yi Wang, Dr. Wei Xu and Dr. Gang Lei for their suggestions and comments. I would like to thank all my colleagues and friends, including, Prof. Qingfang Teng, Dr. Helen Lu, Dr. Yongjian Li, Dr. Jianbin Zeng, Mr. Jiefeng Hu, Mr. Md Rabiul Islam, Mr. Dung Pham, Mr. Yiying Wei, Mr. Yanqing Qu and Mr. Sonki Prasetya.

Finally, I would like to express my deepest gratitude to my wife Shuyang Liu, my father Yanqing Wang and my mother Xiaoyun Jiang for their love and financial support during my study.

TABLE OF CONTENTS

LIST OF SYMBOLS

$*$	Reference value
$\alpha\beta$	Stationary stator reference frame axes
dq	Rotary rotor reference frame axes
f	Frequency (Hz)
f_{av}	Average switching frequency (Hz)
f_{sp}	Sampling frequency
J	Inertia
$\psi_a,\ \psi_b,\ \psi_c$	Three-phase flux linkages (Wb)
ψ_α, ψ_β	α- and β- axis stator flux linkages (Wb)
ψ_d, ψ_q	d- and q-axis stator flux linkages (Wb)
θ_r	Angle between two stator reference frame and rotor reference frame
L_d, L_q	d- and q-axis inductance (H)
ψ_f	Flux linkage generated by the rotor permanent magnet (Wb)
ψ_{rip}	Flux ripple
p	Number of the machine pole pairs
u_a, u_b, u_c	Stator voltages (V)
u_α, u_β	α- and β- axis stator voltages (V)
i_a, i_b, i_c	Stator currents (A)
i_α, i_β	α- and β- axis stator currents (A)
i_d, i_q	d- and q-axis stator currents (A)
R_s	Per-phase stator winding resistance (Ω)
T_e	Electromagnetic torque (Nm)
T_L	Load torque applied on the rotor shaft
T_{rip}	Torque ripple

$u_0 \cdots u_6$	Space voltage vectors produced by the two level inverter (V)
P_{in}	Total input power of a motor (W)
P_{em}	Electromagnetic power obtained by subtracting the mechanical loss from the input power (W)
ω_r	Rotor mechanical speed
ω_e	Electrical speed
C_T	Torque constant gain
C_ψ	Flux constant gain

LIST OF FIGURES

LIST OF TABLES

ABSTRACT

This study focuses on the development of novel model predictive control method for PMSM drive system. The aims of the proposed control method are flux and torque ripples reduction. The performances of the proposed model predictive control method and conventional direct torque control (DTC) are comparatively studied in both simulation and experimental tests.

In recent years, various variable speed drive strategies and structures for PMSMs have been widely investigated and reported. Among these control strategies, the six-step control, field oriented control (FOC) and DTC are the most popular ones. Among them, the conventional DTC, which selects the desired voltage vector based on hysteresis comparators and switching table, features a fast dynamic response and very simple structure. The major demerits of DTC are large torque and flux ripples, variable switching frequency, and acoustic noises. Recently, the model based predictive control (MPC) was introduced to overcome these problems. However, the improvement was limited for the purposes of torque and flux ripple reduction and the MPC still suffered from variable switching frequency.

The conventional DTC and MPC are similar in that they both select only one voltage vector per sampling period. This may result in overregulation, which is the key issue for torque and flux ripples and excessive acoustic noise. In this thesis, an improved MPC method with duty ratio optimization was proposed for PMSMs. The proposed method features low torque and flux ripples and relatively stable switching frequency. It is of most benefit when the drive system is working at a low sampling frequency because in the low frequency range, the proposed MPC drive system can achieve much lower torque and flux ripples than the original MPC and DTC, which is a very desirable feature for high power applications (e.g. electric vehicles). Finally, the numerical simulation and experimental test results of the conventional DTC, MPC, and improved MPC were presented to verify its effectiveness.

CHAPTER 1

INTRODUCTION

1.1 Background and Significance

Modern permanent magnet synchronous machines (PMSMs) are attracting increasing interest for a wide range of applications including industry, household and transportation usage. With the worldwide trend towards energy conservation, there is an increasing need for energy efficient, high performance and reliable electrical drives. PMSMs are the ideal candidates due to their high efficiency, high output power per mass and volume and excellent dynamic performance.

In recent years, various variable speed drive strategies and structures for PMSMs have been widely investigated and reported. Among these control strategies, the field oriented control (FOC) and direct torque control (DTC) are the most popular ones [1.1]-[1.3]. Compared to FOC, the merits of DTC are simple structure, quick dynamic response and strong robustness against motor parameter variation [1.4]-[1.6]. However, the conventional DTC also presents some disadvantages, such as large torque and flux ripples, variable switching frequency and excessive acoustic noises.

To overcome these problems, many methods have been proposed in the literature. Some of them apply space vector modulation (SVM) to DTC, known as SVM-DTC. In the conventional DTC, the switching table only includes a limited number of voltage vectors with fixed amplitudes and positions. The implementation of SVM enables the generation of an arbitrary voltage vector with any amplitude and position [1.7]-[1.9]. In this way, SVM-DTC can generate the torque and flux more accurately. Another merit of using SVM is that the sampling frequency required is not as high as that in the conventional DTC.

Recently, the model predictive control (MPC) has attracted increasing attention in industry and academic communities [1.10]-[1.15]. In SVM-DTC, the power converter with modulation can be considered as a gain in controller design. In the predictive control methods, the discrete nature of power converters is taken into account by considering the converter and the motor from a systemic view. There are various

versions of predictive control, differing in the principle of vector selection, number of applied vectors and predictive horizon.

The conventional DTC and MPC are similar in that they both select only one voltage vector in each sampling period. This can result in overregulation, leading to large torque and flux ripples and acoustic noise.

The major objectives of this thesis project are:

- To conduct a comprehensive comparative study of the existing PMSM drive strategies,
- To propose a novel MPC control scheme for the purposes of torque and flux ripple reduction, and
- To carry out both simulation and experimental tests of the proposed MPC control and compare these to other conventional control schemes.

1.2 Thesis Outline

This thesis is organised in five chapters, including this one as an introduction to the background and structure of the whole thesis.

Chapter 2 presents the state of the art of permanent magnet synchronous machines. Various topologies of PMSMs and classifications are introduced. A literature review of all the major machine control methods is presented. The fundamentals and principles of these drive methods are also investigated.

Chapter 3 discusses the model predictive control in details. The PMSM model for MPC is firstly derived. Then the principle of MPC is introduced as well as some improvements, such as one-step delay compensation and linear multiple horizon prediction. The simulation and experimental tests of DTC, MPC and improved MPC are presented and a comprehensive analysis of the test results is carried out.

In Chapter 4, a novel MPC scheme is proposed, namely MPC with duty ratio optimization. The idea of duty ratio optimization and the duty ratio calculation

algorithm are presented. Both simulation and experimental tests of the original MPC and the new MPC are carried out, in order to demonstrate the effectiveness of the proposed method.

Chapter 5 draws conclusions from this thesis and presents possible future work.

Lists of related references are attached at the end of each chapter.

REFERENCES

[1.1] S. Y. Kim, W. Lee, M.S. Rho, and S. Y. Park, "Effective dead-time compensation using a simple vectorial disturbance estimator in PMSM drives," IEEE Trans. Ind. Electron., vol.57, no.5, 2010, pp.1609–1614

[1.2] J. Lee, J. Hong, K. Nam, R. Ortega, L. Praly, and A. Astolfi, "Sensorless control of surface-mount permanent-magnet synchronous motors based on a nonlinear observer," IEEE Trans. Power Electron., vol.25, no.2, 2010, pp.290–297

[1.3] F. Genduso, R. Miceli, C. Rando, and G. R. Galluzzo, "Back EMF sensorless-control algorithm for high-dynamic performance PMSM," IEEE Trans. Ind. Electron., vol.57, no.6, 2010, pp.2092–2100

[1.4] I. Takahashi and T. Noguchi, "A new quick-response and high-efficiency control strategy of an induction motor," IEEE Trans. Ind. Appl., vol.22, no.5, 1986, pp.820–827

[1.5] M. Depenbrock, "Direct self-control (DSC) of inverter-fed induction machine," IEEE Trans. Power Electron., vol.3, no.4, 1988, pp.420–429

[1.6] G. S. Buja and M. P. Kazmierkowski, "Direct torque control of PWM inverter-fed AC motors—A survey," IEEE Trans. Ind. Electron., vol.51, no.4, 2004, pp.744–757

[1.7] Y. S. Lai and J. H. Chen, "A new approach to direct torque control of induction motor drives for constant inverter switching frequency and torque ripple reduction," IEEE Trans. Energy Convers., vol.16, no.3, 2001, pp.220–

227

[1.8] C. Lascu and A. Trzynadlowski, “A sensorless hybrid DTC drive for high-volume low-cost applications,” IEEE Trans. Ind. Electron., vol.51, no.5, 2004, pp.1048- 1055

[1.9] Y. Zhang, J. Zhu, W. Xu, J. Hu, D. G. Dorrell, and Z. Zhao, “Speed sensorless stator flux oriented control of three-level inverter-fed induction motor drive based on fuzzy logic and sliding mode control,” in Proc. 36th IEEE IECON, 2010, pp.2926–2931.

[1.10] T. S. Wang, J. G. Zhu, and Y. C. Zhang, "Model predictive torque control for PMSM with duty ratio optimization," International Conference on Electrical Machines and Systems (ICEMS), 20-23 Aug. 2011

[1.11] H. Miranda, P. Cortes, J. Yuz, and J. Rodriguez, “Predictive torque control of induction machines based on state-space models,” IEEE Trans. Ind. Electron., vol.56, no.6, 2009, pp.1916–1924

[1.12] T. Geyer, G. Papafotiou, and M. Morari, “Model predictive direct torque control—Part I: Concept, algorithm, and analysis,” IEEE Trans. Ind. Electron., vol.56, no.6, 2009, pp.1894–1905

[1.13] S. Kouro, P. Cortes, R. Vargas, U. Ammann, and J. Rodriguez, “Model predictive control—a simple and powerful method to control power converters,” IEEE Trans. Ind. Electron., vol.56, no.6, 2009, pp.1826–1838

[1.14] F. Morel, J.-M. Retif, X. Lin-Shi, and C. Valentin, “Permanent magnet synchronous machine hybrid torque control,” IEEE Trans. Ind. Electron., vol.55, no.2, 2008, pp.501–511

[1.15] K. Drobnic, M. Nemec, D. Nedeljkovic, and V. Ambrozic, “Predictive direct control applied to AC drives and active power filter,” IEEE Trans. Ind. Electron., vol.56, no.6, 2009, pp.1884–1893

CHAPTER 2

LITERATURE SURVEY ON PERMANENT MAGNET SYNCHRONOUS MACHINES AND ELECTRICAL MACHINE CONTROL STRATEGIES

2.1 Introduction

Permanent magnet synchronous machines (PMSMs) have been widely applied in both industrial and domestic markets because of their high power density, high torque to current ratio, and high power factor. However, the major drawbacks of PMSMs are high cost, narrow speed range, less robustness when compared to induction motors (IMs) and the need for a complex control scheme. Recently, various topologies have been proposed for PMSMs to overcome these problems.

During the 1990s, the vector control (VC) or field oriented control (FOC) scheme was thoroughly investigated resulting in a significant improvement in the performance of AC drives. However, these schemes have several main limitations, such as the high sensitivity to machine parameters and large computing cost. To overcome the drawbacks of the conventional VC schemes, the direct torque control (DTC) scheme was proposed with attractive advantages, such as insensitivity to machine parameters, fast torque response and simple algorithms. Much effort has been made to improve the performance of both VC and DTC schemes.

In this chapter, the state of the art of PMSMs is firstly introduced in section 2.2, including various topologies of PMSMs and classification. Section 2.3 presents a literature review of all the major machine control methods. The fundamentals and principles of these drive methods are introduced in sections 2.4 and 2.5.

2.2 State of the Art of PMSMs

Permanent magnet (PM) machines are the most efficient of all types of electrical machines due to the use of permanent magnets for the excitation, which consumes no power. Other merits of PM machines include simple control technique, high power density and ease of cooling. However, PM machines also suffer from some disadvantages, such as narrow constant power speed range, possible demagnetization, and high cost.

The topologies of PM machines are various. According to the location of PMs, they can be divided into two categories: PMs on rotor and PMs on stator.

2.2.1 Permanent magnets on rotor

This is a classical topology of PM machines, including the surface mounted permanent magnet machine (SPM) and interior permanent magnet machine (IPM), as shown in Fig. 2.1.

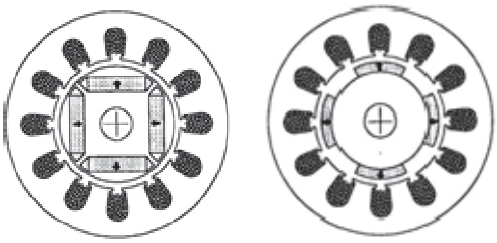

(a) **(b)**

Fig. 2.1 Structure of PM machines
(a) IPM and (b) SPM

Numerous novel designs of IPMs have been proposed. In 1995, M. Azizur Rahman and Ruifeng Qin designed a PM hysteresis hybrid synchronous motor which is the combination of conventional stator and hybrid rotor [2.1], as shown in Fig.2.2(a). On the rotor, PMs are inserted in the slots at the inner surface of the hysteresis material ring. The merit of this design is the high starting torque due to the magnet brake torque of a conventional PM motor compensated by the high eddy current and hysteresis torques.

At the synchronous speed, the motor behaves as a permanent magnet motor due to the absence of eddy current torque [2.1].

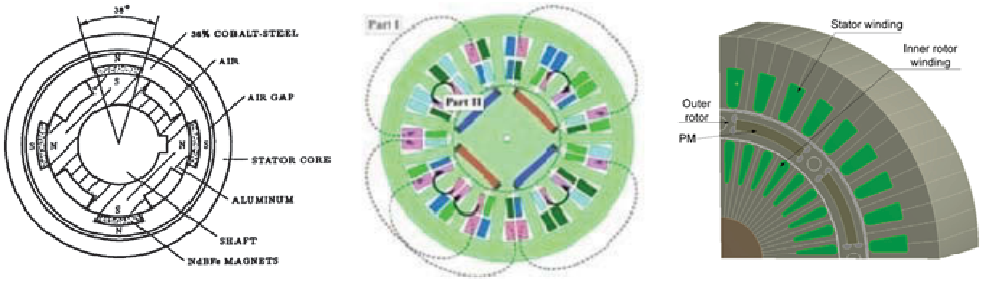

(a) (b) (c)

Fig. 2.2 Cross sectional view of (a) PM hysteresis hybrid machine [2.1], (b) 4-layer hybrid winding machine [2.2], and (c) double rotor synchronous PM machine [2.3]

In 2010, Won-ho Kim, and Jae-Nam Bae, *et al*., suggested a 4-layer hybrid winding (concentrated and distributed winding) layout designing to extend the operating range of IPMSM [2.2], shown in Fig.2.2(b). This design has more sinusoidal air-gap flux density and higher power density.

Also in 2010, Peter Pisek, and Bojan Stumberger, *et al*., designed a double rotor synchronous PM machine which can be used in HEVs or EVs as a traction motor or generator [2.3], as shown in Fig.2.2(c). The merits of this design are high torque density and low torque ripples.

2.2.2 Permanent magnets on stator

When the permanent magnets are located on the stator, the rotor must have salient pole geometry, making it similar to a switched reluctance motor (SRM). This topology has inherently the advantages of a simple and rugged structure, high speed operation and good heat dissipation. Some machines have PMs located in stator back-iron, which are named doubly salient permanent magnet (DSPM) machines; others have PMs fitted in the stator teeth, which are named flux switching permanent magnet (FSPM) machines.

The DSPM was first proposed by Yuefeng Liao and Feng Liang in 1992 [2.4], which is an evolution of the doubly salient homopolar inductor machine. In a DSPM, the field excitation is supplied by the PMs which are planted in the stator or rotor. The torque is

produced by both PMs' flux and current excitation flux in the windings. The basic structure of DSPM is similar to that of SRM as shown in Fig. 2.3(a) [2.4]. The major advantages of the DSPM are high torque density, high efficiency, simple and rugged structure, high speed capability, small VA rating of the power converter and fast response times. The drawbacks of DSPM are poor torque quality and limited speed range which is critical for EVs.

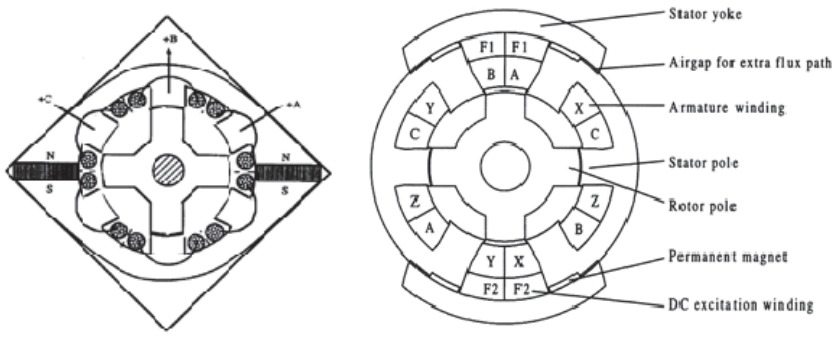

(a) **(b)**

Fig. 2.3 Cross sectional view of (a) the first proposed DSPM [2.4], and (b) stator doubly fed DSPM [2.5]

In recent years, to extend the speed range and improve the efficiency of DSPM for EV applications, numerous novel designs have been proposed. In 2003, K.T. Chau suggested a stator doubly fed DSPM [2.5], which consists of two types of stator windings, a three-phase armature winding and a DC field winding as shown in Fig. 2.3(b). The three-phase armature winding operates like that in the conventional DSPM, whereas the DC field winding works as a tool for flux weakening or flux strengthening. Moreover, an extra flux path is added in this topology to reinforce the effect of flux weakening and flux strengthening. With the help of these artful designs, the constant power operation range can be extended to four times that of the base speed which is suitable for EV applications. The efficiency on the flux weakening operation is also improved [2.5].

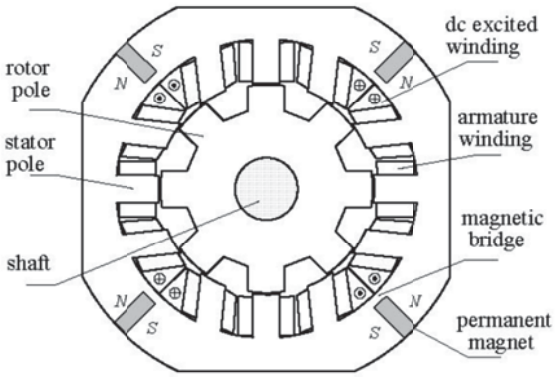

Fig. 2.4 Structure of SHEDS-PM [2.6]

In 2005, Xiaoyong Zhu and Ming Cheng proposed a stator hybrid excited doubly salient permanent magnet (SHEDS-PM) brushless machine with a magnetic bridge as shown in Fig. 2.4 [2.6], which is a similar approach to that suggested by K.T. Chau in 2003. The magnetic bridge could maintain the entirety of the stator lamination as well as amplify the effect of DC excitation flux on PM flux.

The concept of FSPM was firstly proposed by S.E. Rauch and L.J. Johnson in 1955 and was used in 4/2 pole and 4/6 pole flux-switch alternators which are designed for missiles as shown in Figs. 2.5(a) and (b) [2.7].

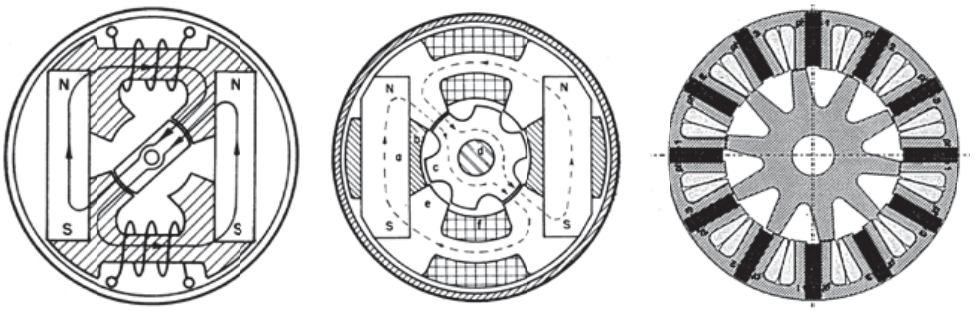

Fig. 2.5 Structure of (a) 4/2 pole flux-switch alternator [2.7], (b) 4/6 pole flux-switch alternator [2.7], and (c) FSPM proposed by E. Hoang in 1997 [2.8]

In 1997, E. Hoang presented a new structure of FSPM with PMs inserted in the stator teeth and full pitch concentrated stator winding which can be considered as the modern

conventional FSPM [2.8]. As shown in Fig. 2.5(c), due to the air gap flux being a compound of the PM flux and the winding excitation flux, in theory, the capability of flux weakening is infinite. Besides the inherent merits of the SRM and PM machine, the most prominent advantage of the proposed design is its wide operating speed range. Although the structure of FSPM is similar to that of SRM, the acoustic noise of FSPM is lower than that of SRM by the help of a different flux control method.

In the last five years, numerous novel FSPM topologies have been developed for various applications as shown in Fig. 2.6. The fault-tolerant design proposed by R.L. Owen and Z.Q. Zhu in 2008, is achieved by employing an alternate pole and wound windings topology, as shown in Fig. 2.6(b) [2.9]. However, the conventional FSPM machine has the demerit of high magnet volume, which can be improved by replacing the stator pole without armature winding with a simple stator tooth, as shown in Fig. 2.6(c) E-core FSPM [2.10]. Moreover, the simple stator tooth can be removed to enlarge the slot area, and consequently the C-core FSPM is produced as presented in Fig. 2.6(d). As shown, the rotor pole number is twice of the stator pole number in the E- and C-core FSPM design, whilst they are equal in the conventional FSPM. In order to improve the torque density, in 2008, Z.Q. Zhu, and J.T. Chen, *et al*., presented a multi-tooth FSPM topology as shown in Fig. 2.6(e) [2.10]. However, as the magnetic circuit becomes saturated more quickly as the current is increased, its torque capability becomes inferior to that of a conventional FSPM machine, due to the higher armature reaction.

In 2009, A. Zulu suggested a novel FSPM design with segmental rotor, as shown in Fig. 2.6(f) [2.11]. The idea of this design is to provide a defined magnetic path for conveying the field flux to adjacent stator armature coils as the rotor rotates, in order to shorten the end-winding and improve the overall efficiency. However, further study should be carried out, due to the normal experimental performance compared with the conventional FSPM. Also, the hybrid excited FSPM evolved from the conventional FSPM was proposed in 2007 by E. Hoang and M. Lecrivain as shown in Fig. 2.6(g) [2.8]. A DC excitation winding was added in the back of the PMs, in order to modulate the excitation of the permanent magnets. In this way, both the flux weakening and flux strengthening effect can be achieved for a wide speed range in a constant power region and high torque at starting period. In 2011, W. Xu and J. Zhu, *et al*. proposed an axially

laminated FSPM (ALFSPM) machine, as shown in Fig. 2.6(h) [2.12]. The windings and magnets of this machine are located in the stator, while the rotor is passive with great mechanical robustness. For inheriting the merits of both switched reluctance machine and traditional rotor-PM machine, it has good attributes of high torque/power density, high efficiency, excellent flux-weakening capability, strong robustness, and convenience of cooling

Most PM machines have excellent features like high power density, high efficiency, high controllability and fast dynamic response. The major weaknesses are the delicate rotor structure due to the low mechanical strength of PMs and the narrow operating speed range due to the difficulty of weakening the field of PMs.

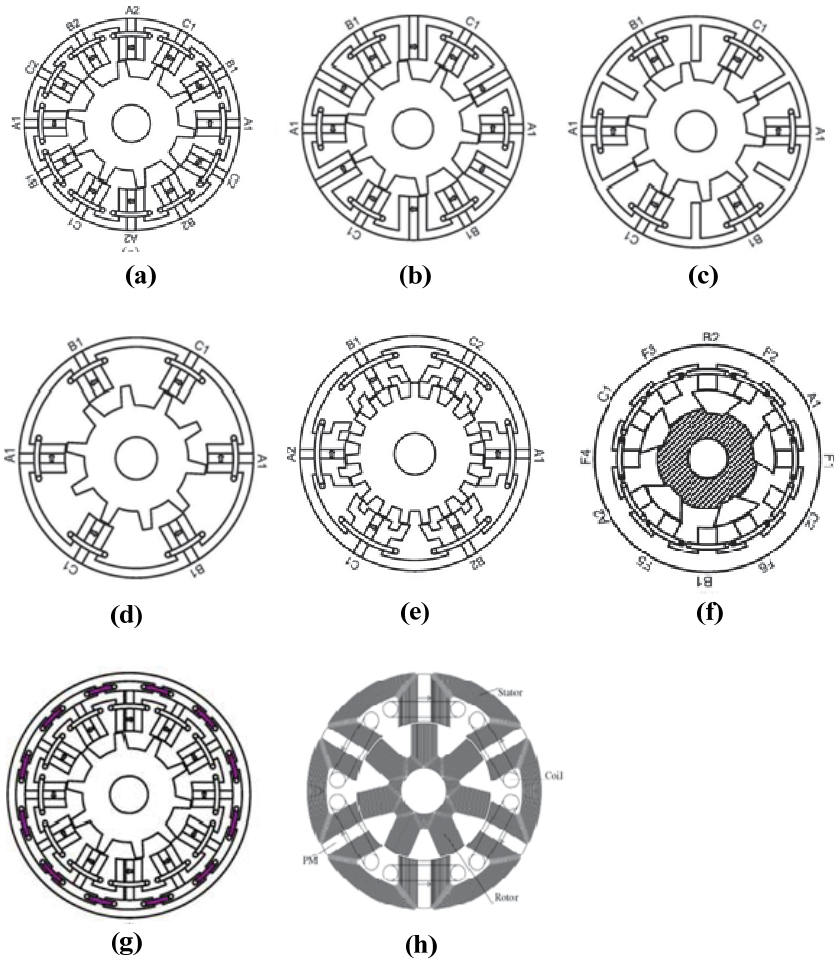

Fig. 2.6 Topologies of modern FSPM, (a) conventional FSPM, (b) fault-tolerant FSPM [2.9], (c) E-core FSPM [2.10], (d) C-core FSPM [2.10], (e) multi-tooth FSPM [2.10], (f) segmental rotor FSPM [2.11], (g) hybrid excited FSPM [2.8], and (h) axial laminated structure FSPM [2.12]

2.3 History of Motor Control Methods

2.3.1 Six-step control

The conventional DC machines feature high performance and high efficiency. However, the major drawback is that they need a commutator and brushes which are subject to wear and require maintenance. The development of solid-state switches enabled the realization of maintenance-free machines which are known as electronically commutated motors (ECMs) [2.13] or brushless DC (BLDC) motors [2.14-15]. The BLDC motor was first developed in 1964 by the National Aeronautics and Space Administration (NASA) [2.16].

The basic principle of BLDC motors and conventional DC motors are almost the same. The primary difference is the inverse relationship of rotating and stationary components. The conventional DC motors have a stationary magnetic field and rotating armature, while the BLDC motors have a rotating PM rotor and stationary armature windings. In the six-step control method, the solid-state switches function as the commutators and brushes, in order to commutate the stator current. [2.17].

The PM BLDC motors are different from PMSMs in that the former‘s back *emf* waveform is rectangular or trapezoidal, whereas the latter is sinusoidal, as shown in Fig. 2.7. The electrical cycle of the BLDC rotor is divided into six sectors, and the control method of BLDC motors, known as the six-step method, can be implemented by detecting the rotor position to generate gating signals to control the six solid state switches of the three phase inverter. The most common position sensor used in BLDC motors is the Hall element, or switching Hall sensor. The installation position of the sensors is shown in Fig. 2.8. Compared with the other rotating position sensors, such as encoder, resolver or linear Hall sensors, the Hall elements are cheaper and more robust. However, they can only produce low resolution feedbacks as shown in Fig. 2.9.

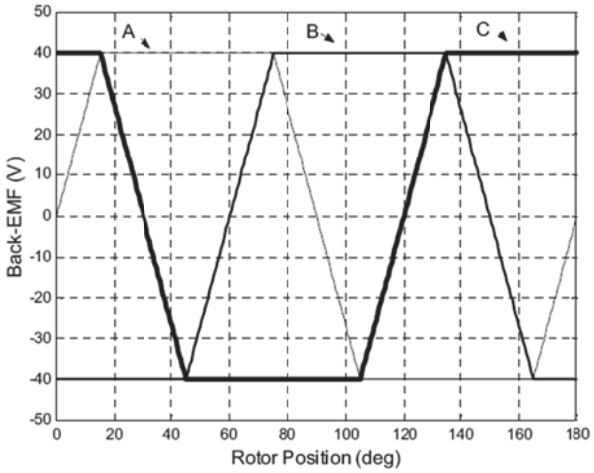

(a)

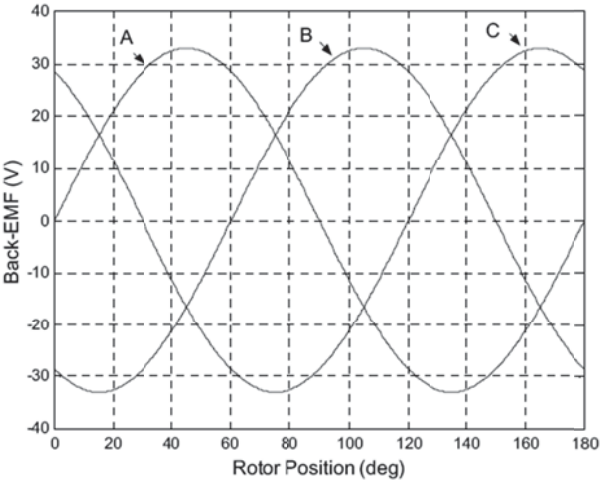

(b)

Fig. 2.7 Back *emf* waveform of BLDC and PMSM: (a) Trapezoidal back *emf* of BLDC motor, and (b) Sinusoidal back *emf* of PMSM.

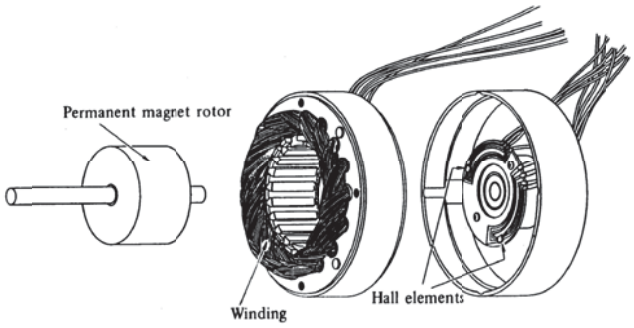

Fig. 2.8 Disassembled view of a BLDC motor: PM rotor, winding and Hall elements [2.18]

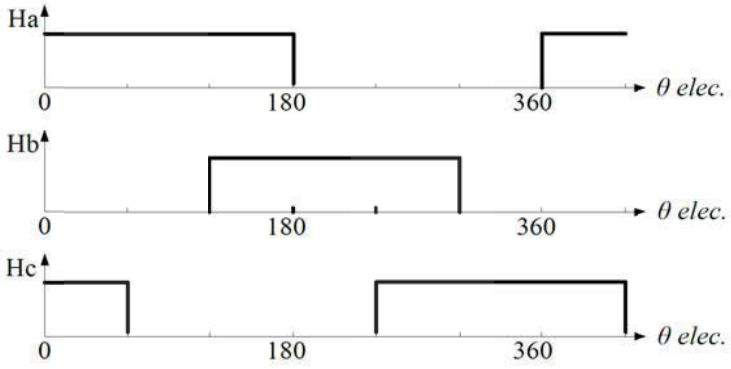

Fig. 2.9 Feedback signals generated by Hall elements

The six-step control methods for BLDC motors can be classified into 120° and 180° conduction modes [2.19]. In the 120° conduction mode, known as the two-phase feeding mode [2.20], only two switches are turned on at a time and the electronic commutation takes place every 60 electrical degrees. The inverter operates as a commutator feeding the DC current into two phases of the motor. The third phase can be considered as open circuit. The rotating magnetic field is created by commutating the DC current from phase to phase at intervals equivalent to 60 electrical degrees. The commutation is synchronized to the rotor position sensor signals. Under this mode, each inverter switch works for 120 electrical degrees in every cycle.

Under the 180° conduction mode, the electronic commutation interval is still 60 electrical degrees but three switches are turned on at one time. All inverter switches conduct for 180° in one cycle. The 120° conduction method is more popular in the controller design and applications (as will be explained below). The inverter status in these conduction modes are shown in Fig. 2.10.

For a star connected BLDC motor, the overall torque generation depends on the conduction modes. For example, when the DC bus current fed to the armature windings is constant and the switches T1 and T2 are turned on in the 120° conduction mode, the currents in phase *A* and *C* have the same magnitude but different direction. The total electromagnetic torque is equal to $\sqrt{3}T_a$, which can be obtained by the arithmetic sum as shown in Fig. 2.11 (a), where T_a is the electromagnetic torque produced by phase *a* current. In 180° conduction mode, inverter T1, T2, and T6 are turned on and the total electromagnetic torque is only 1.5 T_a, as shown in Fig. 2.11 (b).

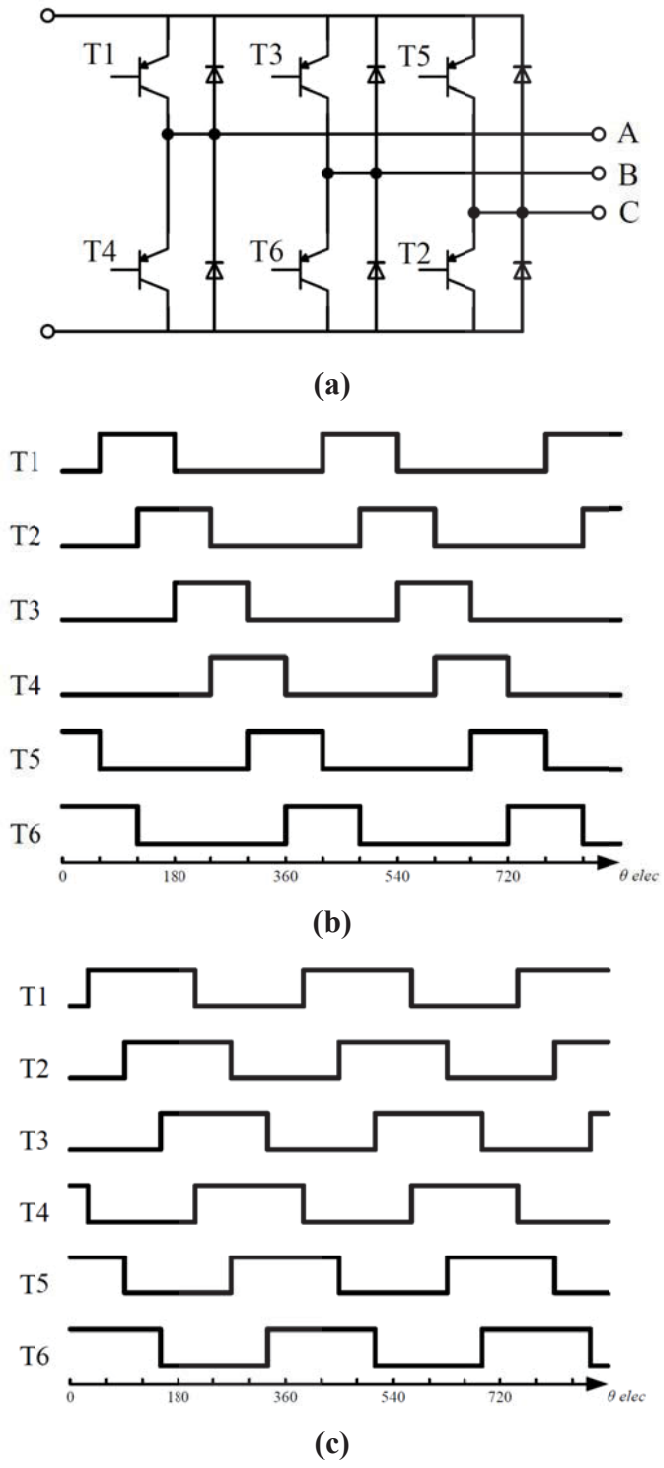

Fig. 2.10 Inverter diagram and conduction modes for six-step control: (a) Inverter structure, (b) Switch status at 120° conduction mode, and (c) Switch status at 180° conduction mode

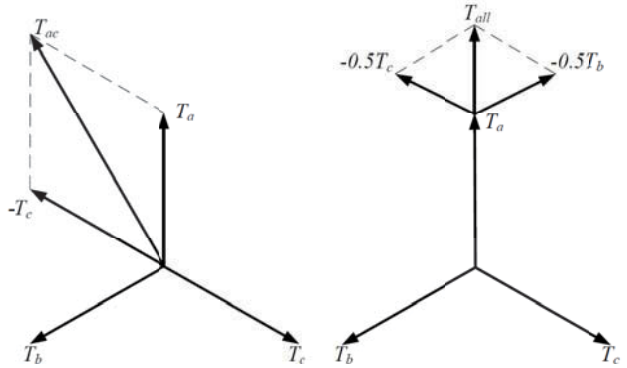

Fig. 2.11 Torque generation under different conduction modes: (a) Torque composition in 120° conduction mode, and (b) Torque composition in 180° conduction mode

2.3.2 Vector control

In the 1990s, with the availability of high energy permanent magnet materials and fast switching power electronic devices, much progress has been achieved for PMSM drives. However, the nonlinear characteristics and inherent coupling problem of the PMSM make the torque control difficult. Fortunately, vector-controlled PMSM drives play an important role in providing good performance characteristics similar to or even better than those of DC motors.

The vector control (VC) or field oriented control (FOC) scheme was proposed in the 1970s by Blaschke [2.21]. It is a fundamental method for controlling AC machines by essentially transforming their dynamic structure into that of DC machines. The VC method was developed based on the Park transform [2.22], which was proposed to model the synchronous machines [2.23]. The control objective is to decouple the stator current i_s, into its flux producing and torque producing components, i_d and i_q, respectively. This method enables independent control of the field and torque of the machine by manipulating the corresponding field-oriented quantities. This system adapts to any load disturbances and/or set-point variation as fast as a DC motor can operate.

The VC controller for PMSMs was proposed based on the original FOC concepts, transferring the electrical excitation field to a permanent magnet based field [2.24]. Striving for a sinusoidal *emf* of the motor, the power and the torque transmitted are

independent of time and rotor angle. The stator current can be subdivided into its *d*-axis and *q*-axis components, i_d and i_q, respectively. Only the component i_q develops the torque for non-salient pole rotor machines, whereas i_d influences the magnitude of the air-gap field. In order to develop the required torque at minimum current, the phase angle of the current is chosen in a way such that no i_d component exists. The desired locus of stator current spatial vector is that of a round circle. Fig. 2.12 shows the diagram of the classical VC scheme for PMSMs.

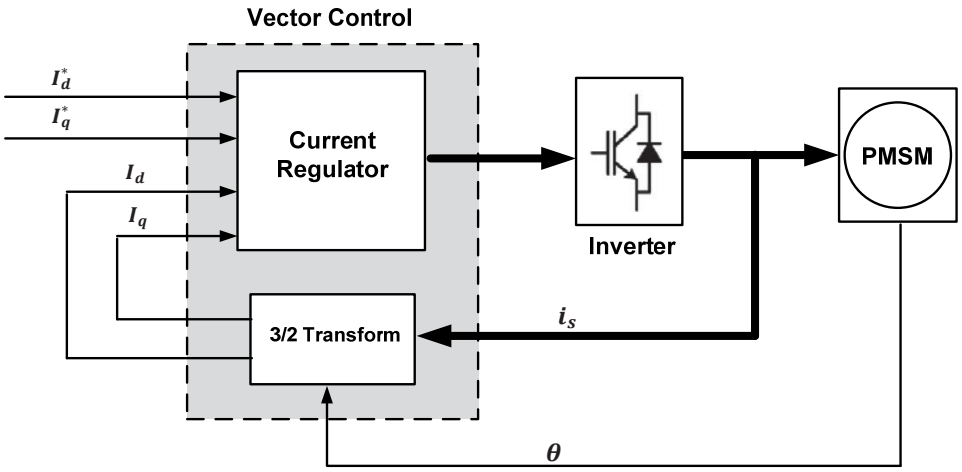

Fig. 2.12 Diagram of vector control drive system

Based on the VC scheme, the motor currents and voltages are manipulated in the *dq* reference frame. This means that the measured motor currents must be mathematically transformed from the three phase static reference frame of the stator windings to the stator *dq* reference frame, prior to being processed by the PI controller. Later, the voltages have to be transformed from the *dq* frame to the *abc* reference frame for the PWM output. For these transformations, the fast and intensive calculation capability of a high performance microprocessor or digital signal processor (DSP) is necessary. The powerful microprocessors or DSP have presented an effective solution to the high performance digital PMSM controllers. Additionally, the availability of the unexpected computation of microprocessors or DSPs has also made the current controller possible.

In 1986, a digital-based speed loop was reported with an analogue internal current controller [2.25]. In 1988, a DSP vector controller was reported, but the detailed implementation was not proposed [2.26]. The theoretical background to the digital

implementation of vector and current control was proposed in [2.27], which makes a fully operational digital implementation of the vector/current controllers available and reliable. Based on the previous research, in [2.28], Allen applied a dual digital signal processor board for the control of PMSMs. As system reliability and cost reduction can be achieved by the full digital solution, a digital VC scheme has been developed with a space voltage modulation algorithm by Boldea and Nasar [2.29].

In 1992, Cecati presented the fully digital implementation of a classical rotor flux orientation (RFO) VC scheme for a PMSM drive [2.30]. Based on the cascade control, the whole system is composed of two loops. The well-known principle of rotor flux oriented control is applied in the current control loop as the inner control loop, and the outer loop is for speed control, which is realised by PI controllers.

With the application of fast digital signal processors, the space vector modulation technique has been digitally implemented together with the VC scheme. In 1993, a new VC drive scheme was presented with an application specific integrated circuit for pulse width modulation (PWM) [2.31].

In 2002, Bolognani and Zigliotto designed a novel vector control scheme [2.32] whereby the current space vector in the synchronous *d-q* reference frame is controlled. The best voltage vector is applied in order to reduce the mean prediction based on motor equations, which somewhat recalls the DTC methodology. The proposed algorithm is a hysteresis control on both current vector amplitude and torque angle. Simulation and experiment have confirmed the validity and simplicity of the method, which is particularly suited for low-cost and full-digital DSP based applications. In addition, the switching count is impressively reduced.

2.3.3 Direct torque control

In a VC based PMSM drive system, the output torque is controlled indirectly by regulating the stator current, meaning the efforts to improve the system's performance are mainly focused on estimating accurate machine feedback and developing an

effective current controller, which will unfortunately increase the computation load, and slow down the system's dynamic response.

Another drive method for PMSMs was then proposed as direct torque control (DTC), which regulates the generated torque and air-gap flux directly. The DTC scheme was developed firstly for induction machines, by Takahashi as the DTC [2.33] and by Depenbrock as the direct self-control (DSC) [2.34]. The basic idea of DTC for the induction motor is to control the torque and flux linkage by selecting the voltage space vectors properly, which is based on the relationship between the slip frequency and torque [2.35]. It has been proven that DTC could be used for PMSM drives although there is little difference from that of induction motors. Fig. 2.13 shows a typical structure of the DTC system. The current controller followed by a PWM comparator is not used in DTC systems, and the parameters of the motor are also not used, except the stator resistance. Therefore, the DTC possesses advantages such as less parameter dependence and faster torque response when compared with the torque control via VC based current control. The switching state of the inverter is updated once only in every sampling interval and it does not change until the output of the hysteresis controller change states [2.36]. Therefore, the ripples in torque and flux are relatively high when compared with those of the vector control drive system. Although a smaller hysteresis bandwidth may result in less torque ripples, the switching loss of the inverter will dramatically increase. Furthermore, the switching frequency of the inverter is not constant. The switching action only depends on the observed torque and flux linkage values. Therefore, the inverter switching frequency varies against the rotor speed, load torque and the bandwidth of the two hysteresis controllers [2.37] [2.38].

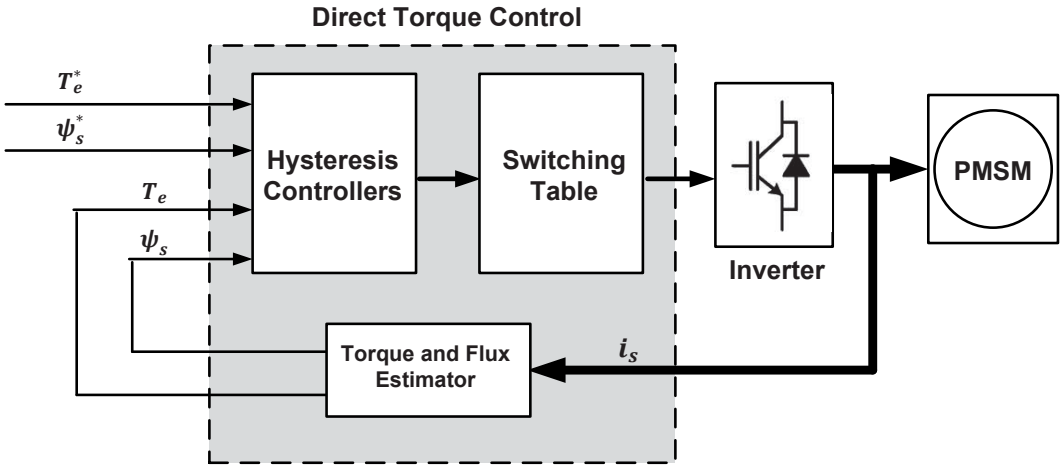

Fig. 2.13 Diagram of direct torque control drive system

Many schemes have been proposed to improve the DTC scheme to achieve better performance and they are summarised in Fig. 2.14. In [2.39]-[2.41], the hysteresis controllers are replaced by a fuzzy logic controller, which considers not only the sign of the error, but also the amplitude. In [2.42], neural network is used to select the vector. In [2.43]-[2.45], Output space regulation (OSR) is used to select the vector. The proposed strategies focus on a direct regulation of two outputs, namely torque and flux amplitude. These strategies are based on the minimization of a weighted function of quadratic or absolute value functions of the output errors. The classic DTC is considered as a special case of OSR and it belongs to the class of strategies based on a quadratic criterion. In [2.46], a 3-level inverter fed DTC scheme with modified switching table is proposed to improve performance at low speed. However, it failed to consider other problems, such as neutral point balance and voltage jump. In [2.47], the duration time, i.e. duty ratio of the selected vector is obtained by solving the optimal value which will lead to minimum torque ripple RMS during one period. In [2.48], the duty of the active vector in one period can also be obtained from a fuzzy logic controller. However, the performance improvement is quite limited. In [2.49], a band-constrained technique is proposed, which aims at limiting the torque ripple to the hysteresis band, not the minimal RMS of torque ripple. A completely different approach to achieve better performance has been proposed in [2.50] and [2.51], which consists of replacing the hysteresis torque and flux controllers with proportional–integral (PI) regulators and voltage modulators. However, it reduces the simplicity of the classic DTC scheme.

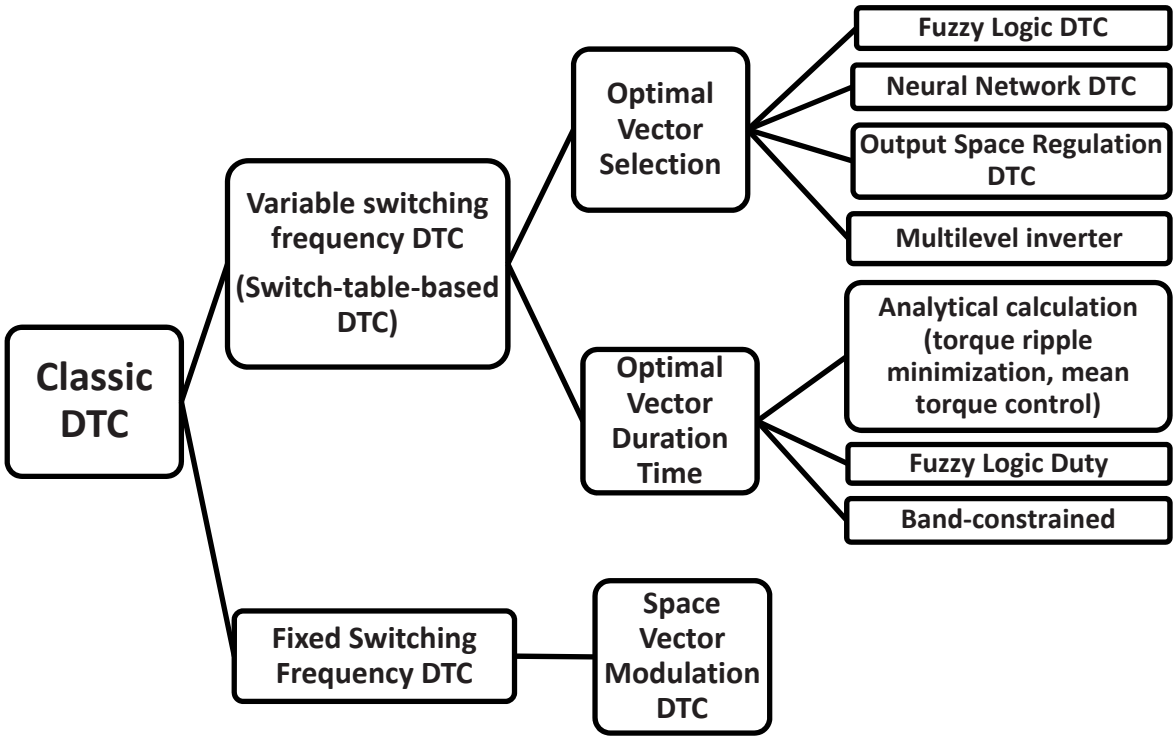

Fig. 2.14 Development of DTC scheme

2.3.4 Model predictive control

The linear PID-controllers used in electrical drive system were widely built with analogue operational amplifiers and used the control deviation to generate the commanding signal [2.52]. This type of controller does not include any knowledge of the plant and this knowledge is only required for designing the controller. With the availability of inexpensive microcomputers and digital control techniques in drive system, the idea to precalculate the plant's behaviour via a mathematic model and to determine optimum values for the actuating variables from these pre- calculated values was born, i.e. predictive control.

Considering the functional principles of the different predictive control algorithms, it can be found that they can be classified into three main groups: hysteresis-based, trajectory-based and model-based strategies.

The basic principle of hysteresis-based control strategies is to keep the value of the controlled variable within a tolerance band or a tolerance area, the so-called hysteresis. The simple form of such a controller is the well-known hysteresis or bang-bang controller. Hysteresis-based strategies have the advantage that precise knowledge of the drive system is not required. Even with possible model divergences the control error can be kept within the specified limit band by the hysteresis controller. To achieve this, it must always be ensured that the hysteresis controller reacts very quickly if the actual value has gone outside of the hysteresis band. This is a major problem if the hysteresis-based predictive controller is implemented in a digital processor, as the detection of the reference signal crossing the hysteresis band will be done only during the next sampling instant. At this time, it may happen that the error has grown to a large value. Hence, hysteresis-based predictive control is more suitable when the realization is done using analogue operational amplifier rather than microprocessor controllers.

The trajectory-based control methods are based on the principle to force the system onto precalculated system trajectories. Once the system has been pushed onto one of these trajectories, it remains there because of its own properties until a change is enforced form outside. The trajectory-based control is based on a very precise prediction of the

future control system behaviour. Hence, in contrast to hysteresis controllers, controllers of this type require an exact model of the system to be controlled. Because of the quite complex pre-calculation of the system trajectories, these methods are better suited for implementations in the form of digital controllers on microprocessors.

Both hysteresis and trajectory-based predictive controllers use the current system state to precalculate the value of the controlled variable for the next sampling cycle. The past is not explicitly taken into consideration as it is hidden in the actual system state. Although there is a relationship between hysteresis and trajectory-based predictive control algorithms, model-based strategies are based on completely different ideas. Model-based predictive control methods are able to consider the past and to optimize future values of the actuating variables, not only for the next sampling cycle, but also up to a specified future cost or control horizon.

The model predictive control (MPC) is derived from a rather old approach whose first ideas were published more than 20 years ago [2.53] [2.54]. Its strategies are based on an explicit and identifiable model of the controlled system, which is used to precalculate the behavior of the plant and to choose an optimal value of the control variables. Because of the great computational power required by MPC, its implementation has been formerly limited to slowly varying systems, such as chemical processes, in which the time interval is long enough to process the complete control algorithm. As the performance of the available computing hardware has rapidly increased and new faster algorithms have been developed, it is now possible to implement MPC for fast systems using shorter time steps.

MPC makes explicit use of the system mathematical model to predict the future behaviour of the system. An optimal aim is defined and solved in MPC to obtain the most appropriate control input. Similar to the nature of FOC and DTC, MPC can also be classified into two categories: continuous MPC [2.55], [2.56] and finite control set MPC (FCSMPC) [2.57], [2.58]. Like FOC, the continuous MPC also requires the use of PWM or the concept of duty cycle, which fails to consider the discrete nature of the converter. In contrast, FCSMPC evaluates the effects of each possible voltage vector and the one that minimizes the error between the reference value and the feedback value

is selected. FCSMPC is similar to DTC in that they both directly select one and only one voltage vector during one control period. Due to its intuitive concept and simple principle, FCSMPC has been widely studied and applied to the control of power converters and motor drives. FCSMPC can be categorized into two groups according to the predictive horizon N [2.58], [2.59]. With a short predictive horizon of N = 1, the calculation burden is relatively small and can be easily implemented in modern DSPs. With a longer predictive horizon of N > 1, it is possible to obtain a better control performance [2.59]. In [2.59], for a three-level inverter-fed DTC motor drive, a predictive horizon greater than one is employed to obtain reduced switching frequency whilst keeping the torque, flux, and neutral point potential within their respective hysteresis bands.

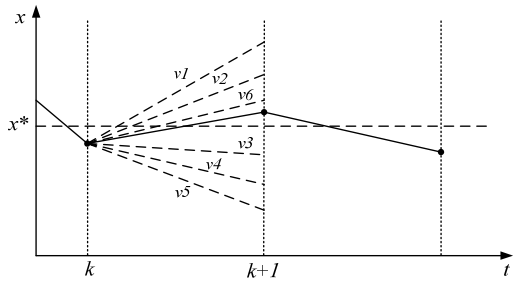

Fig. 2.15 Finite control set MPC scheme

Delay compensation is an important issue in the implementation of FCSMPC [2.60], [2.61]. It is widely recognized that there is a one-step delay between the commanding voltage and the applied voltage, which means that the commanding voltage obtained at any current instant will not be applied until the next instant. This delay is usually caused by the update mechanism in DSP. The influence of one-step delay is especially serious when the sampling frequency is low. As MPC uses the internal model to predict the future behaviour of the system, it is natural to further use the predictive results to eliminate the one-step delay, which is called a two-step prediction in [2.62].

For power converters and inverter-fed drives, it is desirable to reduce the switching frequency to obtain reduced switching loss and higher efficiency [2.59], [2.60], [2.63]. However, so far the incorporation of switching frequency reduction in MPC for motor drives is very rare. In [2.62], the application of MPC for the torque and flux control of an induction motor drive is investigated, but the switching frequency reduction is not addressed. Reference [2.61] considered the switching frequency reduction in a

three-level inverter fed induction motor drive by using hysteresis controllers. The implementation is complex and requires the use of ASIC to accomplish the fast computation requirement [2.64].

A cost function suitable for electrical machine drive systems was proposed by Kouro and Cortes [2.65]. The cost function evaluates all predictions and the one with the minimum cost is chosen. Then future control actions are implemented. In addition to torque and stator flux, other control variables, such as switching frequency, efficiency and spectrum shaping can also be included in the cost function. The priority of each control variable is adjusted by weighting factors. This paper presents great ideas on implementation of MPC. However, it lacks experimental results to verify the effectiveness of the proposed method.

In [2.66], a guideline of the weighting factor design is presented, but it does not mention any analytical or numerical solution. The weighting factors are still determined by empirical methods.

In [2.67], Zhang and Zhu proposed a model-based predictive torque control (MPTC) method for permanent magnet synchronous machine (PMSM) drive system. A linear PMSM model is used in this paper, in order to reduce the computational cost as well as maintain the accuracy. The one step delay compensation is considered and two additional components are added to the cost function in order to improve the stability of the system and reduce the switching frequency. The simulation test demonstrates the effectiveness of the proposed method. However, it still needs further verification of the experimental test.

2.3.5 Qualitative comparison of control methods

In general, the classic VC method can bring good performance to PMSM drive systems. However, in order to control the drive system in real time, a high computational power microprocessor is needed to perform complicated coordinate transformations. The classic DTC method works with hysteresis controllers and a switching table to achieve rapid response times and it is insensitive to machine parameter variations, whereas its

steady state performance is poor. In contrast, the MPC features both good dynamic and steady state performance. The most attractive feature of the MPC is the great flexibility of the cost function, i.e. the controllable variables such as torque ripple, switching frequency and power loss can be included in the cost function.

The details of each control method are compared in Table 2-1.

Table 2-1 Qualitative comparison of control methods

	Classic FOC	**Classic DTC**	**MPC**
Speed Estimation	Encoder output	Encoder output	Encoder output
Speed Controller	PI controller	PI controller	Cost function definition
Flux-linkage Estimation	N/A	*abc*-to- *αβ* transformation with Integration	*abc*-to-*dq* transformation
Flux-linkage Controller	N/A	Hysteresis controller	Cost function definition
Current/Torque Estimation	*abc*-to-*dq* transformation	Calculation from flux linkage and currents	*abc*-to-*dq* transformation
Current/Torque Controller	PI controller	Hysteresis controller	Cost function definition
Inverter Control	PWM	Look-up table	Cost function definition

2.4 Vector Control of PMSM

The vector control (VC) technique proposed by Blaschke [2.68] in 1971 was initially developed for induction motor drives with the aim of optimising efficiency and dynamic performance. Since its first proposal, the VC scheme has provided an interesting and challenging innovation field to researchers and engineers. In the VC for PMSMs, the stator current and voltage vectors are directly controlled in the *dq* reference frame. These motor voltage and currents are processed by a series of reference frame transformations to produce voltage control signals for control of the PWM output modulator.

The main feature of vector-controlled PMSM drives is that the direction of the stator flux vector is oriented with respect to the rotor *d*-axis by instantaneous control of the amplitude and instantaneous direction of the stator current vector. In the VC scheme, $i_d=0$, $i_s=i_q$ and $\delta=90°$ are the optimal choice for maximum torque per stator current control of PMSM drives, where δ is the load angle between the rotor *d*-axis and stator current vector i_s. Under these conditions, the voltage and current vectors are illustrated in Fig. 2.15.

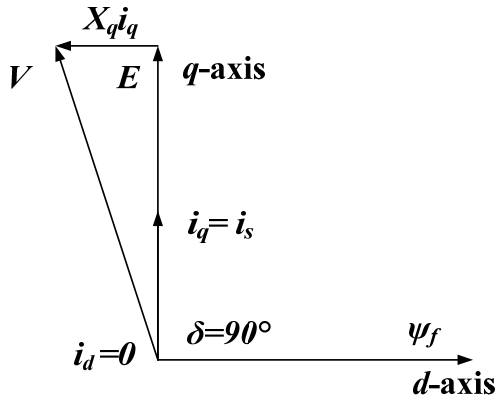

Fig. 2.16 Voltage and current vectors

For a PMSM under sinusoidal excitations, the original voltage equations can be expressed in the stationary reference frame as the following

$$\begin{bmatrix} u_a \\ u_b \\ u_c \end{bmatrix} = R_s \begin{bmatrix} i_a \\ i_b \\ i_c \end{bmatrix} + p \begin{bmatrix} \psi_a \\ \psi_b \\ \psi_c \end{bmatrix} \tag{2.1}$$

where ψ_a, ψ_b and ψ_c are three-phase flux linkages, respectively.

The Park-Clark orthogonal transformation can be expressed in the matrix form as

$$\begin{bmatrix}\psi_d\\ \psi_q\\ \psi_0\end{bmatrix}=\sqrt{\frac{2}{3}}\begin{bmatrix}cos\,\theta_r & \cos\left(\theta_r-\frac{2}{3}\pi\right) & \cos\left(\theta_r+\frac{2}{3}\pi\right)\\ -sin\,\theta_r & -\sin\left(\theta_r-\frac{2}{3}\pi\right) & -\sin\left(\theta_r+\frac{2}{3}\pi\right)\\ \frac{1}{\sqrt{2}} & \frac{1}{\sqrt{2}} & \frac{1}{\sqrt{2}}\end{bmatrix}\begin{bmatrix}\psi_a\\ \psi_b\\ \psi_c\end{bmatrix} \tag{2.2}$$

where θ_r is defined as the angle between two reference frames.

The flux linkages of the *d*- and *q*-axes can be further expressed as

$$\begin{cases}\psi_d = L_d i_d + \psi_f\\ \psi_q = L_q i_q\end{cases} \tag{2.3}$$

where L_d and L_q are constant *d*- and *q*-axes inductance, respectively, and ψ_f is the flux linkage generated by the rotor permanent magnet.

The electrical equations in the rotor reference frame can be rewritten as

$$\begin{cases}u_d = R_s i_d + L_d\frac{di_d}{dt} - L_q i_q\frac{d\theta_r}{dt}\\ u_d = R_s i_q + L_q\frac{di_q}{dt} + (L_d i_d + \psi_f)\frac{d\theta_r}{dt}\end{cases} \tag{2.4}$$

The torque expression after the application of the transformation becomes

$$T_e = \frac{3}{2}p\left(\psi_d i_q - \psi_q i_d\right) = \frac{3}{2}p\left[\psi_f i_q + (L_d - L_q) i_d i_q\right] \tag{2.5}$$

where p is the number of machine pole pairs.

By this transformation, the control of torque and flux are decoupled. The *q*-axis current, in the VC method, is regulated to produce torque while the *d*-axis current is controlling the air-gap flux linkage. In normal operation, the *d*-axis current is set to zero to achieve maximum torque-per-ampere ratio. In the flux weakening control, the *d*-axis current is used to weaken the air-gap flux.

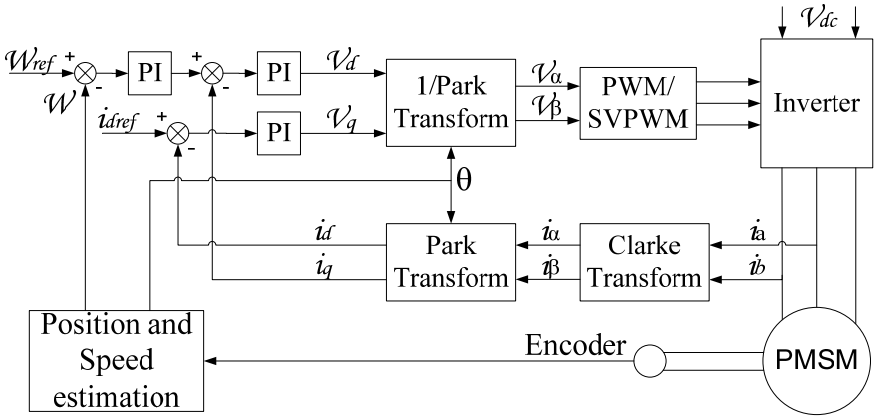

Fig. 2.17 Block diagram of PMSM VC drive system

Fig. 2.16 shows the block diagram of the PMSM FOC drive system. The *d*-axis current is set to zero while the *q*-axis current is controlled by a PI controller with the reference speed. Then the reference voltage vector is sent to a PWM generator to control the inverter.

2.5 Direct Torque Control of PMSM

In the DTC strategy, the flux linkage and torque are calculated in the two-phase stator reference frame, i.e. the *α-β* frame, which is transferred from the three-phase *a-b-c* reference frame by using the Clark transformation. The flux linkage components in *α-β* frame can be calculated as

$$\begin{cases} \psi_\alpha = \int (u_\alpha - R_s i_\alpha) dt \\ \psi_\beta = \int (u_\beta - R_s i_\beta) dt \end{cases} \tag{2.6}$$

The torque observer can then be designed as

$$T_e = \frac{3}{2} \cdot \frac{p}{2} (\psi_\alpha i_\beta - \psi_\beta i_\alpha) \tag{2.7}$$

Fig. 2.17 shows the implementation diagram of the classic DTC scheme for the PMSM drive. Two hysteresis controllers are applied to the flux linkage and torque control loops. The calculated flux linkage is also sent to the switching table to identify the current flux vector position. The switching table for controlling both the amplitude and rotating

direction is shown in Table 2-2, and the inverter voltage vector and spatial sector definitions are illustrated in Fig. 2.18.

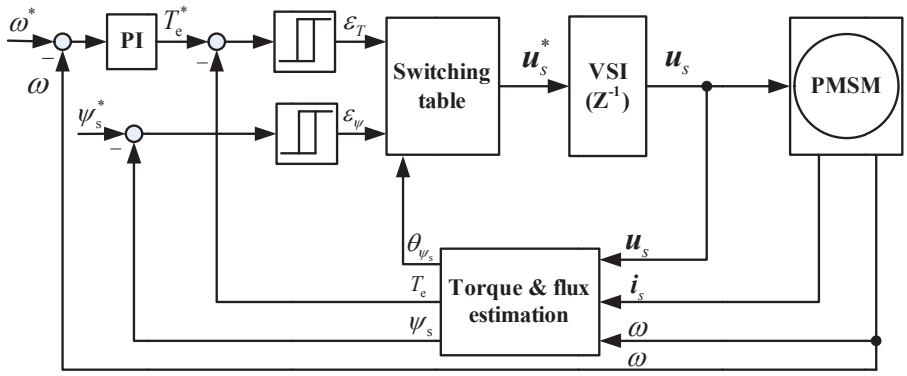

Fig. 2.18 Block diagram of PMSM DTC drive system

Table 2-2 Switching table of classic DTC scheme for PMSM drive

$\boldsymbol{\varphi}$	$\boldsymbol{T_e}$	$\boldsymbol{\theta}$					
		θ_1	θ_2	θ_3	θ_4	θ_5	θ_6
$\Delta\varphi = 1$	$\Delta T_e = 1$	$V_2(110)$	$V_3(010)$	$V_4(011)$	$V_5(001)$	$V_6(101)$	$V_1(100)$
	$\Delta T_e = 0$	$V_6(101)$	$V_1(100)$	$V_2(110)$	$V_3(010)$	$V_4(011)$	$V_5(001)$
$\Delta\varphi = 0$	$\Delta T_e = 1$	$V_3(010)$	$V_4(011)$	$V_5(001)$	$V_6(101)$	$V_1(100)$	$V_2(110)$
	$\Delta T_e = 0$	$V_5(001)$	$V_6(101)$	$V_1(100)$	$V_2(110)$	$V_3(010)$	$V_4(011)$

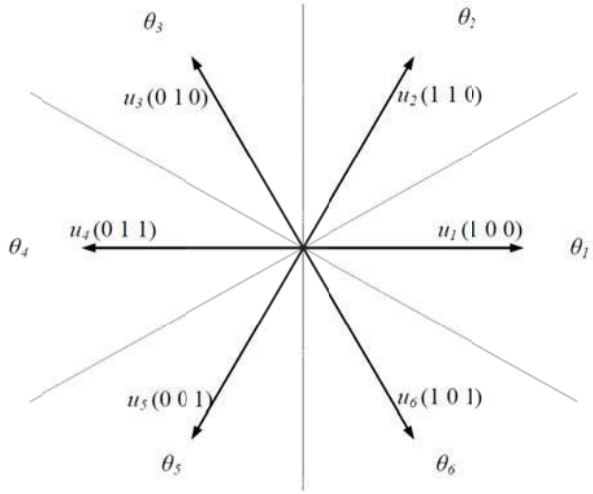

Fig. 2.19 Voltage vector and spatial sector definition

2.6 Conclusion

In this chapter, a thorough literature survey on PM machines and machine drive control methods has been conducted. Firstly, the PM machines definition and classification were introduced. The control strategies were then studied, including the six-step method, vector control and direct torque control. The fundamentals and the state of the art of each strategy were reviewed and reported improvements for each method were then summarized.

REFERENCES

[2.1] M. A. Rahman and Q. Ruifeng, "A permanent magnet hysteresis hybrid synchronous motor for electric vehicles," *Industrial Electronics, IEEE Transactions on*, vol. 44, pp. 46-53, 1997.

[2.2] W. H. Kim, J. N. Bae, et al., "A study on 4-layer hybrid winding layout of the IPMSM and location of the permanent magnets," in *Electromagnetic Field Computation (CEFC), 2010 14th Biennial IEEE Conference on*, 2010, pp. 1-1.

[2.3] P. Pisek, B. Stumberger, *et al*., "Design and FE analysis of a double rotor synchronous PM machine," in *Electromagnetic Field Computation (CEFC), 2010 14th Biennial IEEE Conference on*, 2010, pp. 1-1.

[2.4] Y. Liao, F. Liang, *et al*., "A novel permanent magnet motor with doubly salient structure," in *Industry Applications Society Annual Meeting, 1992., Conference Record of the 1992 IEEE*, 1992, pp. 308-314 vol.1.

[2.5] K. T. Chau, J. Z. Jiang, *et al.*, "A novel stator doubly fed doubly salient permanent magnet brushless machine," *Magnetics, IEEE Transactions on*, vol. 39, pp. 3001-3003, 2003.

[2.6] X. Zhu and M. Cheng, "A novel stator hybrid excited doubly salient permanent magnet brushless machine for electric vehicles," in *Electrical Machines and Systems, 2005. ICEMS 2005. Proceedings of the Eighth International Conference on*, 2005, pp. 412-415 Vol. 1.

[2.7] S. E. Rauch and L. J. Johnson, "Design Principles of Flux-Switch Alternators," Power Apparatus and Systems, Part III. *Transactions of the American Institute of Electrical Engineers*, vol. 74, pp. 1261-1268, 1955.

[2.8] E. Hoang, M. Lecrivain, *et al.*, "A new structure of a switching flux synchronous polyphased machine with hybrid excitation," in *Power Electronics and Applications, 2007 European Conference on*, 2007, pp. 1-8.

[2.9] R. L. Owen, Z. Q. Zhu, *et al.*, "Fault-Tolerant Flux-Switching Permanent Magnet Brushless AC Machines," in *Industry Applications Society Annual Meeting*, 2008. IAS '08. IEEE, 2008, pp. 1-8.

[2.10] Z. Q. Zhu, J. T. Chen, *et al*., "Analysis of a Novel Multi-Tooth Flux-Switching PM Brushless AC Machine for High Torque Direct-Drive Applications," *Magnetics, IEEE Transactions on*, vol. 44, pp. 4313-4316, 2008.

[2.11] A. Zulu, B. Mecrow, *et al*., "A wound-field three-phase flux-switching synchronous motor with all excitation sources on the stator," in *Energy Conversion Congress and Exposition, 2009*. ECCE 2009. IEEE, 2009, pp. 1502-1509.

[2.12] W. Xu; J. Zhu; Y. Zhang; Y. Guo and G. Lei; , "New Axial Laminated-Structure Flux-Switching Permanent Magnet Machine With 6/7 Poles," *Magnetics, IEEE Transactions on* , vol.47, no.10, pp.2823-2826, Oct. 2011

[2.13] P. C. Krause, R. R. Nucera, R. J. Krefta, and O. Wasynczuk, "Analysis of a Permanent Magnet Synchronous Machine Supplied from a 180° Inverter with Phase Control," Energy Conversion, IEEE Transactions on, vol. EC-2, no. 3, pp. 423-431, 1987.

[2.14] N. Sato, "A Study of Commutatorless Motor," Elec. Eng. Jap., vol. 84, pp. 42-51, 1964.

[2.15] A. H. Hoffmann, "Brushless Synchronous Motors for Large Industrial Drives," Industry and General Applications, IEEE Transactions on, vol. IGA-5, no. 2, pp. 158-162, 1969.

[2.16] P. A. Studer, "Development of Brushless DC Motors for Space Applications," NASA TN-D-2108, Feb. 1964.

[2.17] S. Murugesan, "An Overview of Electric Motors for Space Applications," Industrial Electronics and Control Instrumentation, IEEE Transactions on, vol. IECI-28, no. 4, pp. 260-265, 1981.

[2.18] T. Kenjo and S. Nagamori, Permanent-Magnet and Brushless DC Motors. New York: Oxford University Press, 1985.

[2.19] S. D. Sudhoff and P. C. Krause, "Average-value Model of the Brushless DC 120° inverter system," Energy Conversion, IEEE Transactions on, vol. 5, no. 3, pp. 553-557, 1990.

[2.20] H. Le-Huy, R. Perret, and R. Feuillet, "Minimization of Torque Ripple in Brushless DC Motor Drives," Industry Applications, IEEE Transactions on, vol. IA-22, no. 4, pp. 748-755, 1986.

[2.21] F. Blaschke, "Das Prizip der Feldorientierung, die Grundlage far die TRANSVEKTOR-Regerung von Drehfeldmaschinen," Siemens-Zeitschrift, vol. 45, pp. 757-760, Oct, 1971.

[2.22] R. H. Park, "Definition of an Ideal Synchronous Machine and Formula for the Armature Flux Linkages," General Electric Review, vol. 31, p. 332, 1928.

[2.23] R. H. Park, "Two-Reaction Theory of Synchronous Machines Generalized Method of Analysis: Part I," American Institute of Electrical Engineers, Transactions of the, vol. 48, pp. 716-727, 1929.

[2.24] G. Pfaff, A. Weschta, *et al*., "Design and Experimental Results of a Brushless AC Servo Drive," Industry Applications, IEEE Transactions on, vol. IA-20, pp. 814-821, 1984.

[2.25] M.F Rahman, T.S. Low and L.B. Wee, “Development of a digitally controlled permanent magnet brushless DC drive system”, *Proceedings of the IEEE Conference on Applied Control*, 1986, pp. 283-288.

[2.26] B.K. Bose, and P.M. Szczesny, “A microcomputer-based control and simulation of an advanced IPM synchronous machine dreive system for

electric vehicle propulsion", *IEEE Transactions on Industrial Electronics*, Vol. 35, No. 4, Nov. 1988, pp. 547-559.

[2.27] N. Matsui and H. Ohashi, " DSP-based adaptive control of a brushless motor", *Conference Record of the 1988 IEEE IAS Annual Meeting*, Vol. 1, Oct. 2-7, 1988, pp. 375-380.

[2.28] C. Allen and P. Pillay, "TMS320 design for vector and current control of AC motor drives", *Electronics Letters*, Vol. 28, No. 23, Nov. 5, 1992, pp. 2188-2190.

[2.29] J. Boldea and A. Nasar, "Vector control of AC machines', CRC Press, ISBN/ISSN 0849344085, 1992.

[2.30] C. Cecati, F. Parasiliti, and M. Tursini, "Multicomputer-based speed control of permanent magnet synchronous motor drives', *Proceedings of the 1992 International Conference on Iddustrial Electronics, Control, Instrumentation, and Automation (Power Electronics and Motion Control)*, Vol. 1, Nov. 9-13, 1992. Pp. 101-106.

[2.31] N. Bennett, J. Wang, D.W. Shimmin, and K.J. Binns, "A new vector control scheme for an adjustable sped AC drive system utlising a high field permanent magnet synchronous machine", *Proceedings of the Sixth International Conference on Electrical Machines and Drives*, (Conf. Publ. No. 376), Sep. 8-10, 1993, pp. 121-126.

[2.32] Bolognani, S. and Zigliotto, M., "A space-vector approach to the analysis and design of three-phase current controllers," *Industrial Electronics, 2002. ISIE 2002. Proceedings of the 2002 IEEE International Symposium on* , vol.2, no., pp. 645- 650 vol.2, 2002

[2.33] Takahashi and T. Noguchi, "A New Quick-Response and High-Efficiency Control Strategy of an Induction Motor," *Industry Applications, IEEE Transactions on*, vol. IA-22, pp. 820-827, 1986.

[2.34] U. Baader, M. Depenbrock, *et al*., "Direct self control (DSC) of inverter-fed induction machine: a basis for speed control without speed measurement," *Industry Applications, IEEE Transactions on*, vol. 28, pp. 581-588, 1992.

[2.35] C. French and P. Acarnley, "Direct torque control of permanent magnet drives," Industry Applications, IEEE Transactions on, vol. 32, pp. 1080-1088, 1996.

[2.36] M. F. Rahman and L. Zhong, "Comparison of torque responses of the interior permanent magnet motor under PWM current and direct torque controls," in Industrial Electronics Society, 1999. IECON '99 Proceedings. The 25th Annual Conference of the IEEE, 1999, pp. 1464-1470 vol.3.

[2.37] P. Vas, "Sensorless Vector and Direct Torque Control," Oxford, UK: Oxford University Press, 1998.

[2.38] M. P. K. a. H. Tunia, "Automatic Control of Converter-fed Drives," Amsterdam, the Netherlands: Elsevier, 1994.

[2.39] A. Bouafia, F. Krim, *et al*., "Fuzzy-Logic-Based Switching State Selection for Direct Power Control of Three-Phase PWM Rectifier," *Industrial Electronics, IEEE Transactions on*, vol. 56, pp. 1984-1992, 2009.

[2.40] X. Yang and W. Oghanna, "Fuzzy direct torque control of induction motor with stator flux estimation compensation," in *Industrial Electronics, Control and Instrumentation*, 1997. IECON 97. 23rd International Conference on, 1997, pp. 505-510 vol.2.

[2.41] S. A. Mir, M. E. Elbuluk, *et al*., "Fuzzy implementation of direct self-control of induction machines," *Industry Applications, IEEE Transactions on*, vol. 30, pp. 729-735, 1994.

[2.42] L. A. Cabrera, M. E. Elbuluk, *et al*., "Learning techniques to train neural networks as a state selector for inverter-fed induction machines using direct torque control," *Power Electronics, IEEE Transactions on*, vol. 12, pp. 788-799, 1997.

[2.43] G. Escobar, A. M. Stankovic, *et al*., "A family of switching control strategies for the reduction of torque ripple in DTC," *Control Systems Technology, IEEE Transactions on*, vol. 11, pp. 933-939, 2003.

[2.44] R. Ortega, N. Barabanov, *et al*., "Direct torque control of induction motors:

stability analysis and performance improvement," *Automatic Control, IEEE Transactions on*, vol. 46, pp. 1209-1222, 2001.

[2.45] M. A. M. Prats, G. Escobar, *et al*., "A switching control strategy based on output regulation subspaces for the control of induction motors using a three-level inverter," *Power Electronics Letters*, IEEE, vol. 1, pp. 29-32, 2003.

[2.46] K. B. Lee, J. H. Song, *et al*., "Improvement of low-speed operation performance of DTC for three-level inverter-fed induction motors," *Industrial Electronics, IEEE Transactions on*, vol. 48, pp. 1006-1014, 2001.

[2.47] Jun-Koo and S. Seung-Ki, "New direct torque control of induction motor for minimum torque ripple and constant switching frequency," *Industry Applications, IEEE Transactions on*, vol. 35, pp. 1076-1082, 1999.

[2.48] L. Romeral, A. Arias, *et al*., "Novel direct torque control (DTC) scheme with fuzzy adaptive torque-ripple reduction," *Industrial Electronics, IEEE Transactions on*, vol. 50, pp. 487-492, 2003.

[2.49] V. Ambrozic, G. S. Buja, *et al*., "Band-constrained technique for direct torque control of induction motor," *Industrial Electronics, IEEE Transactions on*, vol. 51, pp. 776-784, 2004.

[2.50] C. Lascu and A. M. Trzynadlowski, "Combining the principles of sliding mode, direct torque control, and space vector modulation in a high-performance sensorless AC drive," in *Industry Applications Conference*, 2002. 37th IAS Annual Meeting. Conference Record of the, 2002, pp. 2073-2079 vol.3.

[2.51] Yen-Shin and C. Jian-Ho, "A new approach to direct torque control of induction motor drives for constant inverter switching frequency and torque ripple reduction," *Energy Conversion, IEEE Transaction on*, vol. 16, pp. 220-227, 2001.

[2.52] R. K. A. Linder, R. Kennel, and P. Stolze, "Model-Based Predictive Control of Electric Drives," Germany: Cuvillier Verlag, 2010.

[2.53] D. W. Clarke, C. Mohtadi, and P. S. Tuffs, "Generalized predictive control – part I. the basic algorithm," *Automatica*, vol. 23, pp.137–148, 1987.

[2.54] C. E. Garcia, D. M. Prett, and M. Morari, "Model Predictive Control: Theory and practice – a survey," *Automatica*, vol. 25, pp. 335–348, 1989

[2.55] P. Cortes, M. Kazmierkowski, R. Kennel, D. Quevedo, and J. Rodriguez, "Predictive control in power electronics and drives," *IEEE Trans. Ind. Electron.*, vol. 55, no. 12, pp. 4312 –4324, Dec. 2008.

[2.56] A. Beccuti, S. Mariethoz, S. Cliquennois, S. Wang, and M. Morari, "Explicit model predictive control of dc-dc switched-mode power supplies with extended kalman filtering," *IEEE Trans. Ind. Electron*., vol. 56, no. 6, pp. 1864 –1874, June 2009.

[2.57] S. Kouro, P. Cortes, R. Vargas, U. Ammann, and J. Rodriguez, "Model predictive control—a simple and powerful method to control power converters," IEEE Trans. Ind. Electron., vol. 56, no. 6, pp. 1826 –1838, June 2009.

[2.58] J. Rodriguez, R. M. Kennel, J. R. Espinoza, M. Trincado, C. A. Silva, and C. A. Rojas, "High-performance control strategies for electrical drives: An experimental assessment," IEEE Trans. Ind. Electron., vol. 59, no. 2, pp. 812–820, 2012.

[2.59] T. Geyer, G. Papafotiou, and M. Morari, "Model predictive direct torque control -part I: Concept, algorithm, and analysis," IEEE Trans. Ind. Electron., vol. 56, no. 6, pp. 1894 –1905, june 2009.

[2.60] Y. Zhang, J. Zhu, and W. Xu, "Predictive torque control of permanent magnet synchronous motor drive with reduced switching frequency," in Proc. Int Electrical Machines and Systems (ICEMS) Conf, 2010, pp. 798–803.

[2.61] P. Cortes, J. Rodriguez, C. Silva, and A. Flores, "Delay compensation in model predictive current control of a three-phase inverter," IEEE Trans. Ind. Electron., vol. 59, no. 2, pp. 1323–1325, 2012.

[2.62] H. Miranda, P. Cortes, J. Yuz, and J. Rodriguez, "Predictive torque control of induction machines based on state-space models," IEEE Trans. Ind. Electron.,

vol. 56, no. 6, pp. 1916 –1924, June 2009.

[2.63] R. Vargas, P. Cortes, U. Ammann, J. Rodriguez, and J. Pontt, "Predictive control of a three-phase neutral-point-clamped inverter," IEEE Trans. Ind. Electron., vol. 54, no. 5, pp. 2697 –2705, Oct. 2007.

[2.64] G. Papafotiou, J. Kley, K. Papadopoulos, P. Bohren, and M. Morari, "Model predictive direct torque control-part II: Implementation and experimental evaluation," *IEEE Trans. Ind. Electron*., vol. 56, no. 6, pp. 1906 –1915, June 2009.

[2.65] S. Kouro, P. Cortes*, et al.*, "Model Predictive Control: A Simple and Powerful Method to Control Power Converters," *Industrial Electronics, IEEE Transactions on,* vol. 56, pp. 1826-1838, 2009.

[2.66] P. Cortes, S. Kouro*, et al.*, "Guidelines for weighting factors design in Model Predictive Control of power converters and drives," in *Industrial Technology, 2009. ICIT 2009. IEEE International Conference on*, 2009, pp. 1-7.

[2.67] Y. Zhang, J. Zhu*, et al.*, "Predictive torque control of permanent magnet synchronous motor drive with reduced switching frequency," in *Electrical Machines and Systems (ICEMS), 2010 International Conference on*, 2010, pp. 798-803.

[2.68] F. Blaschke, "Das Prizip der Feldorientierung, die Grundlage far die TRANSVEKTOR-Regerung von Drehfeldmaschinen," *Siemens-Zeitschrift,* vol. 45, pp. 757-760, Oct. 1971.

CHAPTER 3

MODEL PREDICTIVE CONTROL OF PERMANENT MAGNET SYNCHRONOUS MACHINES

3.1 Introduction

The field oriented control (FOC) and direct torque control (DTC) are the two most popular control approaches for the control of permanent magnet synchronous machines (PMSMs) [3.1]-[3.5]. In FOC, the inverter plus pulse width modulation (PWM) is considered as a gain with delay in the controller design [3.6]. Although good performance can be achieved by FOC, it requires synchronous rotary transformation and the dynamic response is limited by the bandwidth of the inner current loop. Furthermore, the cascaded structure of FOC requires a lot of tuning to achieve good a performance over the whole operating range. DTC eliminates the use of PWM and takes the discrete nature of the inverter into account. By directly manipulating the final output voltage vector without the need for inner current loops, the inherent delay caused by current loops is removed and a quick dynamic response is achieved [3.7]-[3.9]. Since all calculations are implemented in stationary coordinate, the structure of DTC is simple. Despite the above merits, the conventional switching-table-based DTC (ST-DTC) also presents some notable drawbacks, such as high torque and flux ripples, variable switching frequency and excessive acoustic noise.

Recently, the model predictive control (MPC) has emerged as an alternative high performance control strategy and is drawing wide attention in both academic and industry communities [3.10]-[3.20]. In fact, MPC has been known for several decades and the first paper regarding the application of MPC in power converters appeared in the 1980s [3.10]. Due to the high computational burden, MPC was mainly applied in the chemical process industry. The development of powerful digital signal processors (DSPs) and micro-controllers has it become possible to use MPC in the area of power

electronics and drives.

3.2 Model of PMSMs

The mathematical model of a machine, in terms of controller design and performance analysis, is usually one or several equations, in which the relationship between the machine input and output variables is analytically expressed, most of the time, by using the machine parameters. This relationship could be generally classified as the electrical and the mechanical processes in the device [3.21].

The conventional PMSM model described in this sector was oriented for PMSMs with sinusoidal back *emf*, which is widely used for development of the machine drive strategies. It was firstly derived in a stationary reference frame and then transformed to a rotating reference frame to achieve field control. Linear assumptions were made to simplify the magnetic properties in the model and the nonlinear saturation effect is neglected.

For a PMSM, it is assumed that the three-phase stator windings are symmetrical and each phase has the same parameter. The electrical model of the device is similar to that of electrically excited synchronous machines (SM) and it is normally expressed by using the per phase voltage equation, in which the phase current is a function of the input voltage signal and the machine electrical parameters, i.e. resistance and inductance. Fig. 3-1 shows the per phase equivalent circuit of traditional SMs.

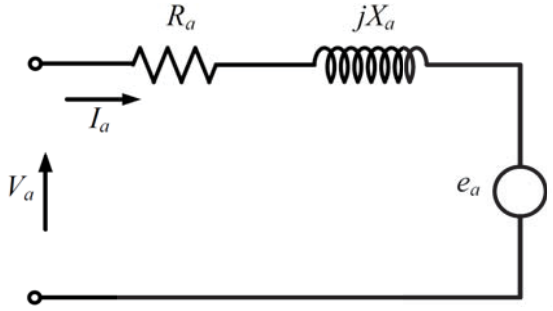

Fig. 3.1 Per phase equivalent circuit diagram for SM

It is different from the electrically excited SM in that the *emf* in PMSM is induced by the permanent magnets fixed on the rotor and it is related to the magnet rotating speed. Therefore, the per phase flux linkage is always utilized to express the machine electrical equation. The voltage equation for the stator phase can be expressed as

$$u_s = R_s i_s + \frac{d\psi_s}{dt} \tag{3.1}$$

where u_s is the stator phase voltage, i_s the stator phase current, R_s the stator resistance, and ψ_s the phase flux linkage.

By assuming the flux linkage is contributed by both the three-phase stator currents and the rotating magnet, the PMSM model in stationary reference frame can be derived as

$$\begin{bmatrix} u_a \\ u_b \\ u_c \end{bmatrix} = R_s \begin{bmatrix} i_a \\ i_b \\ i_c \end{bmatrix} + \begin{bmatrix} L_{aa} & L_{ab} & L_{ac} \\ L_{ba} & L_{bb} & L_{bc} \\ L_{ca} & L_{bc} & L_{cc} \end{bmatrix} \frac{d}{dt} \begin{bmatrix} i_a \\ i_b \\ i_c \end{bmatrix} + \frac{\partial}{\partial \theta} \begin{bmatrix} \psi_a \\ \psi_b \\ \psi_c \end{bmatrix} \omega_e \tag{3.2}$$

where u_a, u_b and u_c are the three-phase voltage, i_a, i_b and i_c the three-phase current, ψ_a, ψ_b and ψ_c the three-phase flux linkage, and $\begin{bmatrix} L_{aa} & L_{ab} & L_{ac} \\ L_{ba} & L_{bb} & L_{bc} \\ L_{ca} & L_{bc} & L_{cc} \end{bmatrix}$ is the inductance matrix, including both the self- and mutual-inductances.

The last part in (3.2) is usually defined as the back *emf* of the machine and it can be found that the *emf* values are proportional to the rotating speed.

In order to decouple the control of flux and torque, the two-phase orthogonal reference frame in stationary and rotation are developed (α-β and *d*-*q* reference frames). Fig. 3.2 shows the spatial vector relationship between these reference-frames, where θ is defined as the angle between the stationary and rotating frames.

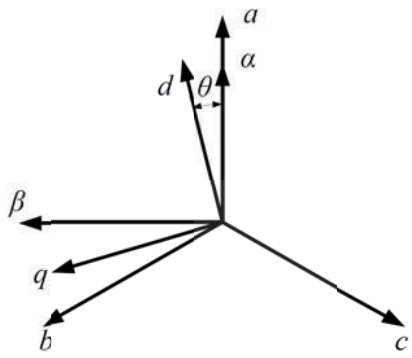

Fig. 3.2 Relationship between different reference frames

The transformations applied to convert the variables between these reference-frames, which are Park and Clark transforms [3.22], are defined as

$$\begin{bmatrix}\psi_a\\ \psi_\beta\end{bmatrix} = \sqrt{\frac{2}{3}}\begin{bmatrix}1 & -\frac{1}{2} & -\frac{1}{2}\\ 0 & \frac{\sqrt{3}}{2} & -\frac{\sqrt{3}}{2}\end{bmatrix}\begin{bmatrix}\psi_a\\ \psi_b\\ \psi_c\end{bmatrix} \tag{3.3}$$

$$\begin{bmatrix}\psi_d\\ \psi_q\end{bmatrix} = \sqrt{\frac{2}{3}}\begin{bmatrix}\cos\theta & \cos\left(\theta-\frac{2}{3}\pi\right) & \cos\left(\theta+\frac{2}{3}\pi\right)\\ -\sin\theta & -\sin\left(\theta-\frac{2}{3}\pi\right) & -\sin\left(\theta+\frac{2}{3}\pi\right)\end{bmatrix}\begin{bmatrix}\psi_a\\ \psi_b\\ \psi_c\end{bmatrix} \tag{3.4}$$

Therefore, the machine electrical variables in stationary form could be expressed by using *d-q* reference frame variables. The voltage, current and flux linkage of phase *a* could be expressed as

$$\begin{cases} i_a = \sqrt{\frac{2}{3}}\left(i_d\cos\theta - i_q\sin\theta\right)\\ u_a = \sqrt{\frac{2}{3}}\left(u_d\cos\theta - u_q\sin\theta\right)\\ \psi_a = \sqrt{\frac{2}{3}}\left(\psi_d\cos\theta - \psi_q\sin\theta\right)\end{cases} \tag{3.5}$$

By substituting (3.5) into (3.1), a simplified expression can be obtained.

$$\left(\frac{d\psi_d}{dt} - \psi_q\frac{d\theta}{dt} + R_s i_d - u_d\right)\cos\theta + \left(-\frac{d\psi_q}{dt} - \psi_d\frac{d\theta}{dt} - R_s i_q + u_q\right)\sin\theta = 0 \tag{3.6}$$

This equation should be satisfied for any value of θ. Therefore, the following *d*-*q* axes voltage equations are always valid.

$$\begin{cases} u_d = R_s i_d + \frac{d\psi_d}{dt} - \psi_q \frac{d\theta}{dt} \\ u_q = R_s i_q + \frac{d\psi_q}{dt} + \psi_d \frac{d\theta}{dt} \end{cases} \tag{3.7}$$

In the conventional machine model, the *d*- and *q*-axes flux linkages are usually defined as

$$\begin{cases} \psi_d = L_d i_d + \psi_f \\ \psi_q = L_q i_q \end{cases} \tag{3.8}$$

where L_d and L_q are the inductance of *d*- and *q*-axes, respectively, and ψ_f is the flux linkage generated by the permanent magnet.

It can be found that the *q*-axis flux linkage is produced by the *q*-axis stator current only. Along the *d*-axis, the flux linkage is produced by both the *d*-axis stator current and the permanent magnet on the rotor. The electrical model in (3.7) can be rewritten as (3.9) and the equivalent circuit in *d*-*q* reference frame is shown in Fig. 3.3.

$$\begin{cases} u_d = R_s i_d + L_d \frac{di_d}{dt} - \omega L_q i_q \\ u_q = R_s i_q + L_q \frac{di_q}{dt} + \omega_e L_d i_d + \omega_e \psi_f \end{cases} \tag{3.9}$$

When the machine operates as a motor, the total input power of the device can be expressed by using three-phase terminal voltages and currents, which can also be transferred to the *d*-*q* rotating reference frame.

$$P_{in} = u_a i_a + u_b i_b + u_c i_c \tag{3.10}$$

$$P_{in} = \frac{3}{2}\left(u_d i_d + u_q i_q\right) \tag{3.11}$$

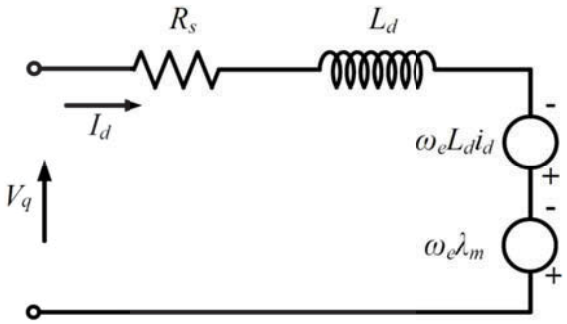

(a)

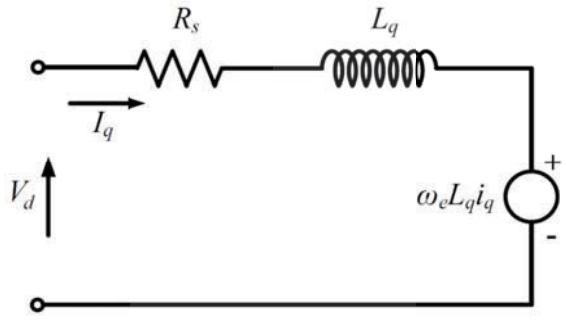

(b)

Fig. 3.3 PMSM equivalent circuits in (a) *d*-, and (b) *q*-axes

By substituting (3.9) in (3.11), the input total power expression can be derived as a composite function of the *d*-*q* axis currents.

$$P_{in} = \frac{3}{2}\left[R_s\left(i_d^2 + i_q^2\right) + i_q \frac{d\psi_q}{dt} + i_d \frac{d\psi_d}{dt} + \omega_e\left(\psi_q i_q - \psi_d i_d\right)\right] \tag{3.12}$$

By eliminating the terms of the copper losses and the variation of magnetic energy, the electromechanical power becomes

$$P_{em} = \frac{3}{2}\frac{p\omega_r}{2}\left(\psi_q i_q - \psi_d i_d\right) \tag{3.13}$$

where ω_r is the rotor mechanical speed converted from the electrical speed

$$\omega_e = \frac{p}{2}\omega_r \tag{3.14}$$

and p is the number of poles

For the mechanical equation of the model, we have

$$T_e = T_L + J\frac{d\omega_r}{dt} + F \cdot \omega_r \tag{3.15}$$

where T_L is the load torque applied on the rotor shaft, J the inertia of the motor, and F the shaft friction coefficient.

By dividing the electromagnetic power by the rotor mechanical speed, the electromagnetic torque expression can be obtained. In this model, the damping effects are ignored because there are no damping windings in the PMSMs. The electromagnetic torque is expressed as

$$T_e = \frac{3}{2}p\left(\psi_d i_q - \psi_q i_d\right) \tag{3.16}$$

By substituting (3.8) into (3.16)

$$T_e = \frac{3}{2}p\left[\psi_f i_q + \left(L_d - L_q\right) i_d i_q\right]$$

$$= \frac{3p|\psi_s|}{4L_d L_q}\left[2\psi_f L_q \sin\delta + |\psi_s|\left(L_d - L_q\right)\sin 2\delta\right] \tag{3.17}$$

where δ is the electrical angle between stator- and rotor-flux vectors.

As shown, the electromagnetic torque is composed of two parts: the permanent-magnet torque and the reluctance torque caused by the rotor saliency.

For a surface-mounted PMSM without saliency, the *d*- and *q*-axis inductances are equal to the synchronous inductance, i.e. *Ld* = *Lq* = *Ls*. The torque does not include the reluctance torque and can be simplified as

$$T_e = \frac{3}{2} p \psi_f i_q = \frac{3}{2} p \frac{\psi_f |\psi_s|}{L_s} \sin \delta \tag{3.18}$$

The voltage and stator-flux equations can also be simplified similarly.

In the stationary frame (the components indicated by $\alpha\beta$), they can be expressed using a complex vector as

$$u_s = R_s i_s + \frac{d\psi_s}{dt} \tag{3.19}$$

$$\psi_s = L_s i_s + \psi_r \tag{3.20}$$

where $\psi_r = \psi_f e^{j\theta_r}$ and the torque in the stationary frame is expressed as

$$T_e = \frac{3}{2} p \psi_s \times i_s = \frac{3}{2} p \left(\psi_{s\alpha} i_{s\beta} - \psi_{s\beta} i_{s\alpha} \right) \tag{3.21}$$

3.3 Model Predictive Control of PMSM

The principle of model predictive control (MPC) was introduced for industrial control applications in the 1970s after the publication of this strategy in the 1960s. The MPC requires great computational effort and it has been formerly limited to slowly varying systems, as chemical processes. With the availability of inexpensive high computing power microcomputers and modern digital control techniques, MPC is able to be applied to the electrical drive system.

Different from the employment of hysteresis comparators and the switching table in conventional DTC, the principle of vector selection in MPC is based on evaluating a defined cost function. The selected voltage vector from the conventional switching table in DTC may not necessarily be the best one for the purposes of torque and flux ripple reduction. Since there are limited discrete voltage vectors in the two-level inverter-fed

PMSM drives, it is possible to evaluate the effects of each voltage vector and select the one minimizing the cost function.

The key technology of MPC lies in the definition of the cost function, which is related to the control objectives. The greatest concern of PMSM drive applications are the torque and stator flux, and thus, the cost function is defined in such a way that both the torque and stator flux at the end of control period are as close as possible to the reference values. In this thesis, the cost function is defined as

$$\begin{aligned} &min.\ \ G = |T_e^* - T_e^{k+1}| + k_1\left||\psi_s^*| - |\psi_s^{k+1}|\right| \\ &s.t. \quad\ u_s^k \in \{V_0, V_1, \cdots V_6, V_7\} \end{aligned} \tag{3.22}$$

where T_e^* and ψ_s^* are the reference values of torque and flux, T_e^{k+1} and ψ_s^{k+1} the predicted values of torque and flux, respectively, and k_1 is the weighting factor. Because the physical natures of electromagnetic torque and stator flux are different, the weighting factor k_1 is introduced to unify these terms. In this paper, k_1 is selected to be T_n / ψ_n, where T_n and ψ_n are the rated values of torque and stator flux, respectively. It should be noted that when a null vector is selected, the specific state (V_0 or V_7) will be determined based on the principle of minimal switching commutations, which is related to the switching states of the old voltage vector.

Equation (3.9) from last section is copied here

$$\begin{cases} u_d = R_s i_d + L_d \frac{di_d}{dt} - \omega L_q i_q \\ u_q = R_s i_q + L_q \frac{di_q}{dt} + \omega_e L_d i_d + \omega_e \psi_f \end{cases} \tag{3.9}$$

From (3.9), the stator current in the *d-q* frame can be expressed in the form of state space equations as

$$\begin{cases} \frac{di_d}{dt} = \frac{-R_s i_d + \omega L_q i_q + u_d}{L_d} \\ \frac{di_q}{dt} = \frac{-\omega L_d i_d - R_s i_q + u_q - \omega \psi_f}{L_q} \end{cases} \tag{3.23}$$

The stator current in *d-q* frame at (*k+1*)*th* instant can be obtained by discretizing (3.23) as

$$\begin{cases} i_d^{k+1} = i_d^k + \frac{1}{L_d} \left(- R_s i_d^k + \omega^k L_q i_q^k + u_d^k \right) T_s \\ i_q^{k+1} = i_q^k + \frac{1}{L_q} \left(- \omega^k L_d i_d^k - R_s i_q^k + u_q^k - \omega^k \psi_f \right) T_s \end{cases} \tag{3.24}$$

With the knowledge of future stator current, both torque and flux at the (*k+1*)*th* instant can be calculated by (3.8) and (3.16).

The block diagram of MPC is shown in Fig. 3.4. The inputs of the system are the reference and estimated values of torque and flux. By evaluating effects of each voltage vector when applied to the machine, the voltage vector which minimizes the difference between reference value and predicted value is first selected, and then it is generated by the inverter.

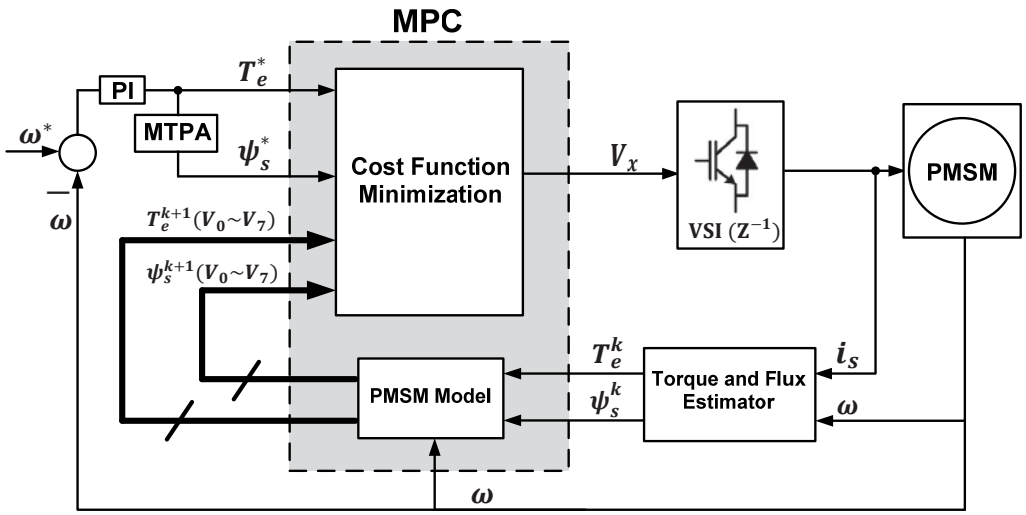

Fig. 3.4 Block diagram of MPC drive system

3.3.1 One-step delay compensation

The cost function in (3.22) assumes that all calculations and judgments are implemented at the *kth* instant and the selected vector will be applied immediately. However, in practical digital implementation, this assumption is not true and the applied voltage vector is not applied until the (*k+1*)*th* instant.

In other words, for the duration between the *kth* and (*k+1*)*th* instants, the applied rotor voltage vector u_s^k has been decided by the value in the (*k—1*)*th* instant and the evolutions of ψ_s and T_e for this duration are uncontrollable. What is left to be decided is actually the stator voltage vector u_s^{k+1}, which is applied at the beginning of the (*k+1*)*th* instant. To eliminate this one step delay, the variables of ψ_s^{k+2} and T_e^{k+2} should be used rather than ψ_s^{k+1} and T_e^{k+1} for the evaluation of the cost function in (3.22). This fact is clearly illustrated in Fig. 3-5, where *x* indicates the state variables of a dynamic system and *u* is the input to be decided. For PMSM, *x* represents torque or stator flux value.

To eliminate the one-step delay in digital implementation, the cost function in (3.22) should be changed to (3.25) as shown below

$$\begin{aligned} &min.\ \ G = |T_e^* - T_e^{k+2}| + k_1\left||\psi_s^*| - |\psi_s^{k+2}|\right| \\ &s.t. \quad u_s^k \in \{V_0, V_1, \cdots V_6, V_7\} \end{aligned} \tag{3.25}$$

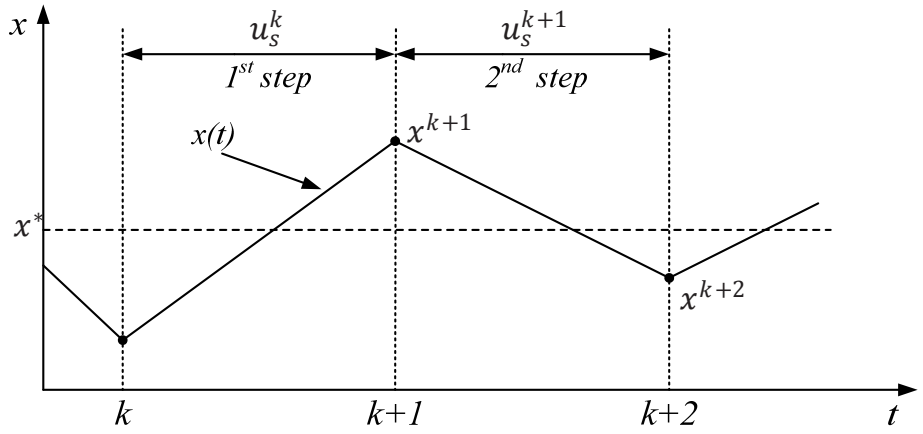

Fig. 3.5 One-step delay in digital control systems

Obtaining $T_e^{k+2}$and ψ_s^{k+2} in (3.25) requires a two-step prediction. The variables at the (*k+1*)*th* instant have been obtained using (3.24), (3.8) and (3.16), where u_s^k is a known variable. To obtain the best voltage vector minimizing the cost function in (3.25), each possible configuration for u_s^{k+1} will be evaluated to obtain the value at the (*k+2*)*th* instant. The predictive model is the same as in (3.24), (3.8) and (3.16), except that the variables in the right side are replaced by the value at the (*k+1*)*th* instant.

3.3.2 Linear multiple horizon prediction

A linear multiple horizon prediction formula is introduced in this section. This formula incorporates two formulas. The first one is the same as in (3.22). The linear multiple horizon prediction formula, which is multiplied by factor *A*, considers the errors in the (*k* + *N*)th instant (*N* > *1*). Different from the model-based predictions for T_e^{k+1} and ψ_s^{k+1}, the stator flux and torque at the (*k*+*N*)th instant are predicted from the value at the *kth* and (*k*+*1*)*th* instants using linear extrapolations, which are expressed as

$$T_e^{k+N} = T_e^k + (N-1)(T_e^{k+1} - T_e^k) \tag{3.26}$$

$$|\psi_s^{k+N}| = \left||\psi_s^k| + (N-1)\left||\psi_s^{k+1}| - |\psi_s^k|\right|\right| \tag{3.27}$$

The expression of the proposed cost function is

$$\begin{aligned} min.\ \ G &= |T_e^* - T_e^{k+1}| + k_1\left||\psi_s^*| - |\psi_s^{k+1}|\right| \\ &\quad + A\left(|T_e^* - T_e^{k+N}| + k_1\left||\psi_s^*| - |\psi_s^{k+N}|\right|\right) \\ s.t. \quad & u_s^k \in \{V_0, V_1, \cdots V_6, V_7\} \end{aligned} \tag{3.28}$$

The introduction of the linear multiple horizon prediction formula can improve the performance of the drive system and reduce the switching frequency. This phenomenon will be deeply investigated in the following sections.

When the one-step delay compensation is taken into account, (3.28) should be changed into

$$min.\ G = |T_e^* - T_e^{k+2}| + k_1\left||\psi_s^*| - |\psi_s^{k+2}|\right| + A\left(|T_e^* - T_e^{k+N}| + k_1\left||\psi_s^*| - |\psi_s^{k+N}|\right|\right)$$

$$s.t. \quad u_s^k \in \{V_0, V_1, \cdots V_6, V_7\} \tag{3.29}$$

3.4 Numerical Simulation of DTC and MPC

In this section, the simulation tests of DTC and MPC are carried out by using Matlab/Simulink. The parameters of the motor are listed in Table 3-1. The sampling frequency of both methods is set to 5 kHz. The values of the control parameters are $k_1 = 25.4,\ \mathrm{A} = 0.1,\ \mathrm{N} = 10$

Table 3-1 Motor parameters

Number of pole pairs	p	3
Permanent magnet flux	ψ_f	0.1057 Wb
Stator resistance	R_s	1.8 Ω
d-axis and *q*-axis inductance	$L_d,\ L_q$	15 mH
Rated torque	T_N	4.5 Nm
DC bus voltage	U_{dc}	200 V

3.4.1 Combined load test at 500 rpm

This simulation test combines start-up, steady-state and external load tests. The motor starts up from 0s with a reference speed (500 rpm, 1000 rpm, 1500 rpm and 2000 rpm). After reaching the reference speed, the motor maintains the speed for at least 0.2s and an external load is applied at 0.3s. From top to bottom, the curves are the stator current, stator flux, torque, motor speed and switching frequency, respectively.

The recorded data from 0.1s to 0.3s is picked to calculate the torque and flux ripples (obtained by standard deviations). The torque and flux ripples of these control methods will be summarized in tables in Section 3.6. A segment (three periods) of the stator current of phase A is used to calculate the total harmonic distortion (THD) and current harmonic spectrum.

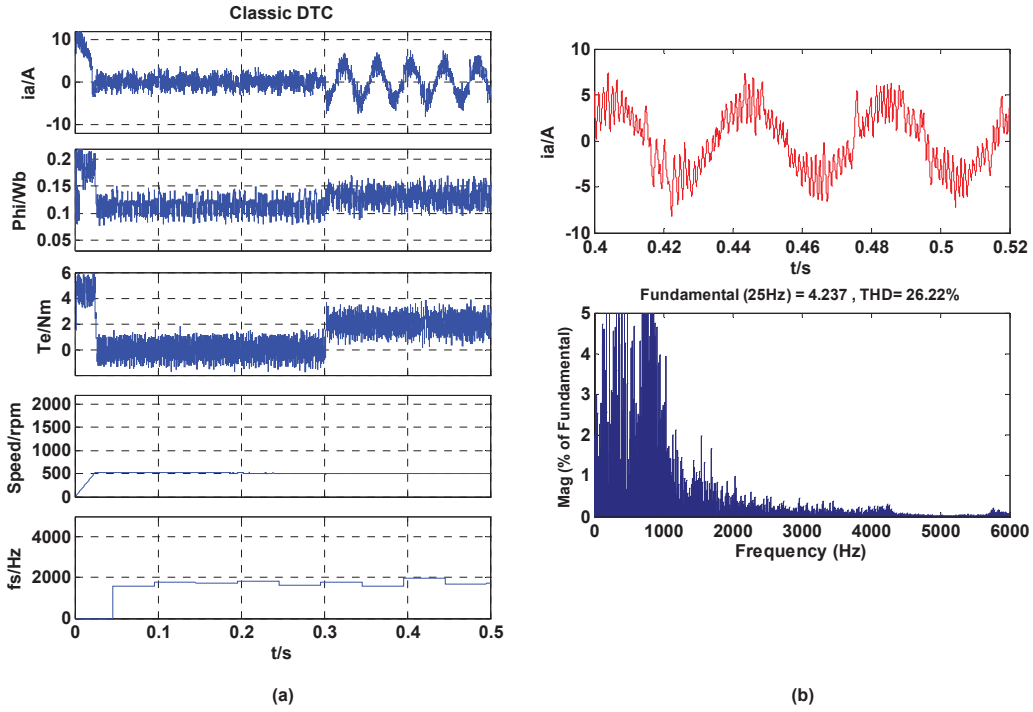

Fig. 3.6 Combined load test for DTC at 500 rpm: (a) start-up, steady-state and external load test, and (b) stator current harmonic spectrum

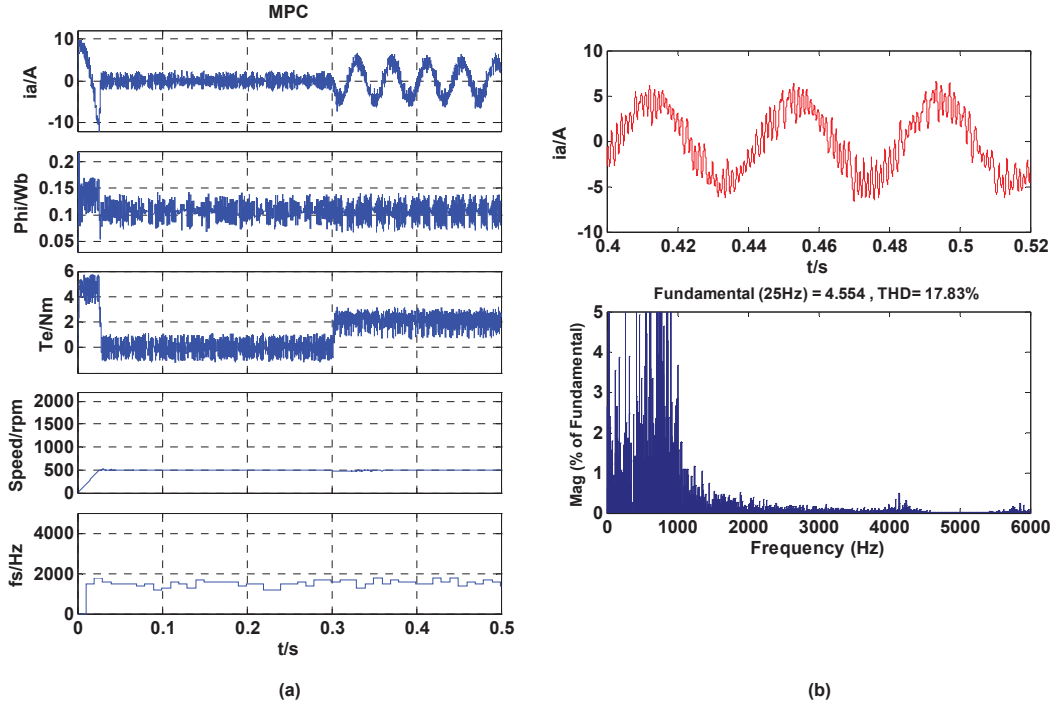

Fig. 3.7 Combined load test for MPC at 500 rpm: (a) start-up, steady-state and external load test, and (b) stator current harmonic spectrum

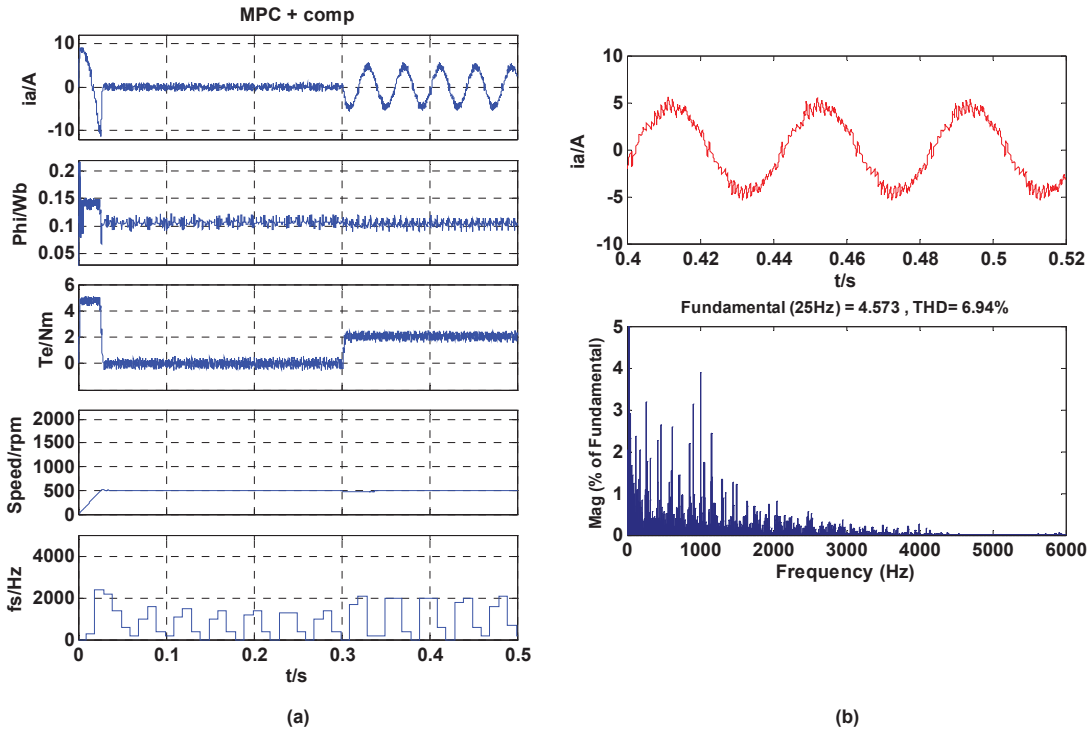

Fig. 3.8 Combined load test for MPC with one-step delay compensation at 500 rpm: (a) start-up, steady-state and external load test, and (b) stator current harmonic spectrum

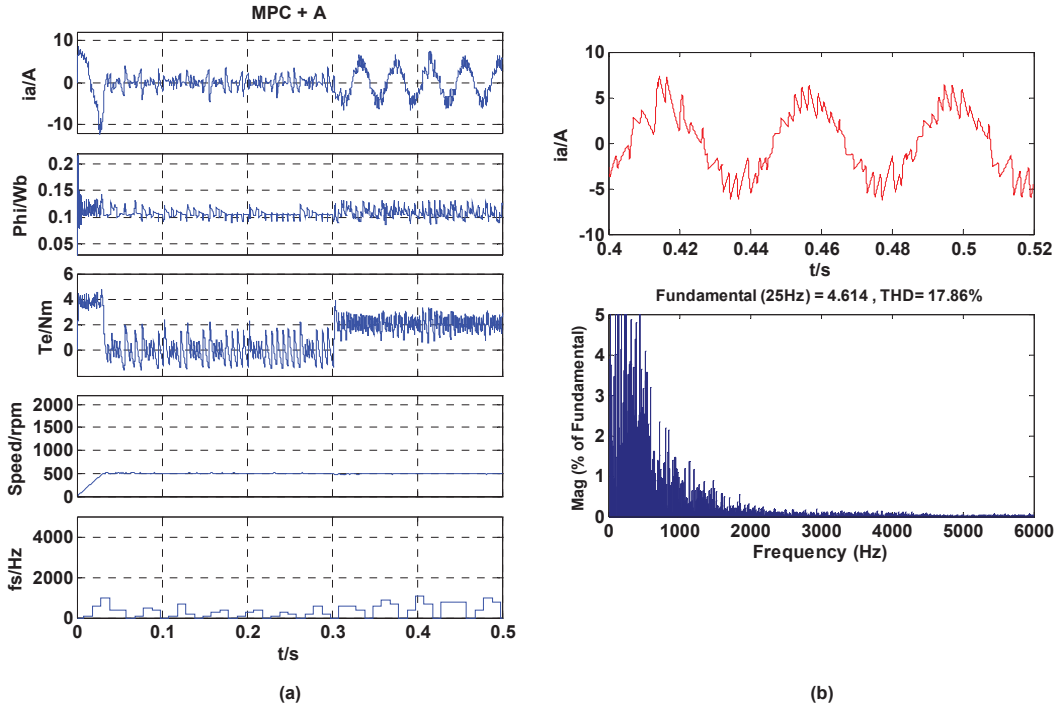

Fig. 3.9 Combined load test for MPC with linear multiple horizon prediction at 500 rpm: (a) start-up, steady-state and external load test, and (b) stator current harmonic spectrum

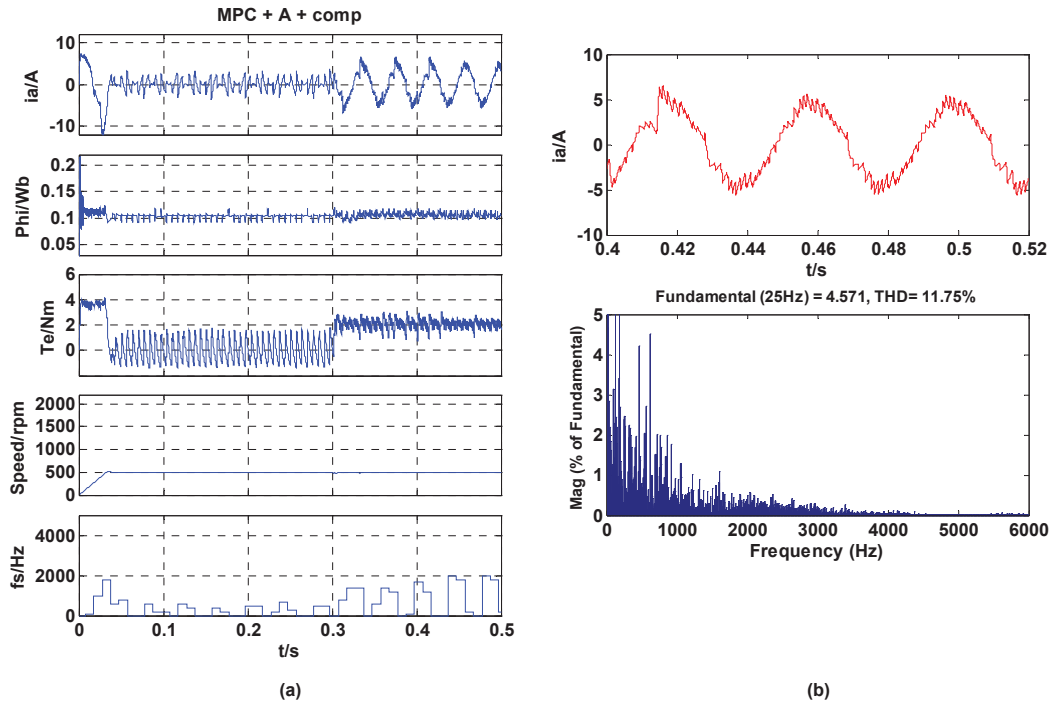

Fig. 3.10 Combined load test for MPC with both linear multiple horizon prediction and one-step delay compensation at 500 rpm: (a) start-up, steady-state and external load test, and (b) stator current harmonic spectrum

From Fig. 3.6 and Fig. 3.7, it is shown that the implementation of MPC can reduce the torque and flux ripples effectively. In Fig. 3.8, the one-step delay compensation algorithm is added to MPC and the torque and flux ripples are further reduced. By comparing Fig. 3.9 with Fig. 3.7, it can be found that the introduction of linear multiple horizon prediction does not affect the torque and flux ripples too much. However, a dramatic reduction in switching frequency can be observed in Fig. 3.9. In the last figure, both one-step delay compensation and linear multiple horizon prediction are introduced to MPC. It is shown that the torque and flux ripples are lower than that of Fig. 3.9 and the switching frequency is slightly increased. From these figures, it can be seen that the dynamic responses of all five methods are similar, but the steady state performance of MPC and improved MPCs is better than that of DTC. The stator current THDs of MPC and improved MPCs are lower than that of DTC and they also present a narrower harmonic spectrum than DTC.

3.4.2 Combined load test at 1000 rpm

The combined load tests at 1000 rpm for DTC, MPC and improved MPCs are presented in this section.

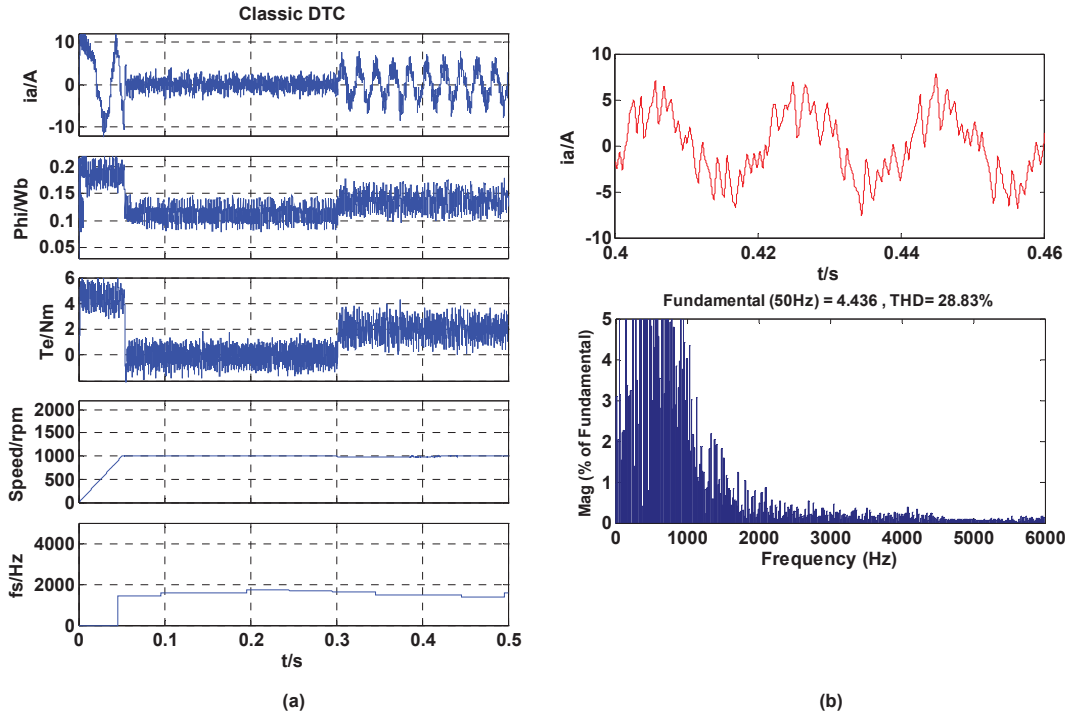

Fig. 3.11 Combined load test for DTC at 1000 rpm: (a) start-up, steady-state and external load test, and (b) stator current harmonic spectrum

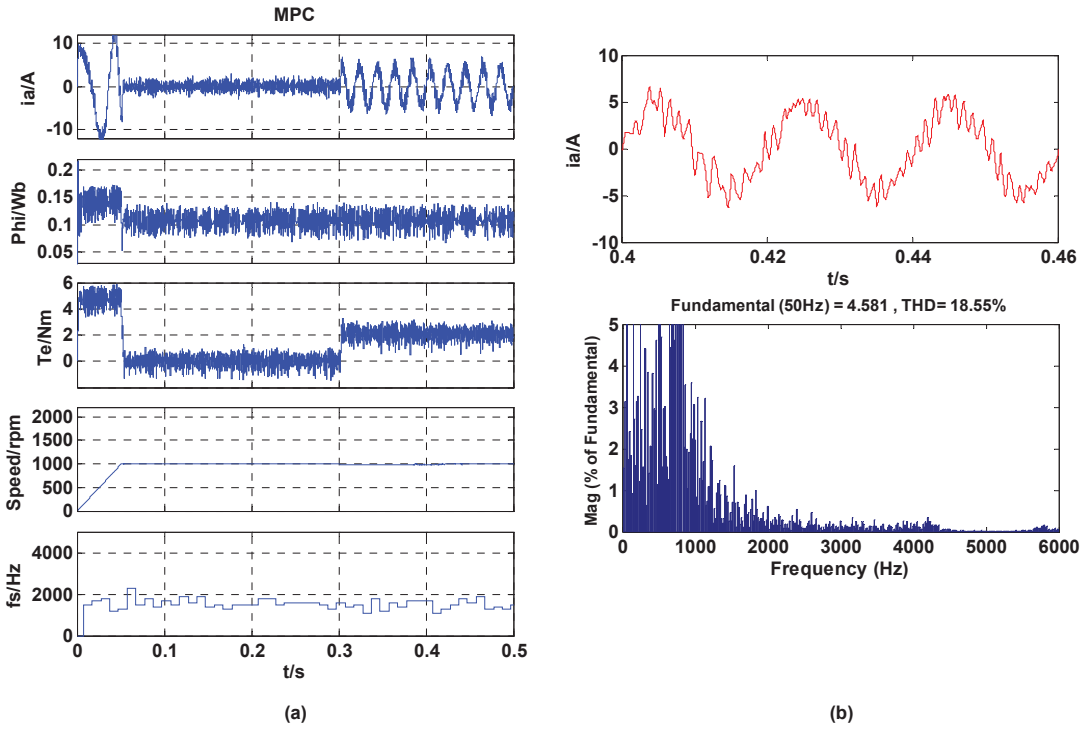

Fig. 3.12 Combined load test for MPC at 1000 rpm: (a) start-up, steady-state and external load test, and (b) stator current harmonic spectrum

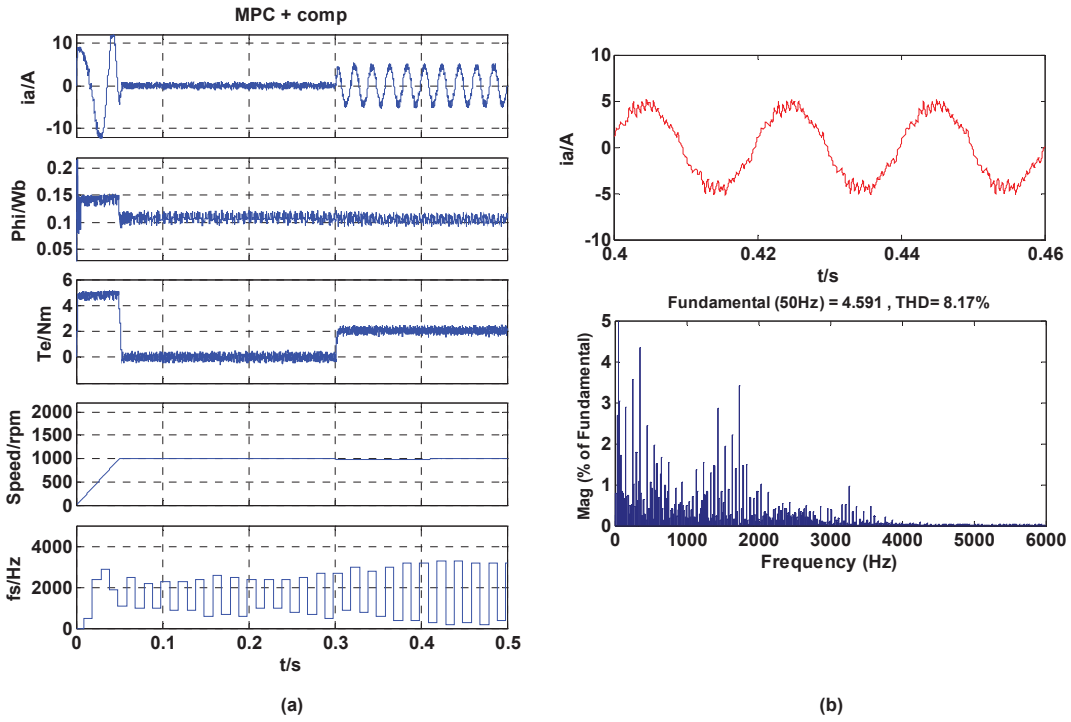

Fig. 3.13 Combined load test for MPC with one-step delay compensation at 1000 rpm: (a) start-up, steady-state and external load test, and (b) stator current harmonic spectrum

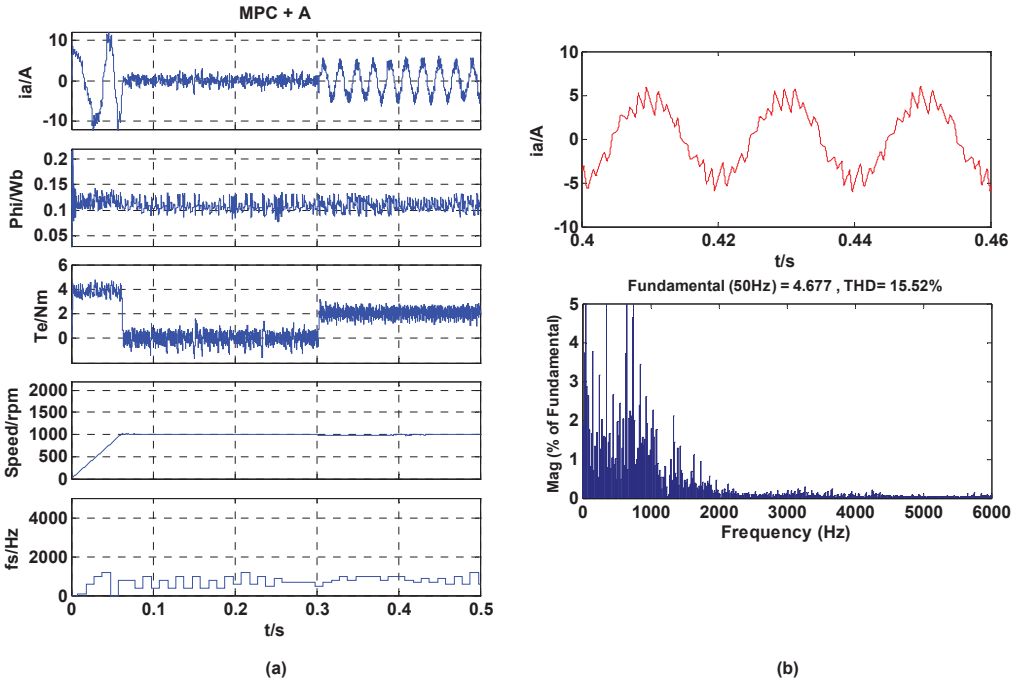

Fig. 3.14 Combined load test for MPC with linear multiple horizon prediction at 1000 rpm: (a) start-up, steady-state and external load test, and (b) stator current harmonic spectrum

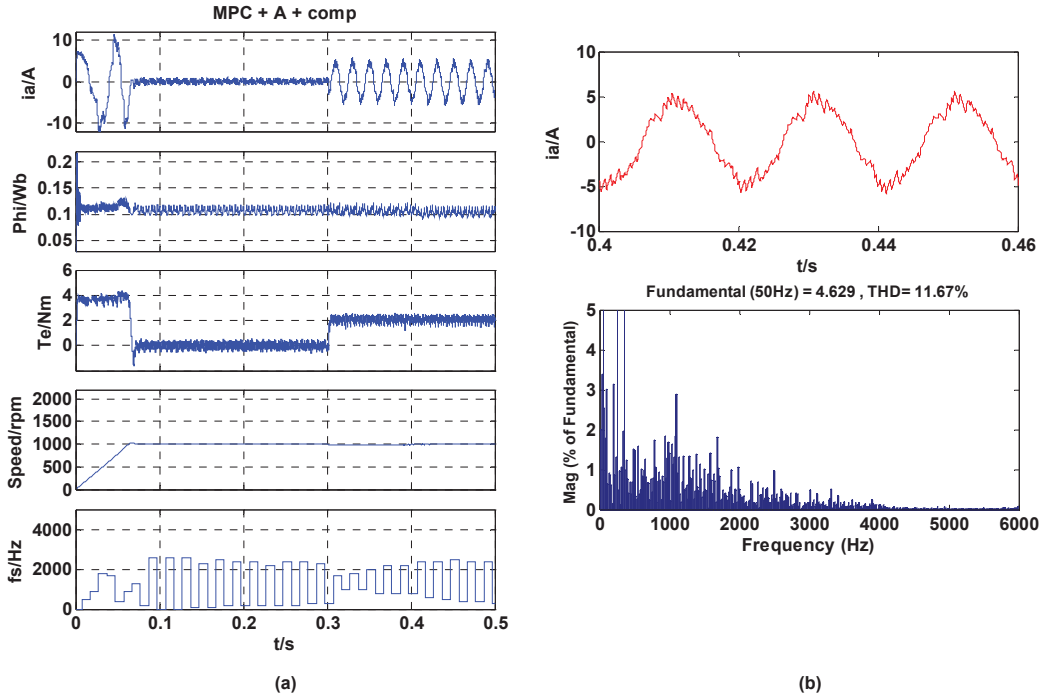

Fig. 3.15 Combined load test for MPC with both linear multiple horizon prediction and one-step delay compensation at 1000 rpm: (a) start-up, steady-state and external load test, and (b) stator current harmonic spectrum

By comparing Fig. 3.12 with Fig. 3.11, it is shown that the torque and flux ripples of MPC are lower than that of DTC. In Fig. 3.13, MPC with one-step delay compensation presents torque and flux ripples even lower than MPC along with an increase in switching frequency. In Fig. 3.14, the introduction of linear multiple horizon prediction can greatly reduce the switching frequency only with a quite limited degradation of torque and flux ripples. With the help of one-step delay compensation in Fig. 3.15, the torque and flux ripple are slightly decreased and a significant increase of switching frequency can be seen. As shown, all these methods present similar dynamic performance and the motor reach the reference speed rapidly. When the load was applied, the motor speed returned to its original value in a very short time period.

3.4.3 Combined load test at 1500 rpm

The combined load tests at 1500 rpm for DTC, MPC and improved MPCs are presented in this section.

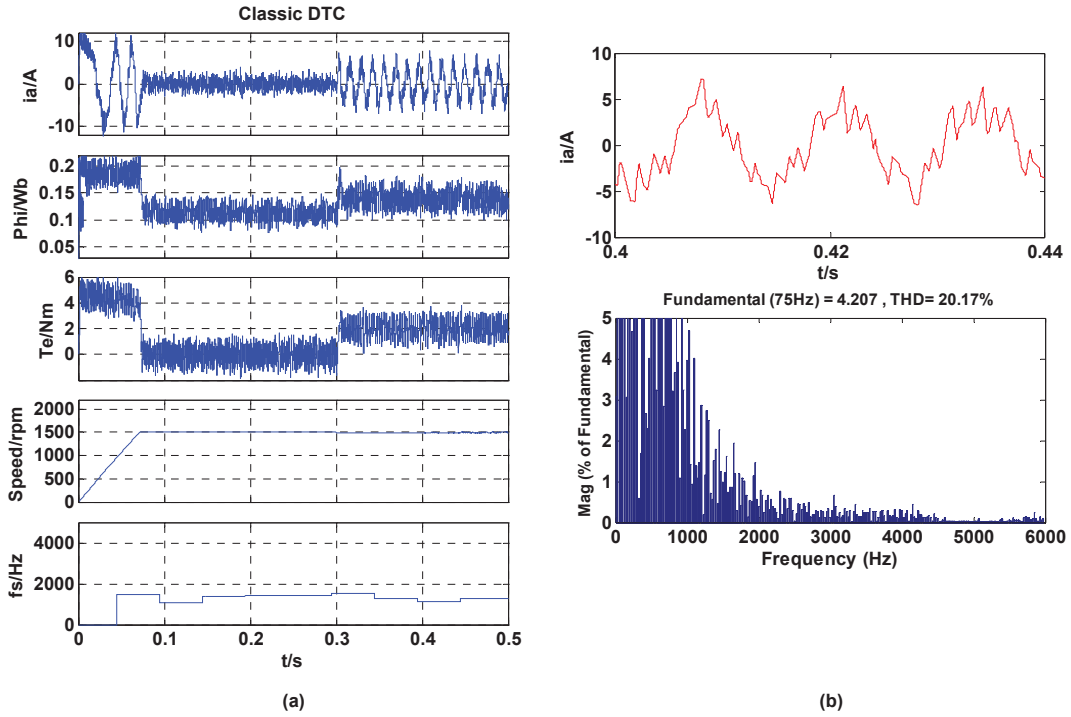

Fig. 3.16 Combined load test for DTC at 1500 rpm: (a) start-up, steady-state and external load test, and (b) stator current harmonic spectrum

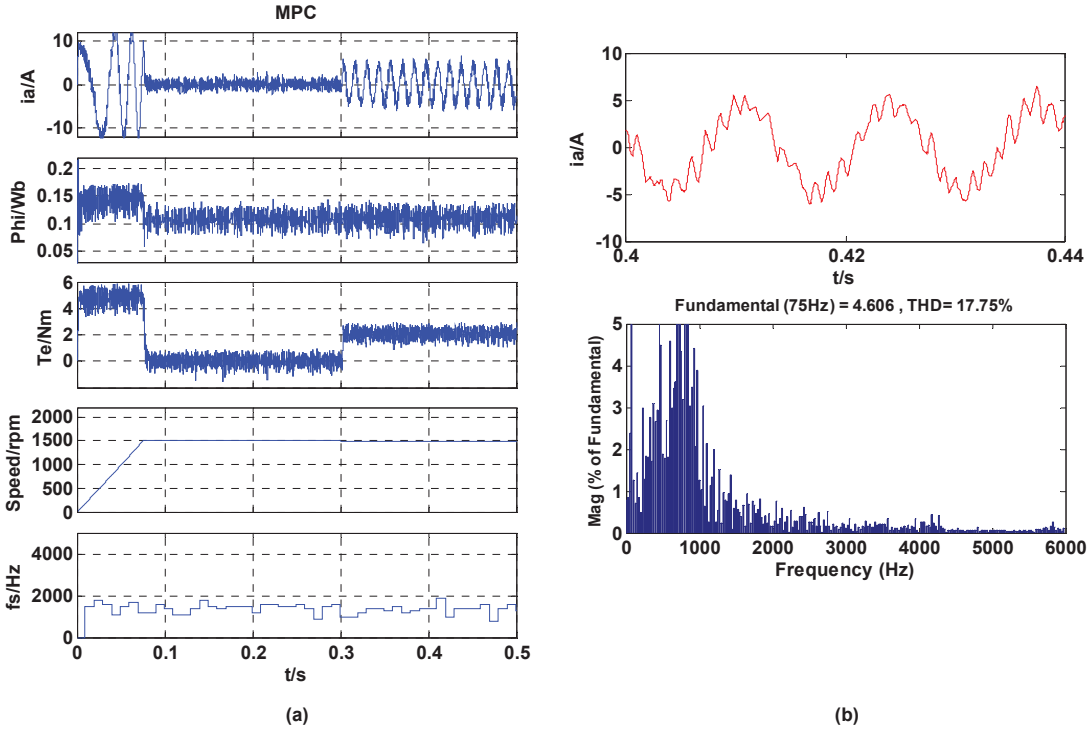

Fig. 3.17 Combined load test for MPC at 1500 rpm: (a) start-up, steady-state and external load test, and (b) stator current harmonic spectrum

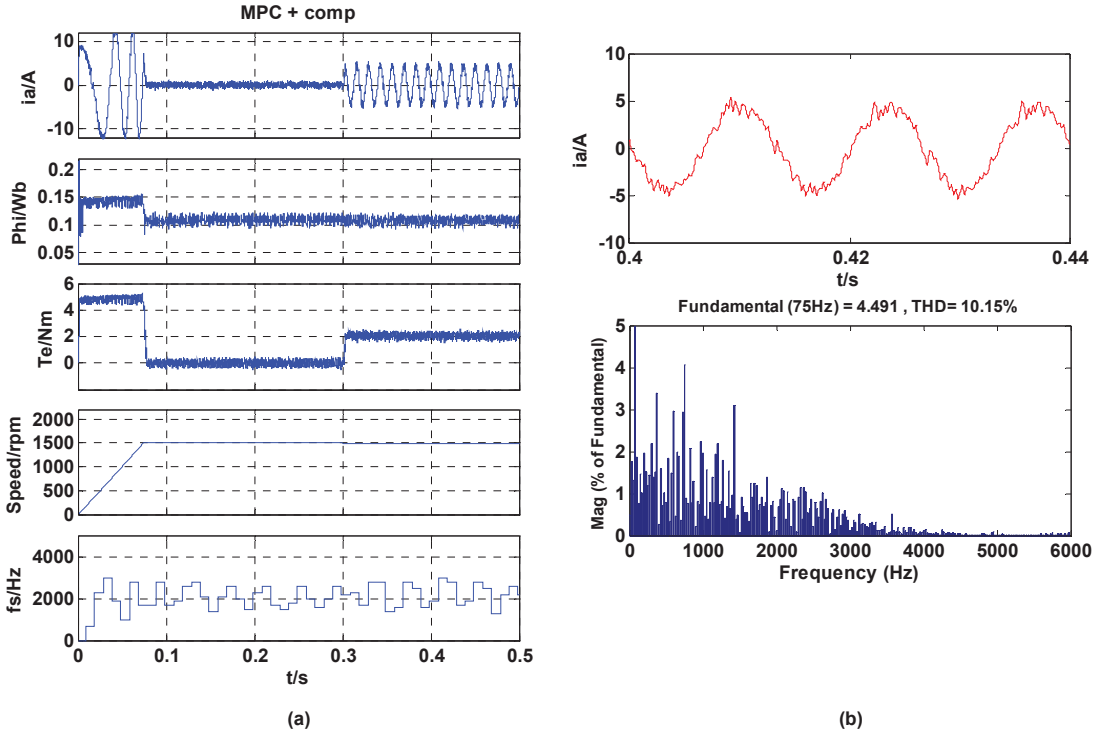

Fig. 3.18 Combined load test for MPC with one-step delay compensation at 1500 rpm: (a) start-up, steady-state and external load test, and (b) stator current harmonic spectrum

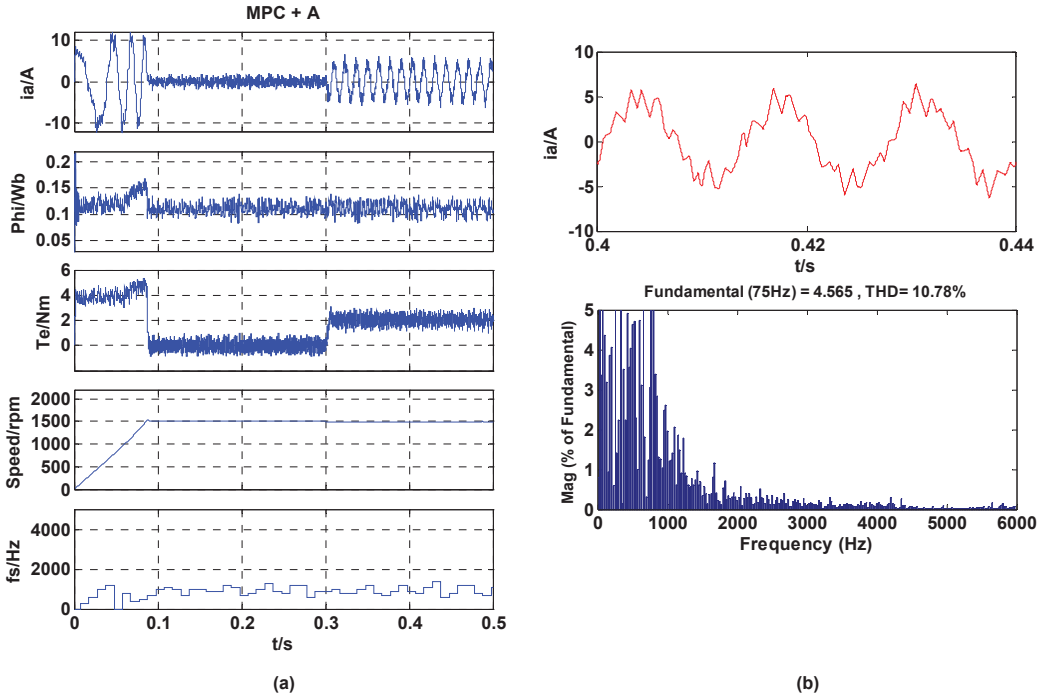

Fig. 3.19 Combined load test for MPC with linear multiple horizon prediction at 1500 rpm: (a) start-up, steady-state and external load test, and (b) stator current harmonic spectrum

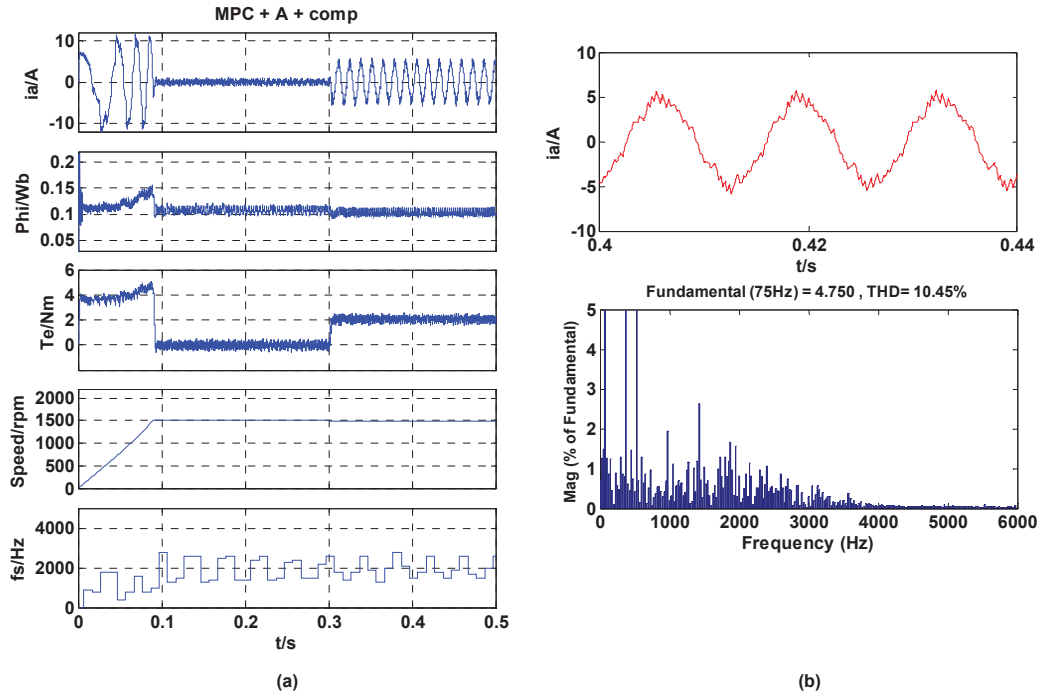

Fig. 3.20 Combined load test for MPC with both linear multiple horizon prediction and one-step delay compensation at 1500 rpm: (a) start-up, steady-state and external load test, and (b) stator current harmonic spectrum

From Fig. 3.16 and Fig. 3.17, it can be seen that MPC present much lower torque and flux ripples than that of DTC whilst maintaining the similar switching frequency. In Fig. 3.18, the torque and flux ripples decrease further due to the introduction of one-step delay compensation. By comparing Fig. 3.19 with Fig. 3.17, it can be found that the switching frequency of 'MPC + A' is almost half of the original MPC and the torque and flux ripples remain the same level. In Fig. 3.20, the additional linear multiple horizon prediction algorithm fails to reduce the switching frequency and also causes a slight increase of torque and flux ripples compared with Fig. 3.18.

3.4.4 Combined load test at 2000 rpm

The combined load tests at 2000 rpm for DTC, MPC and improved MPCs are presented in this section.

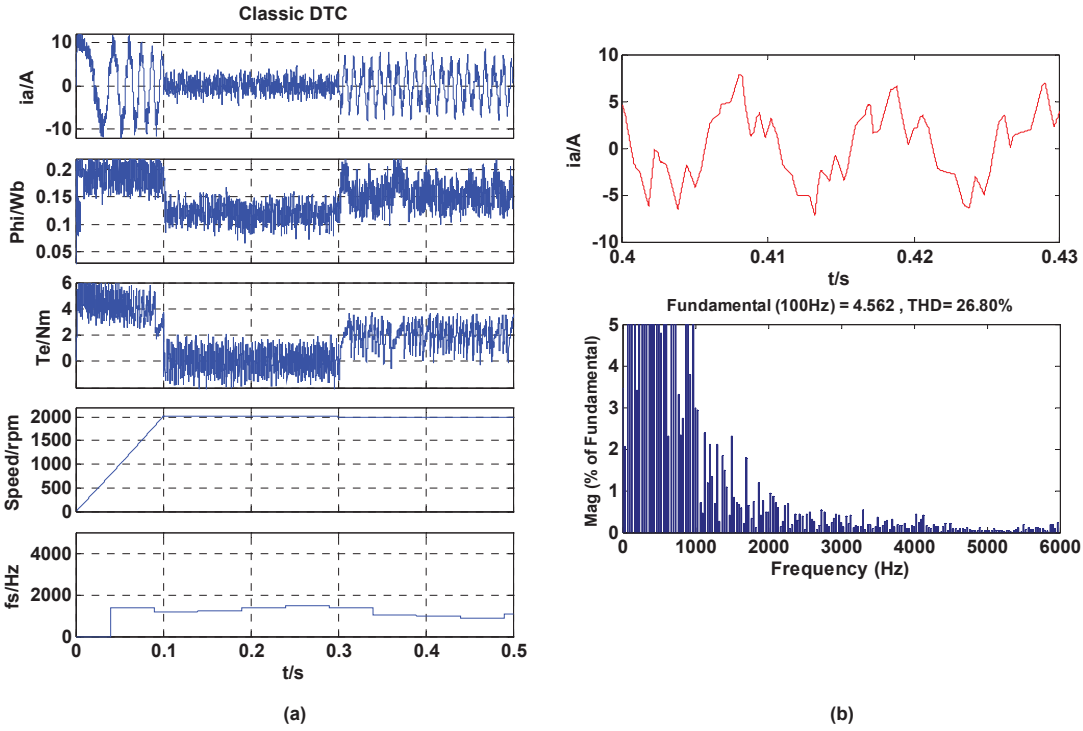

Fig. 3.21 Combined load test for DTC at 2000 rpm: (a) start-up, steady-state and external load test, and (b) stator current harmonic spectrum

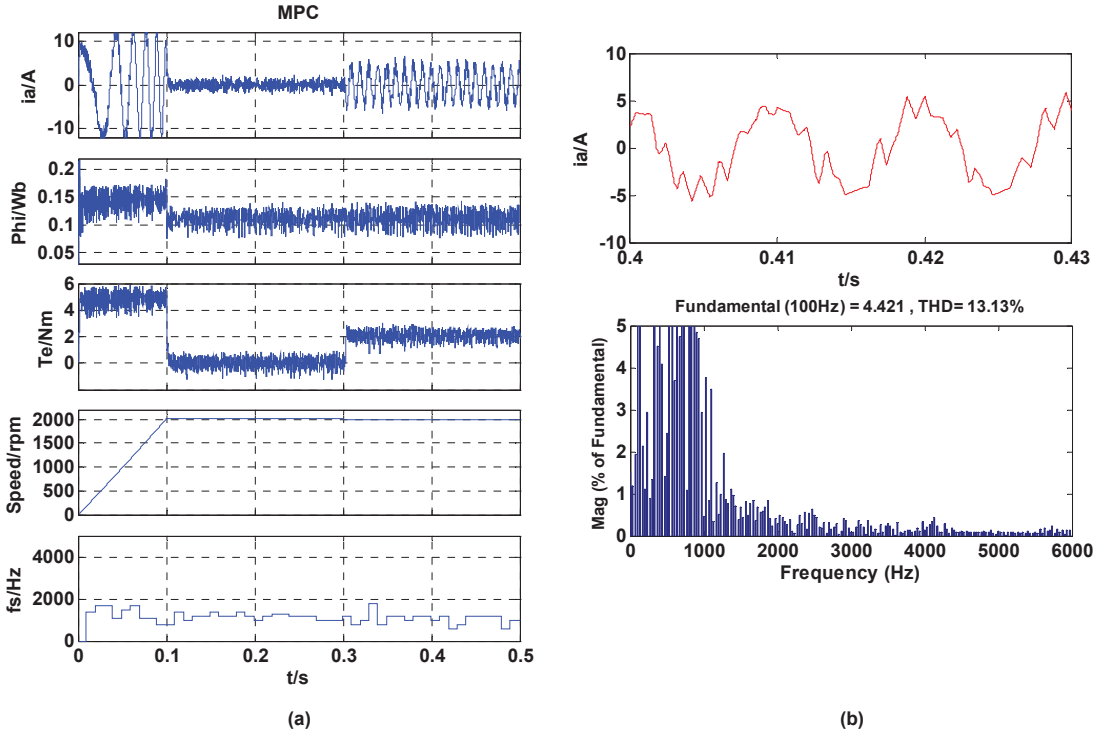

Fig. 3.22 Combined load test for MPC at 2000 rpm: (a) start-up, steady-state and external load test, and (b) stator current harmonic spectrum

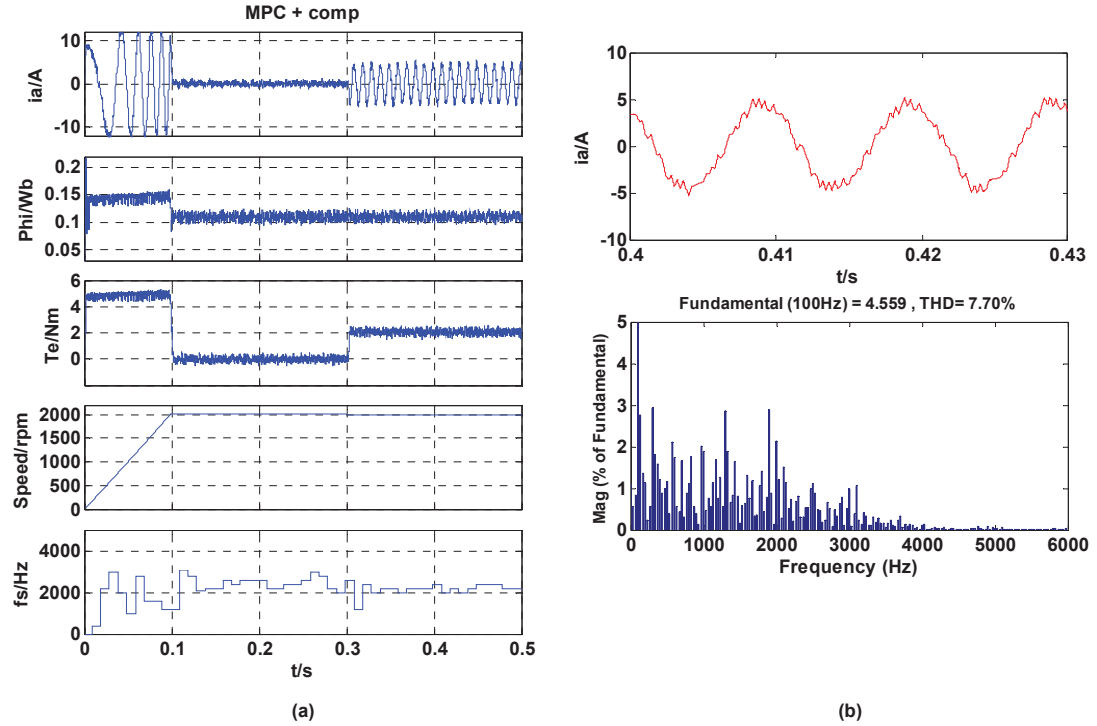

Fig. 3.23 Combined load test for MPC with one-step delay compensation at 2000 rpm: (a) start-up, steady-state and external load test, and (b) stator current harmonic spectrum

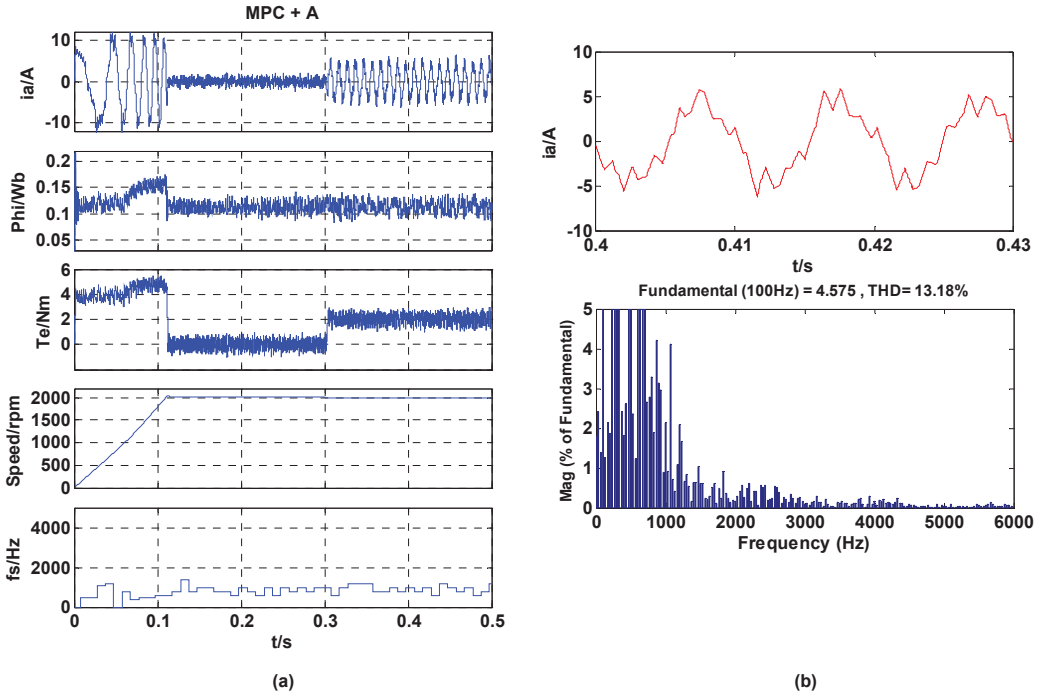

Fig. 3.24 Combined load test for MPC with linear multiple horizon prediction at 2000 rpm: (a) start-up, steady-state and external load test, and (b) stator current harmonic spectrum

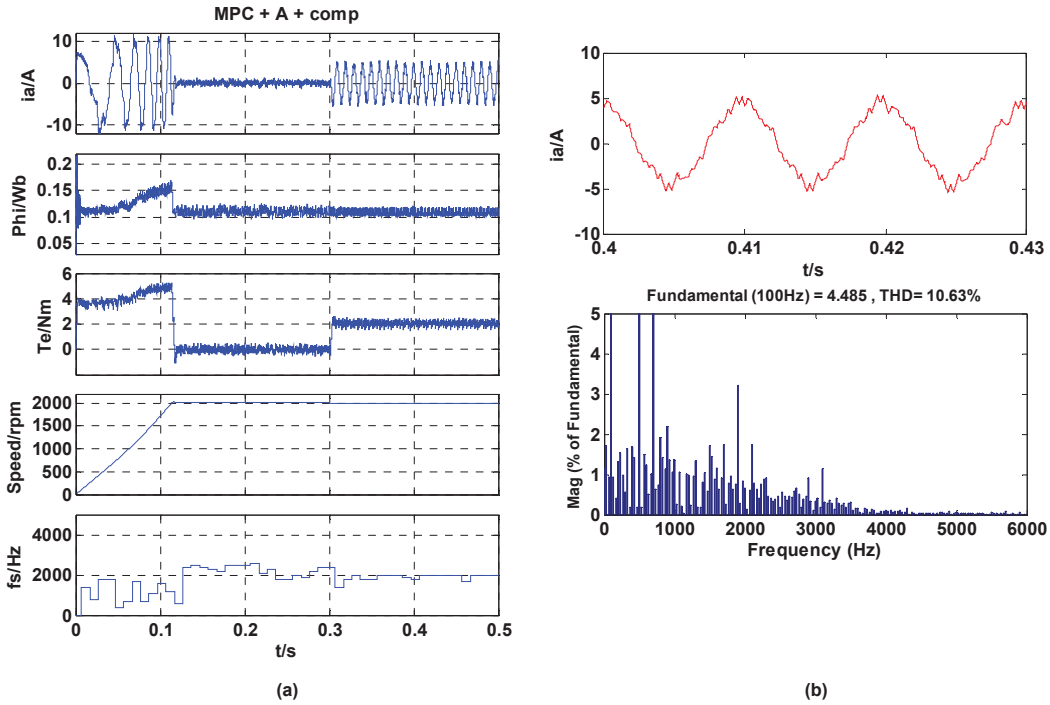

Fig. 3.25 Combined load test for MPC with both linear multiple horizon prediction and one-step delay compensation at 2000 rpm: (a) start-up, steady-state and external load test, and (b) stator current harmonic spectrum

The superiority of MPC can be best presented in Fig. 3.22, the torque and flux ripples and stator current THD of DTC are almost halved by introducing MPC whilst maintaining the similar switching frequency. In Fig. 3.23, the implementation of one-step delay compensation halves the stator current THD of original MPC and almost doubles the switching frequency. In Fig. 3.24, the appearance of linear multiple horizon prediction can significantly reduce the switching frequency and only does quite limited influence to steady-state and dynamic performance. However, the linear multiple horizon prediction seems to fail to reduce the switching frequency when work together with one-step delay compensation algorithm as shown in Fig. 3.25.

3.4.5 Deceleration test (from 1500rpm to 500 rpm)

In this section, the motor maintains the speed of 1500 rpm from 0s and the reference speed is set to 500 rpm from 0.05s. From top to bottom, the curves are the stator current, stator flux, torque and motor speed respectively.

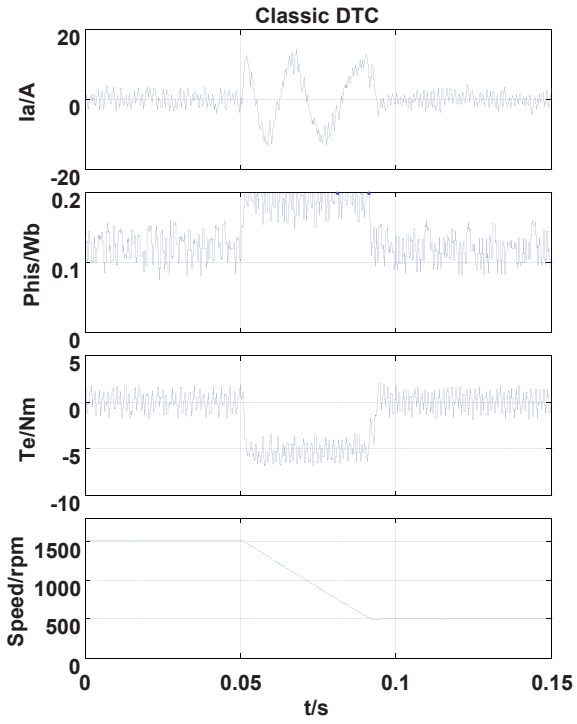

Fig. 3.26 Deceleration test for DTC

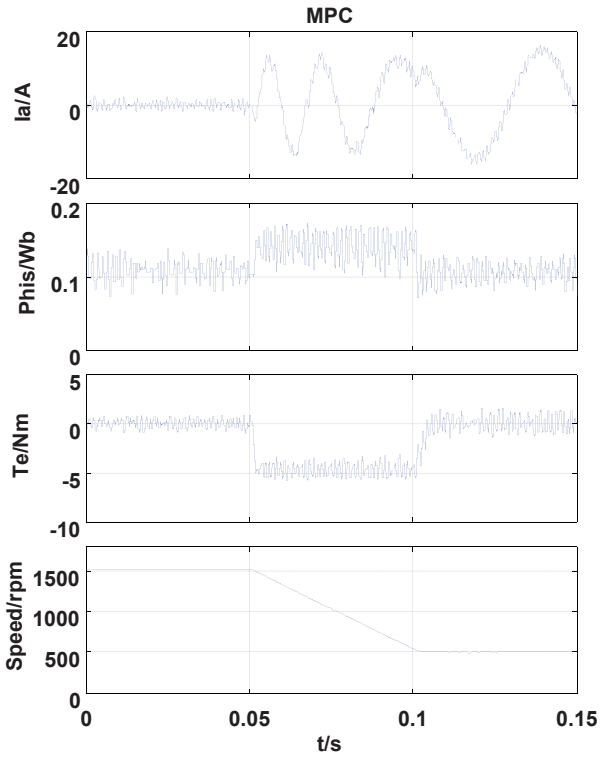

Fig. 3.27 Deceleration test for MPC

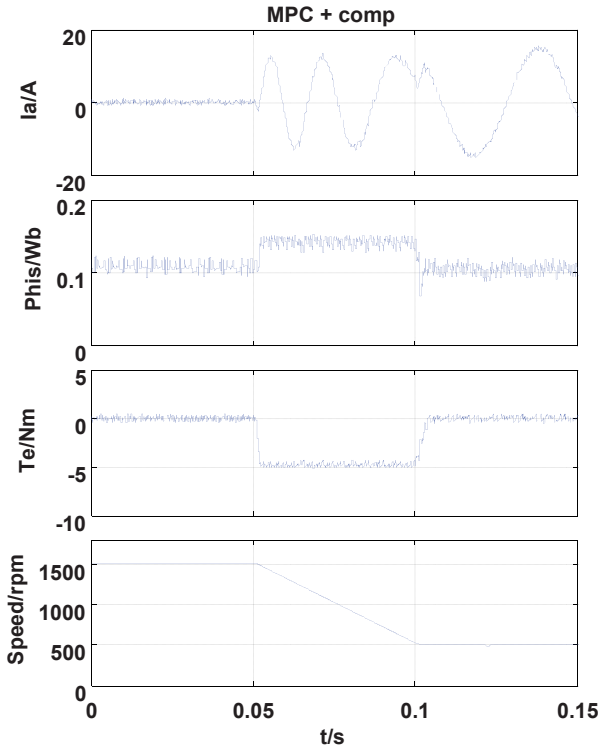

Fig. 3.28 Deceleration test for MPC one-step delay compensation

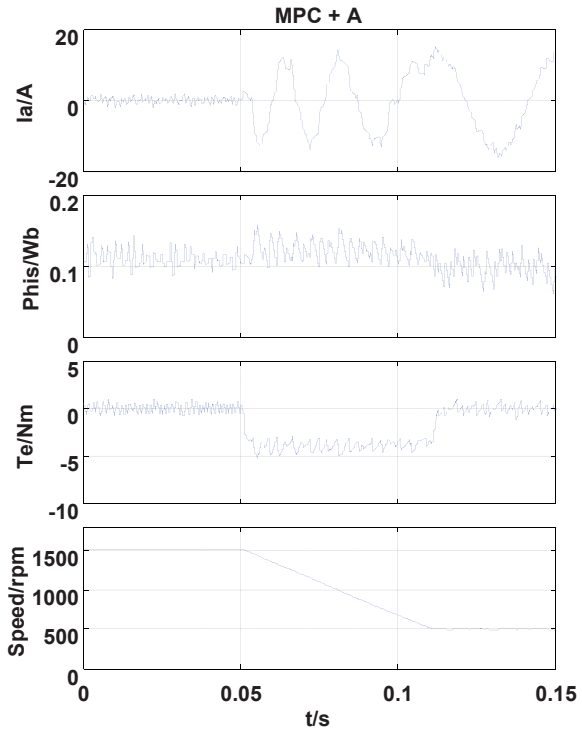

Fig. 3.29 Deceleration test for MPC with linear multiple horizon prediction

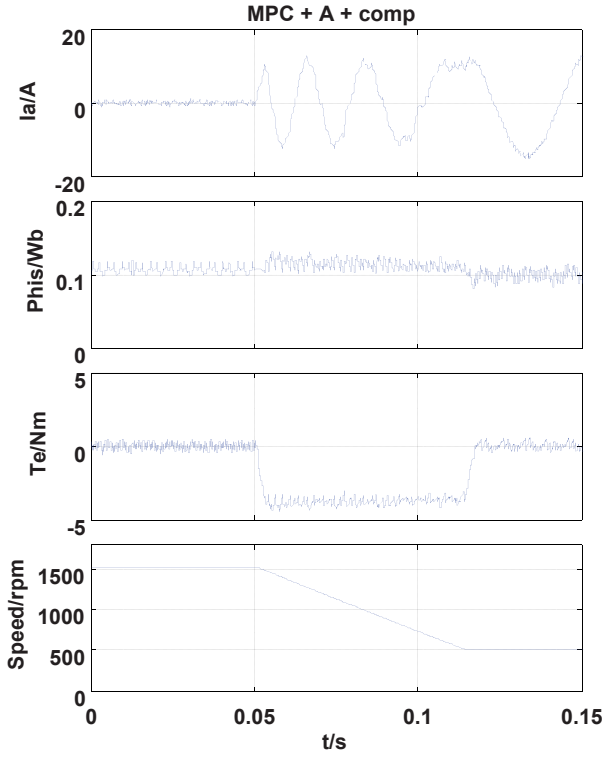

Fig. 3.30 Deceleration test for MPC with both linear multiple horizon prediction and one-step delay compensation

As shown, all these methods performed well. Within a short time period, the motor speed decreased from 1500 rpm to 500 rpm. However, the drive system spent a bit more time to complete the speed deceleration when linear multiple horizon prediction was implemented as shown in Fig. 3.29 and 3.30.

3.5 Experimental Testing of DTC and MPC

In addition to the simulation study, the control methods mentioned above are further experimentally tested on a two-level inverter-fed PMSM motor drive. The control and motor parameters are the same as those introduced in Table I. A dSPACE DS1104 PPC/DSP control board is employed to implement the real-time algorithm coding using C language. A three-phase intelligent power module equipped with an insulated-gate bipolar transistor (IGBT) is used as an inverter. The gating pulses are generated in the DS1104 board and then sent to the inverter. The load is applied using a programmable dynamo-meter controller DSP6000 (Fig. 3.32). A 2500-pulse incremental encoder is equipped to obtain the rotor speed of PMSM. All experimental results are recorded by the ControlDesk interfaced with DS1104 and PC at 5 kHz sampling frequency. The experimental setup is illustrated in Fig. 3.31.

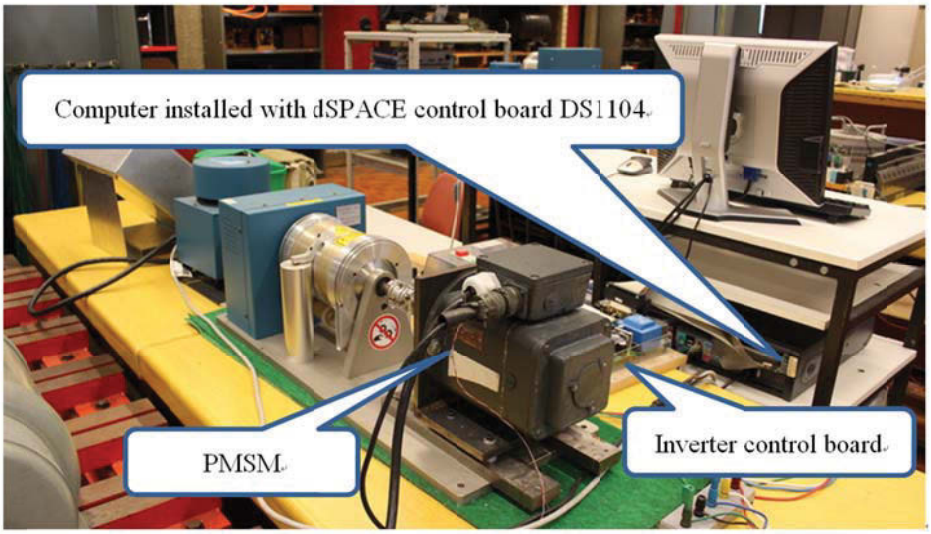

(a)

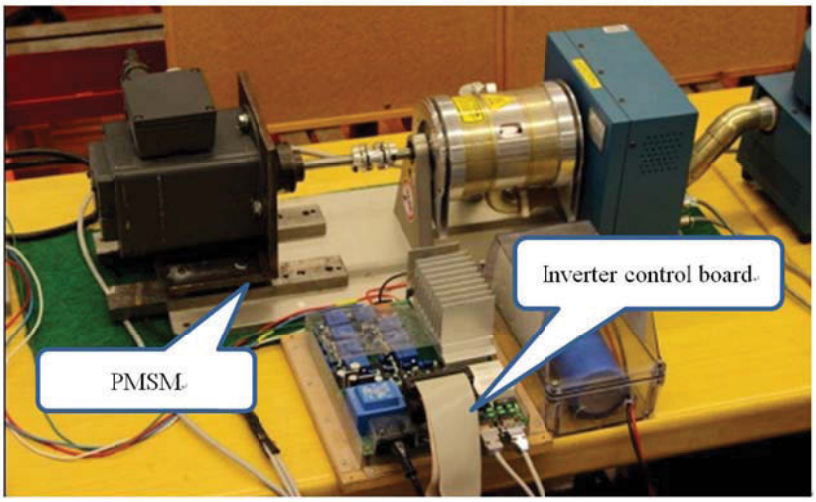

(b)

Fig. 3.31 Experimental setup of testing system: (a) overview of the testing platform and (b) front view of the PMSM and inverter control board

Fig. 3.32 Dynamo-meter controller DSP6000

3.5.1 Steady state responses at 500 rpm

The steady-state responses at 500 rpm, 1000 rpm, 1500 rpm and 2000 rpm respectively are presented in this section. From top to bottom, the curves shown are torque, stator flux and switching frequency.

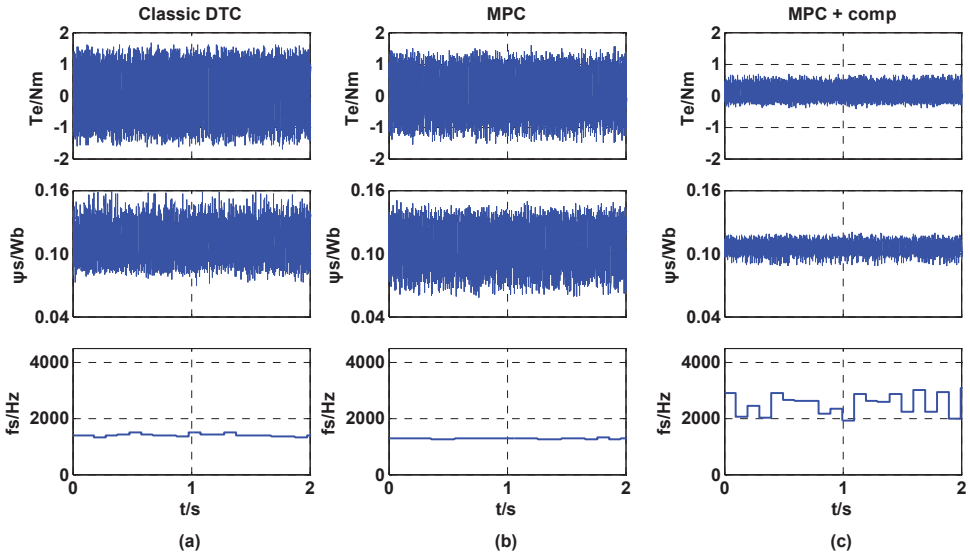

Fig. 3.33 Steady-state response at 500 rpm for: (a) DTC, (b) MPC and (c) MPC with one-step delay compensation

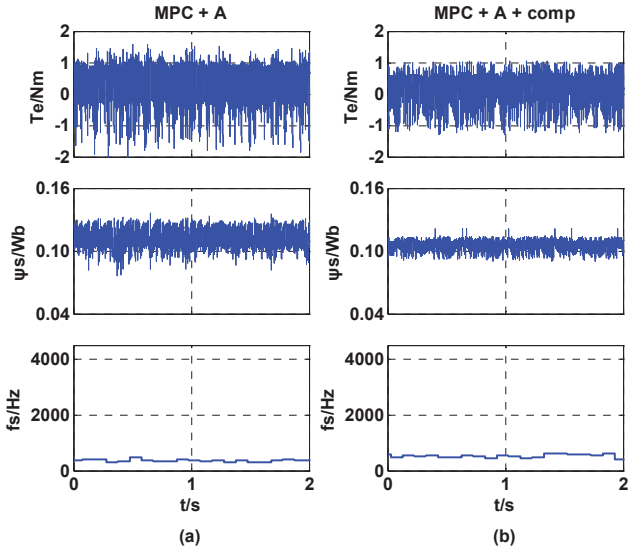

Fig. 3.34 Steady-state response at 500 rpm for: (a) MPC with linear multiple horizon prediction, and (b) MPC with both linear multiple horizon prediction and one-step delay compensation

Fig. 3.33 and 3.34 plot the measured steady-state performance at 500 rpm. It can be found that the torque ripple of MPC is lower than that of DTC. However the flux ripple is higher than DTC. The implementation of one-step delay compensation can greatly reduce the torque and flux ripples and also a significant increase of switching frequency can be observed. By adding linear multiple horizon prediction to MPC, the reduction of the torque and flux ripples can be found as well as the dramatic drop of switching frequency. When the linear multiple horizon prediction is applied to MPC with one-step delay compensation, a significant decrease of switching frequency can be observed and the torque ripple is also increased.

The quantitative index of average switching frequency, stator flux ripple and torque ripple for these tests will be summarized in Section 3.6.

3.5.2 Steady state responses at 1000 rpm

The steady-state responses at 1000 rpm are presented in this section. From top to bottom, the curves shown are torque, stator flux and switching frequency.

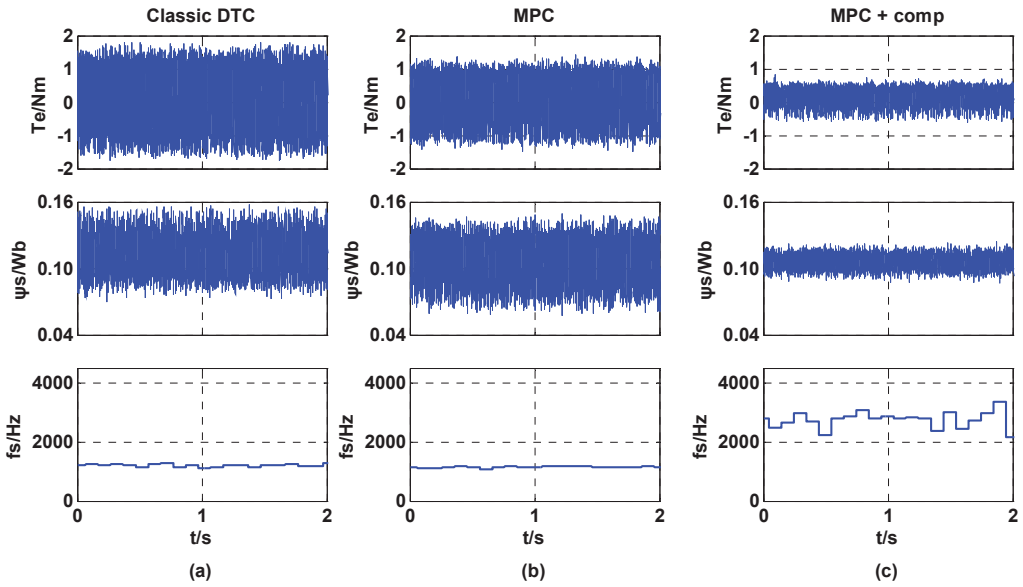

Fig. 3.35 Steady-state response at 1000 rpm for: (a) DTC, (b) MPC and (c) MPC with one-step delay compensation

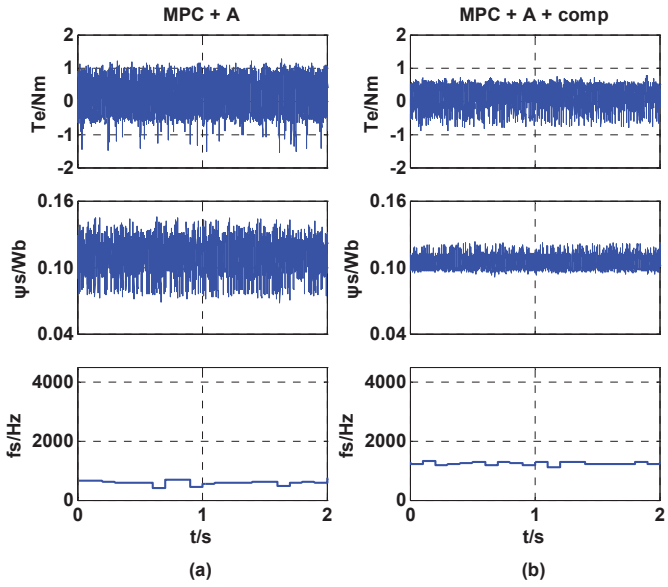

Fig. 3.36 Steady-state response at 1000 rpm for: (a) MPC with linear multiple horizon prediction, and (b) MPC with both linear multiple horizon prediction and one-step delay compensation

Fig. 3.35 and 3.36 plot the measured steady-state performance at 1000 rpm. It is seen that the implementation of MPC can reduce the torque ripple, but does not reduce the flux ripple. When the one-step delay is compensated, a significant decrease of torque and flux ripples can be found as well as an obvious increase of switching frequency. When the linear multiple horizon prediction is added to MPC, it can be seen that the torque and flux ripples are slightly decreased along with a limited reduction of the switching frequency. When the linear multiple horizon prediction is applied to MPC in addition to one-step delay compensation, a remarkable drop of the switching frequency can be seen whilst maintaining the similar steady-state performance.

3.5.3 Steady state responses at 1500 rpm

The steady-state responses at 1500 rpm are presented in this section. From top to bottom, the curves shown are torque, stator flux and switching frequency.

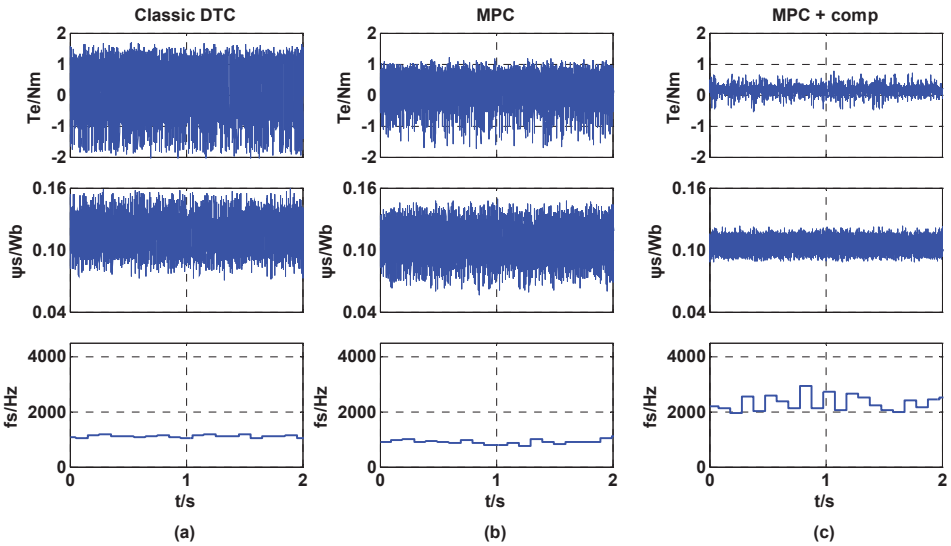

Fig. 3.37 Steady-state response at 1500 rpm for: (a) DTC, (b) MPC and (c) MPC with one-step delay compensation

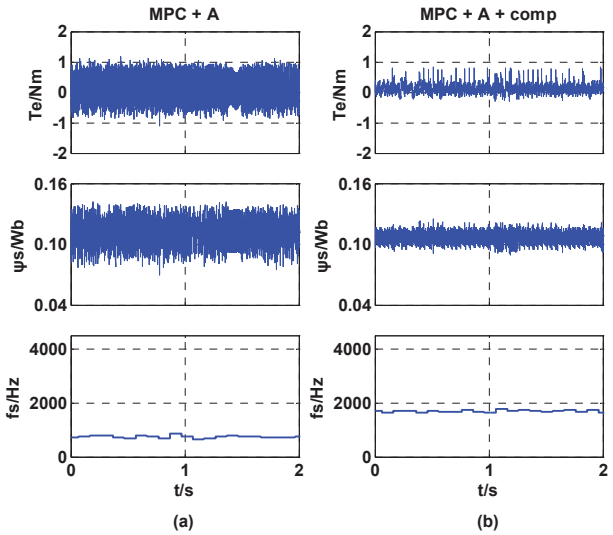

Fig. 3.38 Steady-state response at 1500 rpm for: (a) MPC with linear multiple horizon prediction, and (b) MPC with both linear multiple horizon prediction and one-step delay compensation

Fig. 3.37 and 3.38 plot the measured steady-state performance at 1500 rpm. As shown in Fig. 3.37 (b), the introduction of MPC can reduce the torque ripple, but fails to decrease the flux ripple. In Fig. 3.37 (c), the torque and flux ripples are significantly reduced when one-step delay is compensated. By introducing linear multiple horizon prediction to MPC, an obvious reduction of torque and flux ripples as well as a slight decrease of switching frequency can be observed as shown in Fig. 3.38 (a). In Fig. 3.38 (b), both linear multiple horizon prediction and one-step delay compensation are used in MPC and the switching frequency is slightly reduced whilst maintaining the similar torque and flux ripples as shown in Fig. 3.37 (c).

3.5.4 Steady state responses at 2000 rpm

The steady-state responses at 2000 rpm are presented in this section. From top to bottom, the curves shown are torque, stator flux and switching frequency.

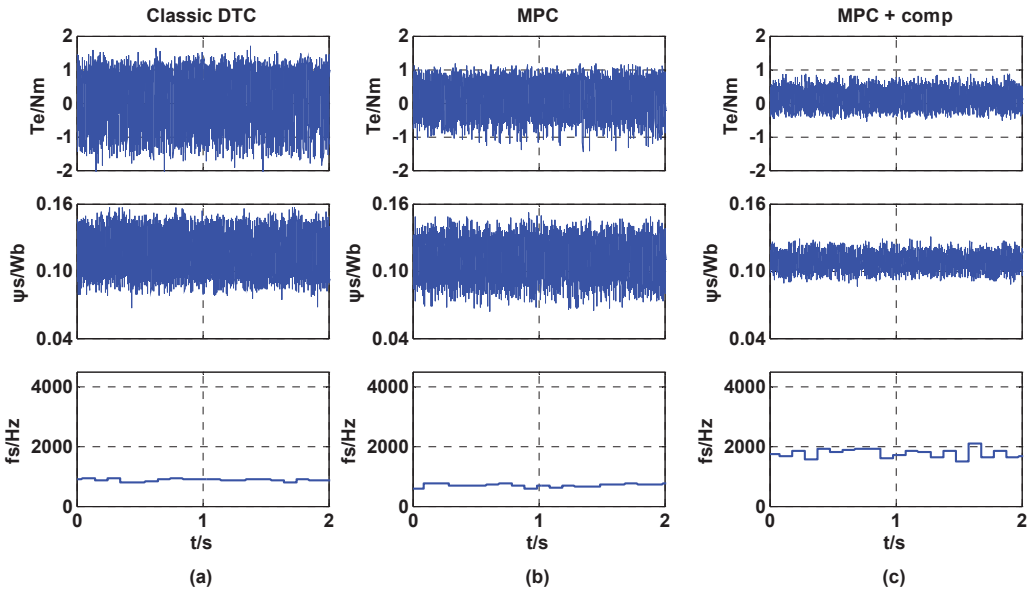

Fig. 3.39 Steady-state response at 2000 rpm for: (a) DTC, (b) MPC and (c) MPC with one-step delay compensation

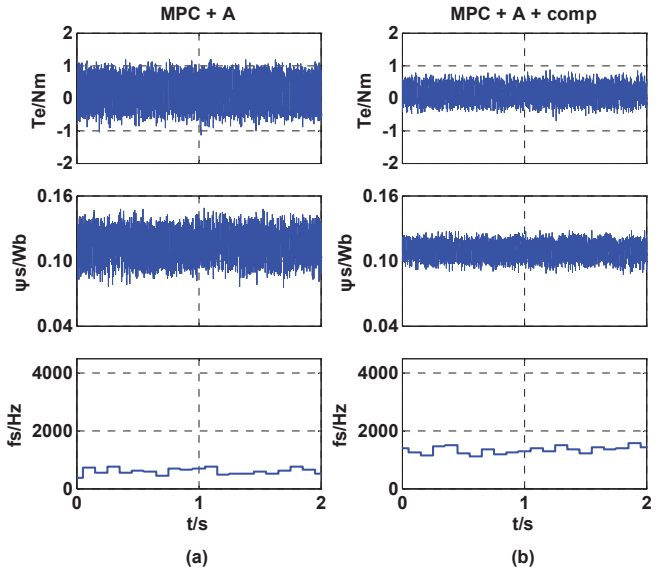

Fig. 3.40 Steady-state response at 2000 rpm for: (a) MPC with linear multiple horizon prediction, and (b) MPC with both linear multiple horizon prediction and one-step delay compensation

Fig. 3.39 and 3.40 plot the measured steady-state performance at 2000 rpm. In Fig. 3.39 (b), an obvious decrease of torque ripple can be seen, but no improvement of flux ripple can be found. When the one-step delay is compensated as shown in Fig. 3.39 (c), the torque and flux ripples are significantly decreased along with a remarkable increase of switching frequency. As shown in Fig. 3.40 (a), the introduction of linear multiple horizon prediction seems to fail with switching frequency reduction, but a slight decrease of both torque and flux ripples can be seen. In Fig. 3.40 (b), with the help of linear multiple horizon prediction, the switching frequency is reduced whilst maintaining the similar torque and flux ripples as shown in Fig. 3.39 (c).

3.5.5 Start-up test

In this section, the start-up response is presented. By introducing a ramp-up function in the PI controller, the motor speed accelerates from 0 to 2000 rpm steadily with a small overshoot. In Figs. 3-41 to 3-45, from top to bottom, the curves shown are the stator current, stator flux, torque and rotor speed. One right hand side of the figure, there is a zoomed view of stator current. It is observed that whilst the dynamic response for these methods are similar, the steady state performance of the MPC with linear multiple horizon prediction is much better.

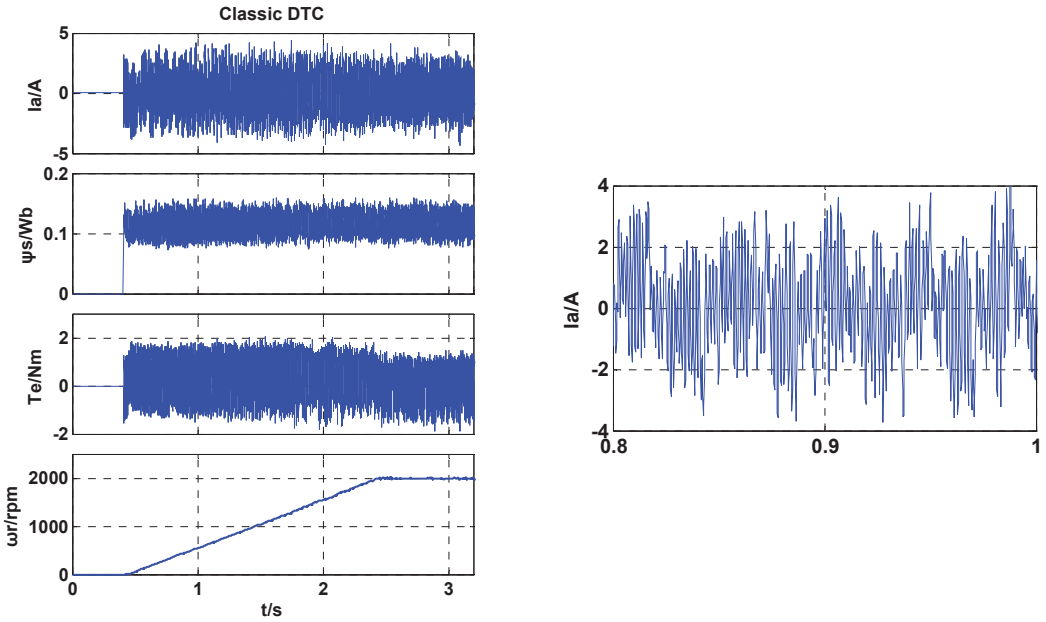

Fig. 3.41 Start-up response from standstill to 2000 rpm for DTC

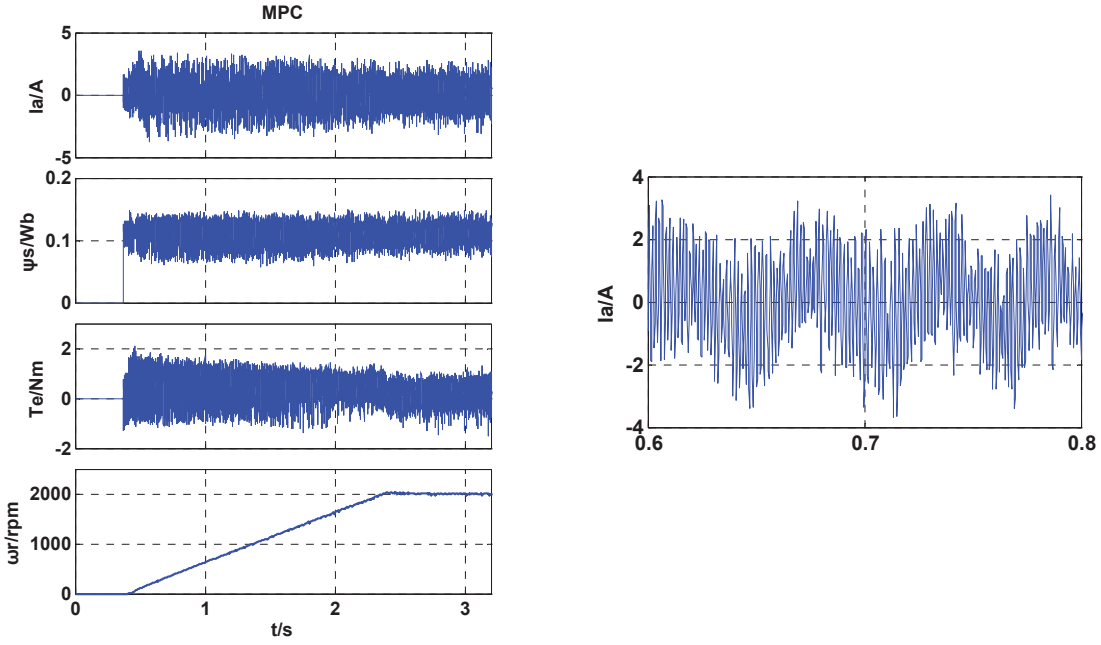

Fig. 3.42 Start-up response from standstill to 2000 rpm for MPC

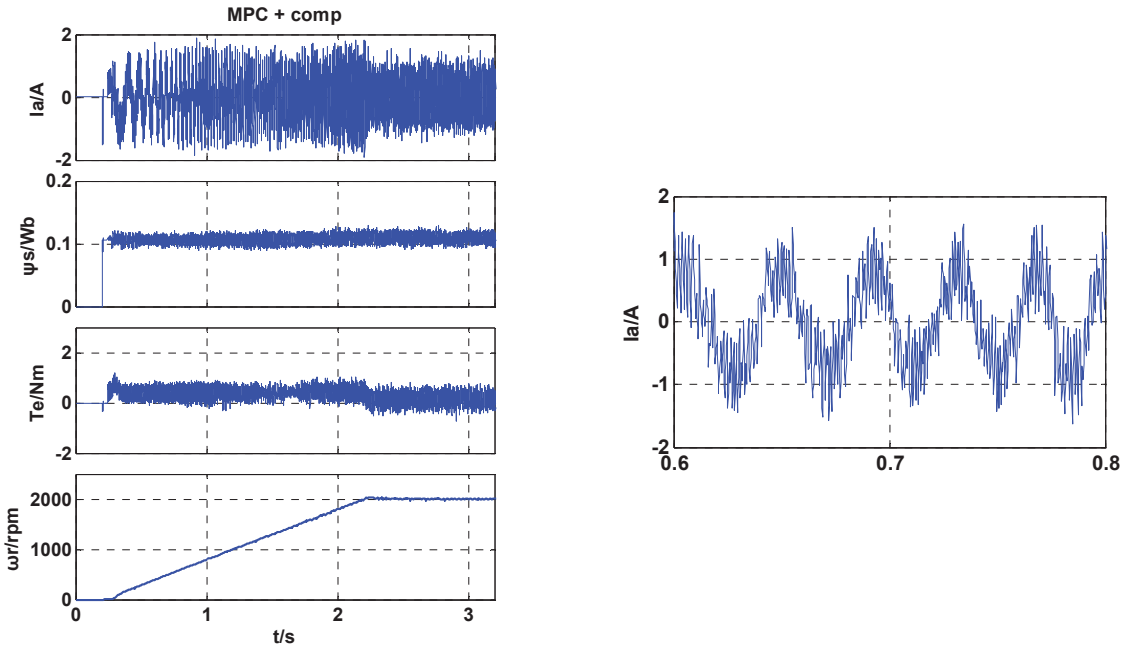

Fig. 3.43 Start-up response from standstill to 2000 rpm for MPC with one-step delay compensation

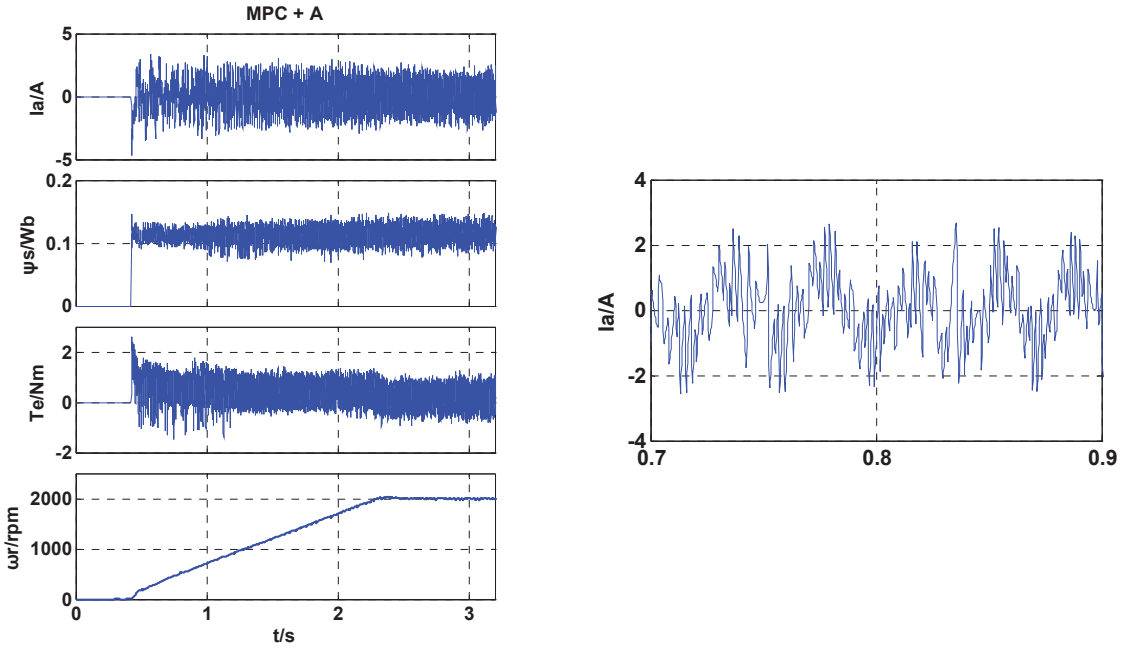

Fig. 3.44 Start-up response from standstill to 2000 rpm for MPC with linear multiple horizon prediction

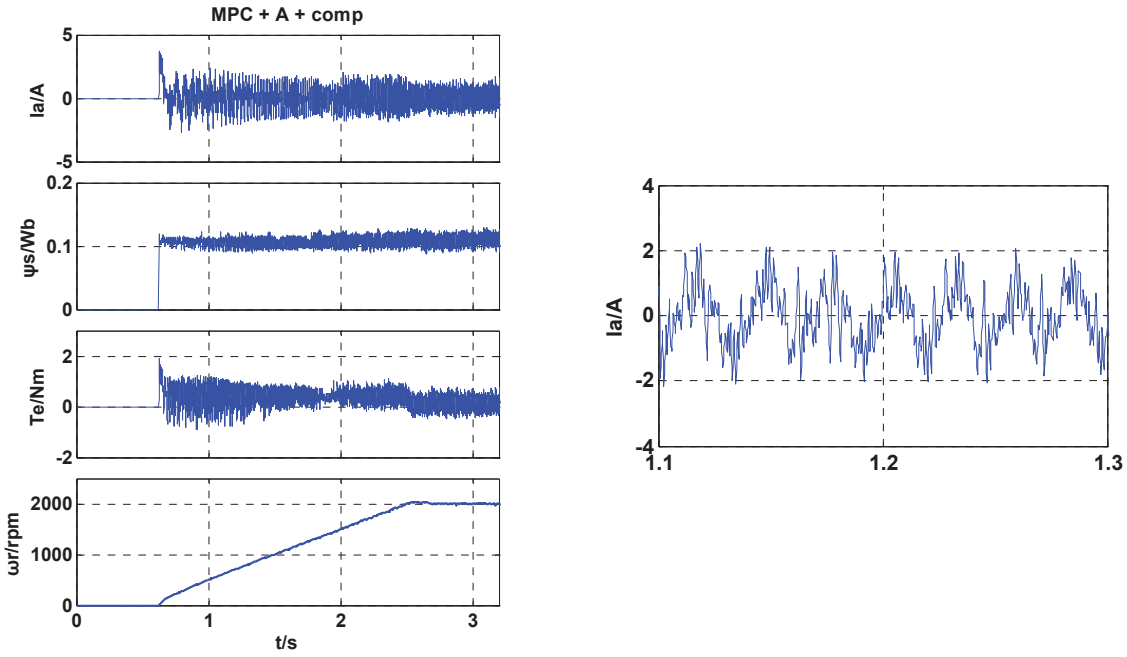

Fig. 3.45 Start-up response from standstill to 2000 rpm for MPC with both linear multiple horizon prediction and one-step delay compensation

3.5.6 Deceleration test (from 1500rpm to 500 rpm)

In this section, the motor maintains the speed of 1500 rpm from 0s and the reference speed is set to 500 rpm at around 1s. In Figs. 3-46 to 3-50, from top to bottom, the curves are stator current, stator flux, torque and motor speed respectively. By introducing a ramp-up function in the PI controller, all these control methods exhibited excellent performance and the motor speed decreased from 1500 rpm to 500 rpm smoothly.

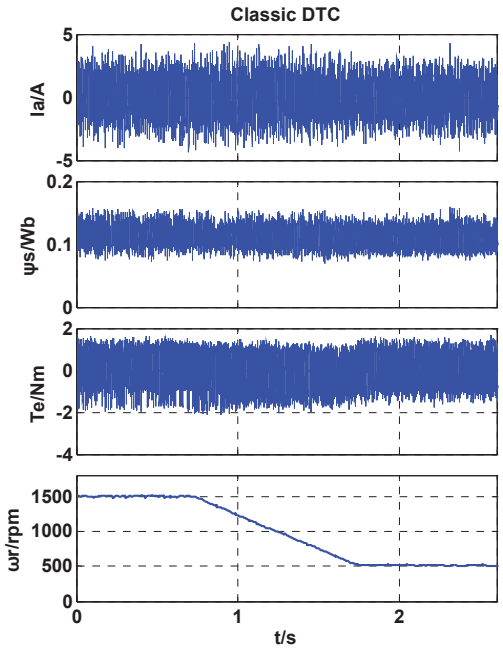

Fig. 3.46 Deceleration test for DTC

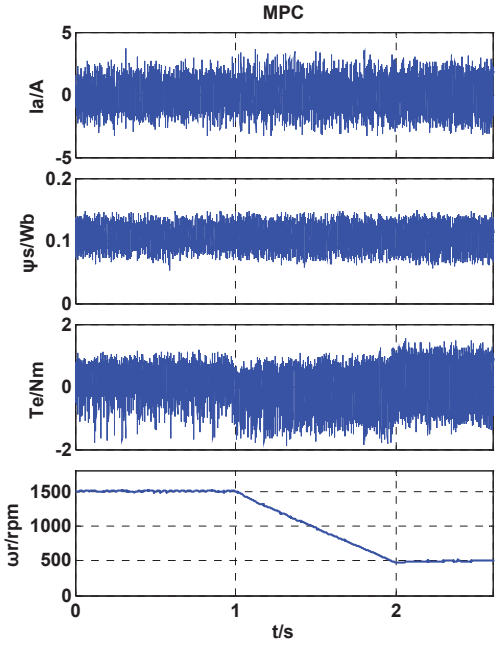

Fig. 3.47 Deceleration test for MPC

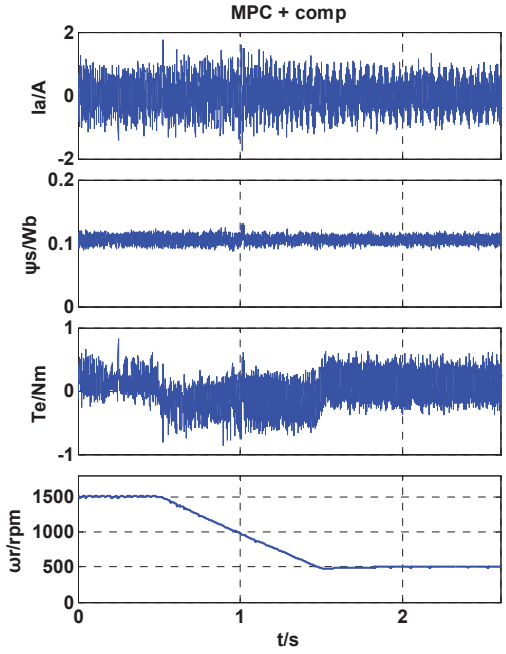

Fig. 3.48 Deceleration test for MPC with one-step delay compensation

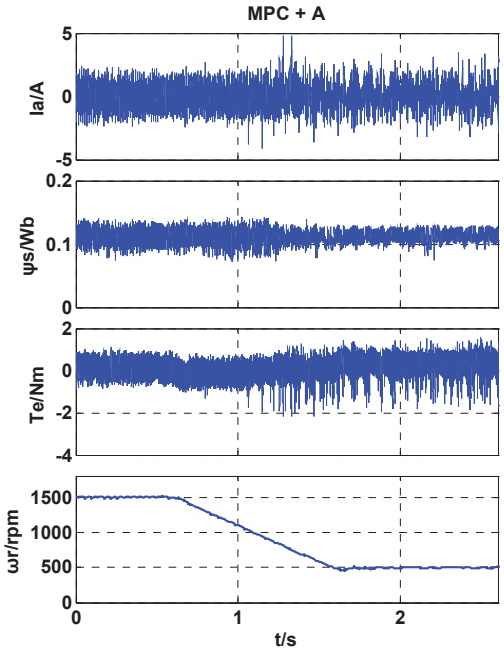

Fig. 3.49 Deceleration test for MPC with both linear multiple horizon prediction

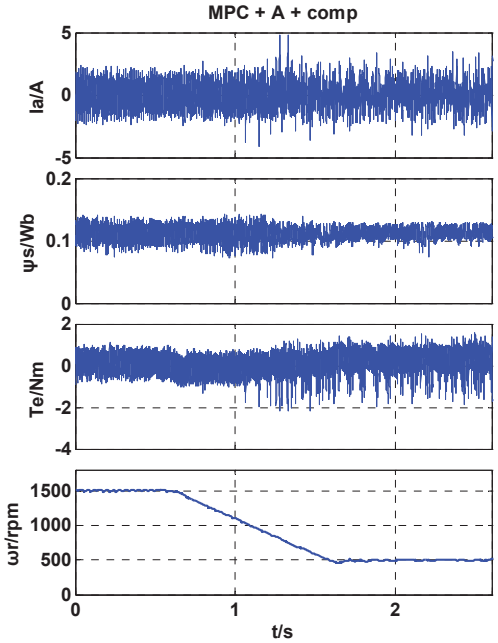

Fig. 3.50 Deceleration test for MPC with both linear multiple horizon prediction and one-step delay compensation

3.5.7 2Nm load test

The section presents the response to external load disturbance of these methods. The motor operates at a steady rate of 1000 rpm and a 2 Nm load is suddenly applied on the shaft. As shown in Figs. 3-51 to 3-55, all these control methods presented good dynamic performance and in a very short period, the motor speed returns to its original value due to the fast torque response. It can be found that the classic DTC spend more than 1s to recover the original speed. For MPC and improved MPCs, the recovery time is less than 0.5s.

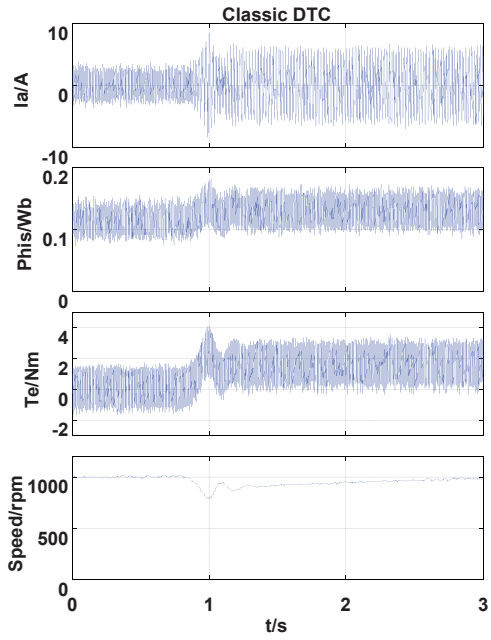

Fig. 3.51 Response to external load for DTC

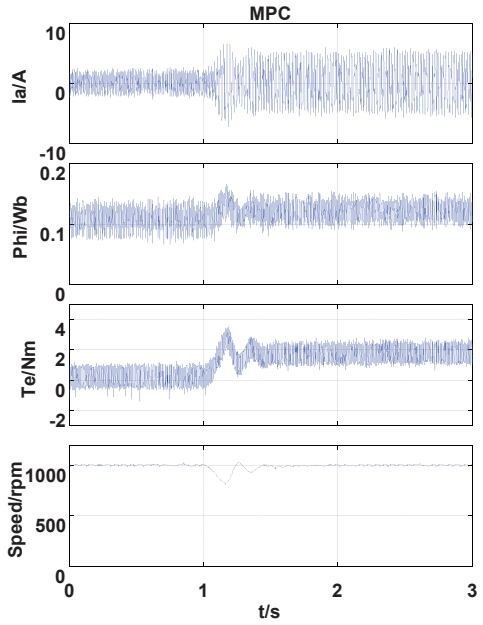

Fig. 3.52 Response to external load for MPC

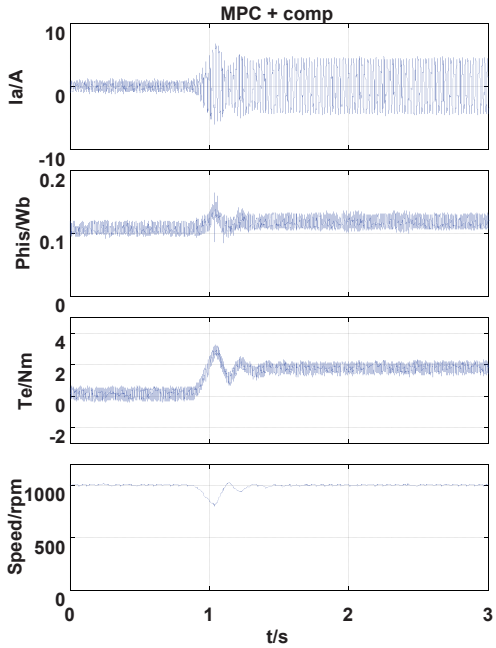

Fig. 3.53 Response to external load for MPC with one-step delay compensation

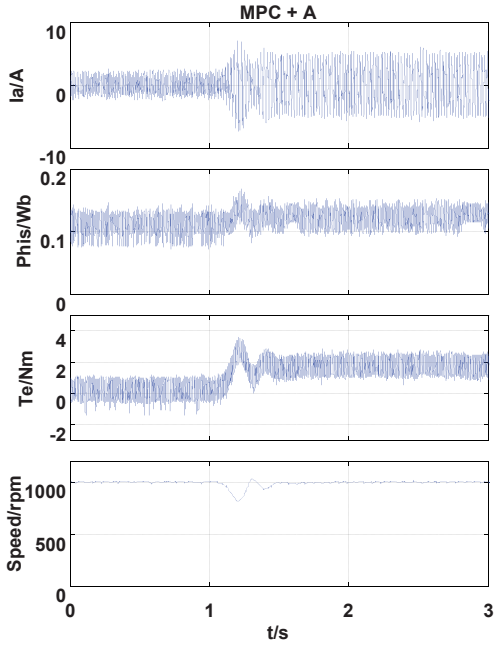

Fig. 3.54 Response to external load for MPC with linear multiple horizon prediction

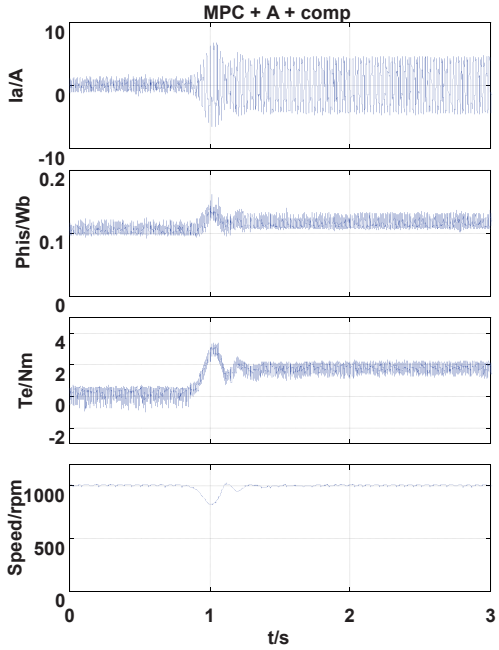

Fig. 3.55 Response to external load for MPC with both linear multiple horizon prediction and one-step delay compensation

3.6 Quantitative Analysis and Comparison of Control Methods

The results of steady-state simulation and experimental tests are summarized in this section.

Group 1

Table 3-2a Steady-state response at 500 rpm (simulation)

Method	THD (%)	f_{av} (Hz)	ψ_{rip} (Wb)	T_{rip} (Nm)
DTC	26.22	1.7411k	0.0151	0.7249
MPC	17.83	1.5200k	0.0150	0.5733
MPC + comp	6.94	0.7320k	0.0059	0.2258
MPC + A	17.86	0.1954k	0.0059	0.8052
MPC + A + comp	11.75	0.1699k	0.0034	0.8527

Table 3-2b Steady-state response at 500 rpm (experimental)

Method	f_{av} (Hz)	ψ_{rip} (Wb)	T_{rip} (Nm)
DTC	1.3989k	0.0166	0.7840
MPC	1.2769k	0.0188	0.6780
MPC + comp	2.4879k	0.0052	0.1985
MPC + A	0.3691k	0.0093	0.6086
MPC + A + comp	0.5117k	0.0049	0.4151

Group 2

Table 3-3a Steady-state response at 1000 rpm (simulation)

Method	THD (%)	f_{av} (Hz)	ψ_{rip} (Wb)	T_{rip} (Nm)
DTC	28.83	1.5972k	0.0155	0.6869
MPC	18.55	1.5692k	0.0138	0.4952
MPC + comp	8.17	1.5812k	0.0059	0.2253
MPC + A	15.52	0.6640k	0.0090	0.5102
MPC + A + comp	11.67	1.3674k	0.0050	0.2493

Table 3-3b Steady-state response at 1000 rpm (experimental)

Method	f_{av} (Hz)	ψ_{rip} (Wb)	T_{rip} (Nm)
DTC	1.2129k	0.0167	0.8446
MPC	1.1393k	0.0173	0.6394
MPC + comp	2.7335k	0.0056	0.2310
MPC + A	0.6045k	0.0136	0.4460
MPC + A + comp	1.2414k	0.0049	0.2644

Group 3

Table 3-4a Steady-state response at 1500 rpm (simulation)

Method	THD (%)	f_{av} (Hz)	ψ_{rip} (Wb)	T_{rip} (Nm)
DTC	20.17	1.2413k	0.0133	0.7191
MPC	17.75	1.4188k	0.0136	0.4432
MPC + comp	10.15	2.0784k	0.0063	0.2103
MPC + A	10.78	0.9834k	0.0095	0.3966
MPC + A + comp	10.45	2.0160k	0.0059	0.2365

Table 3-4b Steady-state response at 1500 rpm (experimental)

Method	f_{av} (Hz)	ψ_{rip} (Wb)	T_{rip} (Nm)
DTC	1.0965k	0.0168	0.8020
MPC	0.9126k	0.0162	0.5084
MPC + comp	2.3440k	0.0069	0.1546
MPC + A	0.7518k	0.0130	0.4581
MPC + A + comp	1.6815k	0.0054	0.1406

Group 4

Table 3-5a Steady-state response at 2000 rpm (simulation)

Method	THD (%)	f_{av} (Hz)	ψ_{rip} (Wb)	T_{rip} (Nm)
DTC	26.80	1.2279k	0.0183	0.9046
MPC	13.13	1.2016k	0.0126	0.5031
MPC + comp	7.70	2.4024k	0.0067	0.2541
MPC + A	13.18	0.9131k	0.0093	0.4193
MPC + A + comp	10.63	2.3611k	0.0064	0.2357

Table 3-5b Steady-state response at 2000 rpm (experimental)

Method	f_{av} (Hz)	ψ_{rip} (Wb)	T_{rip} (Nm)
DTC	0.8774k	0.0165	0.6952
MPC	0.7033k	0.0154	0.4642
MPC + comp	1.8061k	0.0067	0.2380
MPC + A	0.5967k	0.0140	0.4581
MPC + A + comp	1.2798k	0.0065	0.2269

The tests results listed above are discussed in detail:

- **MPC vs. DTC**

From the simulation results, it can be found that the implementation of MPC can reduce the flux ripple by 0.7% (500 rpm), 11.0% (1000 rpm), -2.3% (1500 rpm) and 31.1% (2000 rpm) and reduce the torque ripple by 21.0% (500 rpm), 27.9% (1000 rpm), 38.4% (1500 rpm) and 44.4% (2000 rpm)

From the experimental tests results, it is seen that the implementation of MPC can reduce the flux ripple by -13.3% (500 rpm), -3.6% (1000 rpm), 3.6% (1500 rpm) and 6.7% (2000 rpm) and reduce the torque ripple by 13.5% (500 rpm), 24.3% (1000 rpm), 36.6% (1500 rpm) and 33.2% (2000 rpm)

In conclusion, MPC can achieve lower torque ripple than that of DTC as proven in both simulation and experimental tests. However, MPC's character in flux ripple reduction is quite unstable.

- **MPC+comp vs. MPC**

From the simulation results, it can be found that the implementation of one-step delay compensation can reduce the flux ripple by 60.7% (500 rpm), 57.2% (1000 rpm), 53.7% (1500 rpm) and 46.8% (2000 rpm) and reduce the torque ripple by 60.6% (500 rpm), 54.5% (1000 rpm), 52.5% (1500 rpm) and 49.5% (2000 rpm)

From the experimental tests results, it is seen that the implementation of one-step delay compensation can reduce the flux ripple by 72.3% (500 rpm), 67.6% (1000 rpm), 57.4% (1500 rpm) and 56.5% (2000 rpm) and reduce the torque ripple by 70.7% (500 rpm), 63.9% (1000 rpm), 69.6% (1500 rpm) and 48.7% (2000 rpm)

With the help of one-step delay compensation, the steady-state performance of MPC is improved significantly in both simulation and experimental tests. It should be noticed that the switching frequency almost increase by two times in most tests when one-step delay is compensated.

- **MPC+A vs. MPC**

From the simulation results, it can be found that the implementation of linear multiple horizon prediction can reduce the flux ripple by 60.7% (500 rpm), 34.8% (1000 rpm), 30.1% (1500 rpm) and 26.2% (2000 rpm), reduce the torque ripple by -40.5% (500 rpm), -3.0% (1000 rpm), 10.5 % (1500 rpm) and 16.7% (2000 rpm) and reduce the switching frequency by 87.1% (500 rpm), 57.7% (1000 rpm), 30.7 % (1500 rpm) and 24.0% (2000 rpm).

From the experimental tests results, it is seen that the implementation of linear multiple horizon prediction can reduce the flux ripple by 50.5% (500 rpm), 21.4% (1000 rpm), 19.8% (1500 rpm) and 9.1% (2000 rpm), reduce the torque ripple by 9.1%(500 rpm), 30.2% (1000 rpm), 9.9% (1500 rpm) and 1.3% (2000 rpm) and reduce the switching frequency by 71.1% (500 rpm), 46.9% (1000 rpm), 17.6 % (1500 rpm) and 15.2% (2000 rpm).

As shown in above tests analysis, the introduction of linear multiple horizon prediction can effectively reduce the switching frequency and flux ripple. However, its ability of torque ripple reduction is quite insignificant.

- **MPC+A+comp vs. MPC+comp**

From the simulation results, it can be found that the implementation of linear multiple horizon prediction in addition to 'MPC+comp' can reduce the flux ripple by 42.4% (500 rpm), 15.3% (1000 rpm), 6.3% (1500 rpm) and 4.5% (2000 rpm), reduce the torque ripple by -277.6 % (500 rpm), -10.7% (1000 rpm), -12.5% (1500 rpm) and 7.2% (2000 rpm) and reduce the switching frequency by 76.8% (500 rpm), 13.5% (1000 rpm), 3.0 % (1500 rpm) and 1.7% (2000 rpm).

From the experimental tests results, it is seen that the implementation of linear multiple horizon prediction in addition to 'MPC+comp' can reduce the flux ripple by 5.8% (500 rpm), 12.5% (1000 rpm), 21.7% (1500 rpm) and 3.0% (2000 rpm), reduce the torque ripple by -109.1% (500 rpm), -14.4% (1000 rpm), 9.1% (1500 rpm) and 4.7% (2000 rpm) and reduce the switching frequency by 79.4% (500 rpm), 54.6% (1000 rpm), 28.3 % (1500 rpm) and 29.1% (2000 rpm).

By introducing linear multiple horizon prediction to 'MPC+comp', an obvious reduction in switching frequency and a slight decrease in flux ripple can be found. However, it also comes with heavy penalty of torque ripple increasing, especially at low motor speed.

Summary

According to the analysis above, it can be concluded that:

- MPC can achieve lower torque ripple than that of DTC whilst maintaining/reducing the switching frequency as proven in both simulation and experimental tests. However, MPC's ability in flux ripple reduction is insignificant and even unstable.
- When one-step delay is compensated, the steady-state performance of MPC in

terms of torque and flux ripples reduction is significantly improved. It should be noticed that the performance improvement also comes with a remarkable switching frequency increase (two times or more).

- By introducing linear multiple horizon prediction to MPCs, a significant switching frequency reduction can be found as well as an obvious decrease in flux ripple. However, it comes with heavy penalty of torque ripple increasing, especially at low motor speed

3.7 Conclusion

In this chapter, the model-based predictive control is investigated together with the conventional DTC by both simulation and experiment. The one-step delay issue in digital control systems is also investigated and a model-based compensation method is introduced to MPC. It is shown that the MPC provides better steady state performance, similar dynamic response and lower switching frequency under the condition of the same sampling frequency. When the one-step delay is compensated, the performance can be further improved along with the switching frequency increase.

One major merit of MPC is the flexibility of the cost function, i.e. taking other selection criteria into account. In this chapter, the linear multiple horizon prediction method is introduced and verified experimentally. The implementation of this method can greatly reduce the switching frequency whilst maintaining/improving the performance in terms of the torque and flux ripples.

REFERENCES

[3.1] T. M. Jahns, G. B. Kliman, and T. W. Neumann, "Interior permanent-magnet synchronous motors for adjustable-speed drives," *IEEE Trans*. *Ind. Appl.,* vol. IA-22, no. 4, pp. 738 –747, July 1986.

[3.2] D. Casadei, F. Profumo, G. Serra, and A. Tani, "FOC and DTC: two viable schemes for induction motors torque control," *IEEE Trans. Power Electron*., vol. 17, no. 5, pp. 779–787, Sep. 2002.

[3.3] G. S. Buja and M. P. Kazmierkowski, "Direct torque control of PWM inverter-fed AC motors – a survey," *IEEE Trans. Ind. Electron.,* vol. 51, no. 4, pp. 744–757, Aug. 2004.

[3.4] L. Zhong, M. Rahman, W. Hu, and K. Lim, "Analysis of direct torque control in permanent magnet synchronous motor drives," *IEEE Trans. Power Electron*., vol. 12, no. 3, pp. 528 –536, May 1997.

[3.5] Y. Zhang and J. Zhu, "Direct torque control of permanent magnet synchronous motor with reduced torque ripple and commutation frequency," *IEEE Trans. Power Electron*., vol. 26, no. 1, pp. 235 –248, 2011.

[3.6] J. Holtz, J. Quan, J. Pontt, J. Rodriguez, P. Newman, and H. Miranda, "Design of fast and robust current regulators for high-power drives based on complex state variables," *IEEE Trans. Ind. Appl.*, vol. 40, no. 5, pp. 1388 – 1397, Sept.-Oct. 2004.

[3.7] Y. Zhang and J. Zhu, "A novel duty cycle control strategy to reduce both torque and flux ripples for dtc of permanent magnet synchronous motor drives with switching frequency reduction," *IEEE Trans. Power Electron*., vol. 26, no. 10, pp. 3055–3067, 2011.

[3.8] Y. Zhang, J. Zhu, W. Xu, and Y. Guo, "A simple method to reduce torque ripple

in direct torque-controlled permanent-magnet synchronous motor by using vectors with variable amplitude and angle," *IEEE Trans. Ind. Electron*., vol. 58, no. 7, pp. 2848–2859, 2011.

[3.9] Y. Zhang, J. Zhu, and W. Xu, "Analysis of one step delay in direct torque control of permanent magnet synchronous motor and its remedies," *in Proc. Int Electrical Machines and Systems (ICEMS) Conf,* 2010, pp. 792–797.

[3.10] J. Holtz and S. Stadtfeld, "A predictive controller for the stator current vector of ac machines fed from a switched voltage source," *in Proc. IPEC*, 1983, pp. 1665–1675.

[3.11] P. Cortes, M. Kazmierkowski, R. Kennel, D. Quevedo, and J. Rodriguez, "Predictive control in power electronics and drives," *IEEE Trans. Ind. Electron*., vol. 55, no. 12, pp. 4312 –4324, Dec. 2008.

[3.12] A. Beccuti, S. Mariethoz, S. Cliquennois, S. Wang, and M. Morari, "Explicit model predictive control of dc-dc switched-mode power supplies with extended kalman filtering," *IEEE Trans. Ind. Electron*., vol. 56, no. 6, pp. 1864 –1874, June 2009.

[3.13] S. Kouro, P. Cortes, R. Vargas, U. Ammann, and J. Rodriguez, "Model predictive control—a simple and powerful method to control power converters," *IEEE Trans. Ind. Electron*., vol. 56, no. 6, pp. 1826 –1838, June 2009.

[3.14] J. Rodriguez, R. M. Kennel, J. R. Espinoza, M. Trincado, C. A. Silva, and C. A. Rojas, "High-performance control strategies for electrical drives: An experimental assessment," *IEEE Trans. Ind. Electron*., vol. 59, no. 2, pp. 812–820, 2012.

[3.15] T. Geyer, G. Papafotiou, and M. Morari, "Model predictive direct torque control -part I: Concept, algorithm, and analysis," *IEEE Trans. Ind. Electron*., vol. 56, no. 6, pp. 1894 –1905, June 2009.

[3.16] Y. Zhang, J. Zhu, and W. Xu, "Predictive torque control of permanent magnet synchronous motor drive with reduced switching frequency," *in Proc. Int Electrical Machines and Systems (ICEMS) Conf*, 2010, pp. 798–803.

[3.17] P. Cortes, J. Rodriguez, C. Silva, and A. Flores, "Delay compensation in model predictive current control of a three-phase inverter," *IEEE Trans. Ind. Electron*., vol. 59, no. 2, pp. 1323–1325, 2012.

[3.18] H. Miranda, P. Cortes, J. Yuz, and J. Rodriguez, "Predictive torque control of induction machines based on state-space models," *IEEE Trans. Ind. Electron*., vol. 56, no. 6, pp. 1916 –1924, June 2009.

[3.19] R. Vargas, P. Cortes, U. Ammann, J. Rodriguez, and J. Pontt, "Predictive control of a three-phase neutral-point-clamped inverter," *IEEE Trans. Ind. Electron*., vol. 54, no. 5, pp. 2697 –2705, Oct. 2007.

[3.20] G. Papafotiou, J. Kley, K. Papadopoulos, P. Bohren, and M. Morari, "Model predictive direct torque control-part II: Implementation and experimental evaluation," *IEEE Trans. Ind. Electron*., vol. 56, no. 6, pp. 1906 –1915, June 2009.

[3.21] P. Vas, *Electrical Machines and Drives: A Space-Vector Theory Approach*. New York: Oxford University Press, 1992.

[3.22] R. H. Park, "Definition of an Ideal Synchronous Machine and Formula for the Armature Flux Linkages," *General Electric Review,* vol. 31, p. 332, 1928.

CHAPTER 4
MODEL PREDICTIVE CONTROL WITH DUTY RATIO OPTIMIZATION

4.1 Introduction

The field oriented control (FOC) and direct torque control (DTC) are the most popular control schemes for high performance AC drives [4.1]-[4.3]. Compared with FOC, the merits of DTC are its simple structure, rapid dynamic response and strong robustness against motor parameter variation [4.4]-[4.6]. However, the conventional DTC also presents some disadvantages, such as large torque and flux ripples, variable switching frequency, and excessive acoustic noises.

To overcome these problems, many methods have been proposed in the literature. Some of them employ the space vector modulation (SVM) to DTC, known as SVM-DTC. In the conventional DTC, the switching table only includes a limited number of voltage vectors with fixed amplitudes and positions. The implementation of SVM enables the generation of an arbitrary voltage vector with any amplitude and position [4.7]-[4.9]. In this way, SVM-DTC can generate the torque and flux more accurately. Another merit of using SVM is that the sampling frequency does not need to be as high as that of the conventional DTC.

Another approach is to introduce duty cycle control to the conventional DTC. By adjusting the duty ratio of the active voltage vector in each sampling period, the torque and flux ripples can be greatly reduced. The key issue of this method is the determination of duty ratio. Numerous schemes have been proposed recently to obtain the duty ratio and these differ in vector numbers and optimization goals [4.10]-[4.17]. In [4.10]-[4.12]. The duty ratio is determined by analytical calculation which aims at minimizing the root mean square (RMS) value of torque ripples. The fuzzy logic adaption was introduced in [4.15]. Some of them aim at equalizing the torque with the

reference value over one sampling period [4.13], [4.14]. For the methods in [4.10]-[4.15], they only considered the torque ripple reduction and failed to take the flux ripple reduction into account. Although the effectiveness of these methods has been validated, they are usually complicated and rely heavily on the knowledge of machine parameters. To reduce both torque and flux ripples, a novel strategy using two active vectors and one null vector was proposed in [4.16] for the doubly fed induction generator (DFIG). This method needs two switching tables (one for dynamic process and the other for steady state operation). The details of the machine parameters are also needed to calculate the torque slope. The complexity of the drive system is increased along with the deterioration of the system's robustness. Recently a very simple but effective method was proposed in [4.17]. It reduces both torque and flux ripples and does not require the knowledge of machine parameters for duty ratio calculation. The effectiveness of this method is validated on a PMSM DTC drive [4.17].

The conventional DTC and MPC are similar in that they both select only one voltage vector in each sampling period. However, their selection rules are different and MPC is more advanced and accurate. In this chapter, a novel control scheme is proposed, which is a combination of MPC and the duty determination method proposed in [4.17].

The proposed MPC drive system can achieve much lower torque and flux ripples than the original MPC and DTC, especially at a low system sampling frequency. This is a very desirable feature for high power applications (e.g. electric vehicles). Both simulation and experimental results will be presented to confirm its effectiveness.

In addition, all these control methods mentioned above (the conventional DTC, MPC and MPC with duty ratio optimization) are tested under a wide system sampling frequency range (from 1.5 kHz to 20 kHz).

4.2 Model Predictive Control with Duty Ratio Optimization

The machine model introduced in Chapter 3 is repeated here.

$$u_s = R_s i_s + \frac{d\psi_s}{dt} \tag{3.19}$$

$$\psi_s = L_s i_s + \psi_r \tag{3.20}$$

$$T_e = \frac{3}{2} p\psi_s \times i_s = \frac{3}{2} p\left(\psi_{s\alpha} i_{s\beta} - \psi_{s\beta} i_{s\alpha}\right) \tag{3.21}$$

For voltage source inverter-fed MPC, the voltage vector is the sole controllable input variable, and it is desirable to analytically derive the relationship between the torque and voltage vector.

From (3.19) and (3.20), we can get

$$L_s \frac{di_s}{dt} = u_s - R_s i_s - j\omega\psi_r \tag{4.1}$$

From (3.21), the torque differentiation with respect to time *t* is

$$\frac{dT_e}{dt} = \frac{3}{2} p\left(\frac{d\psi_s}{dt} \times i_s + \frac{di_s}{dt} \times \psi_s\right) \tag{4.2}$$

Substituting (3.19), (3.20), and (4.1) into (4.2) and omitting the tedious derivation process, the final torque differentiation is

$$\begin{aligned} L_s \frac{dT_e}{dt} &= -R_s T_e - \frac{3}{2} p\omega\psi_r \cdot \psi_s + \frac{3}{2} p\psi_r \times u_s \\ &= \Delta T_1 + \Delta T_2 + \Delta T_3 \end{aligned} \tag{4.3}$$

It is seen from (4.3) that the torque differentiation is comprised of three parts, similar to the case in the induction machine [4.16]. The first part ΔT_1 is always negative with respect to T_e, and the second part is also negative and proportional to rotor speed. The last term is a positive one reflecting the effect of stator voltage on T_e. When the zero voltage vector is selected, the torque differentiation becomes

$$L_s \frac{dT_e}{dt} = -R_s T_e - \frac{3}{2} p\omega\psi_r \cdot \psi_s \tag{4.4}$$

indicating that the zero voltage vector always decreases the torque.

In the conventional MPC, the selected voltage vector works during the whole sampling period. In many cases, it is not necessary to work for the entire period to meet the performance requirement of torque and flux. This is one of the main reasons for the torque and flux ripples. By introducing a null vector to each sampling period, the effects of voltage on torque can be adjusted to be more moderate, in order to diminish the ripples of torque and flux.

From (4.3), it can be observed that the torque can be changed by adjusting the amplitude and time duration of u_s. The amplitude is decided by the DC bus voltage and is usually fixed, while the time duration of u_s can be varied from zero to the whole period, which is equivalent to changing the voltage vector length. The null vector only decreases the torque, as shown in (4.4), while appropriate non-zero vectors can increase the torque, and it is possible to employ both null and nonzero vectors during one cycle to reduce the torque ripple. The appropriate non-zero vectors are also referred as ‘active vector’. The key issue is how to determine the time duration of the two vectors, or the duty ratio of the active vector.

The expression of duty ratio for MPC is shown as follows

$$d = \left|\frac{T_e^* - T_e^{k+1}}{C_T}\right| + \left|\frac{\psi_s^* - \psi_s^{k+1}}{C_\psi}\right| \tag{4.5}$$

where d is the duty ratio of the active voltage vector; $T_e^{k+1}\ and\ \psi_s^{k+1}$ are predicted torque and flux values; and C_T and C_ψ the two positive constants.

The idea of this method is that the larger difference between the reference and predicted torque values leads to a larger duty ratio value. The lower C_T and C_ψ value can lead to quicker dynamic response (e.g. take less time to reach the given speed), but poorer steady-state response (e.g. higher torque and flux ripples). Higher values of C_T and C_ψ lead to a better steady-state response, but a slower dynamic response. Therefore, the determination of these values is a compromise between the steady-state and dynamic performances. This phenomenon is deeply investigated in [4.17]. Extensive simulation and experimental results have proven that the permanent magnet flux value and half-rated torque value for C_T and C_ψ can provide a good compromise between the steady state performance and dynamic response.

4.3 Numerical Simulation of DTC and MPC with Duty Ratio Optimization

The parameters of the motor and control system are listed in Table 4-1. The block diagram of the proposed MPC is shown in Fig. 4.1.

Table 4-1

Number of pole pairs	p	3
Permanent magnet flux	ψ_f	0.1057 Wb
Stator resistance	R_s	1.8 Ω
d-axis and q-axis inductance	$L_d,\ L_q$	15 mH
DC bus voltage	V_{dc}	200 V
Inertia	J	0.002 kg · m^2
Torque constant gain	C_T	2
Flux constant gain	C_ψ	0.1
Sampling frequency	f_{sp}	5 kHz

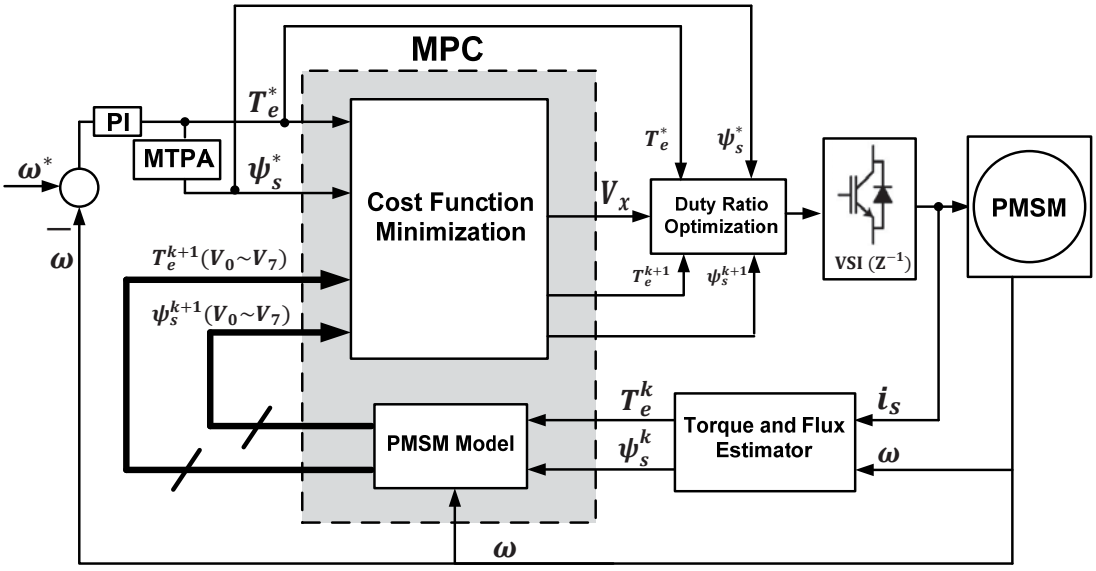

Fig. 4.1 Diagram of a MPC drive system with duty ratio optimization

Motor and control system parameters

4.3.1 Combined simulation test of MPC with duty ratio optimization

This simulation test combines start-up, steady-state and external load tests. The motor starts up from 0s with a reference speed (500 rpm, 1000 rpm, 1500 rpm and 2000 rpm). After reaching the reference speed, the motor maintains this speed for at least 0.2s and an external load is applied at 0.3s. In Figs. 4-2 to 4-5, from top to bottom, the curves are the stator current, stator flux, torque, motor speed, duty ratio and switching frequency, respectively.

The recorded data from 0.1s to 0.3s is picked to calculate the torque and flux ripples (obtained by standard deviations). The torque and flux ripples of these control methods will be summarized in tables in Section 4.5. A segment (three periods) of the stator current of phase A is used to calculate the total harmonic distortion (THD) and current harmonic spectrum.

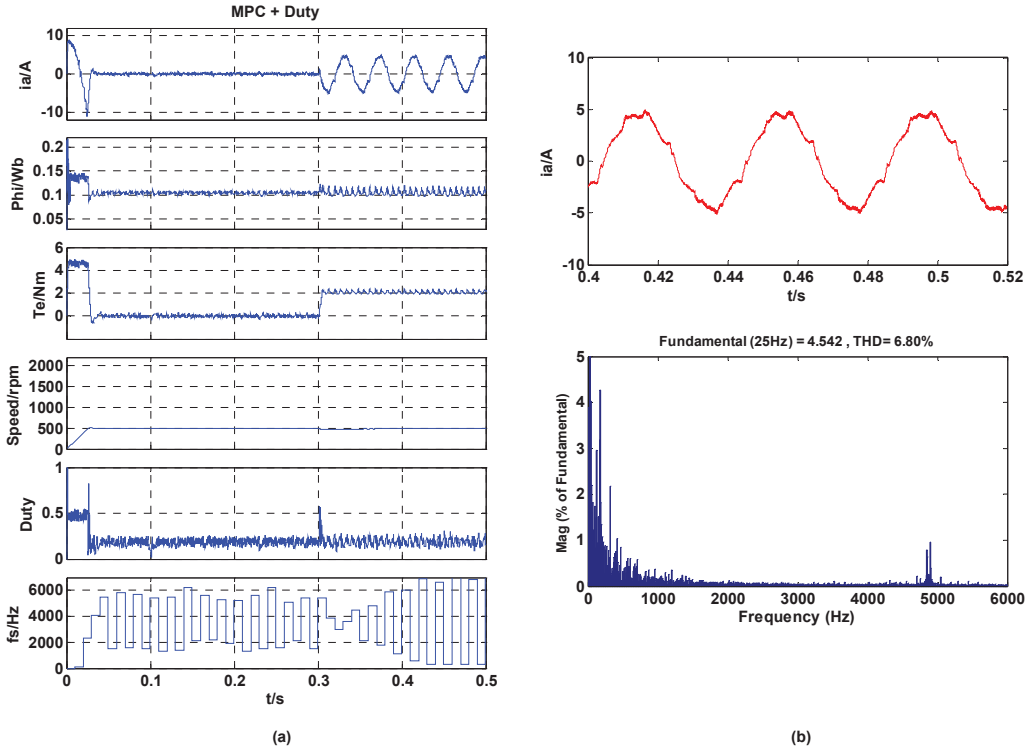

Fig. 4.2 Combined load test for MPC with duty ratio optimization at 500 rpm: (a) start-up, steady-state and external load test, (b) stator current harmonic spectrum

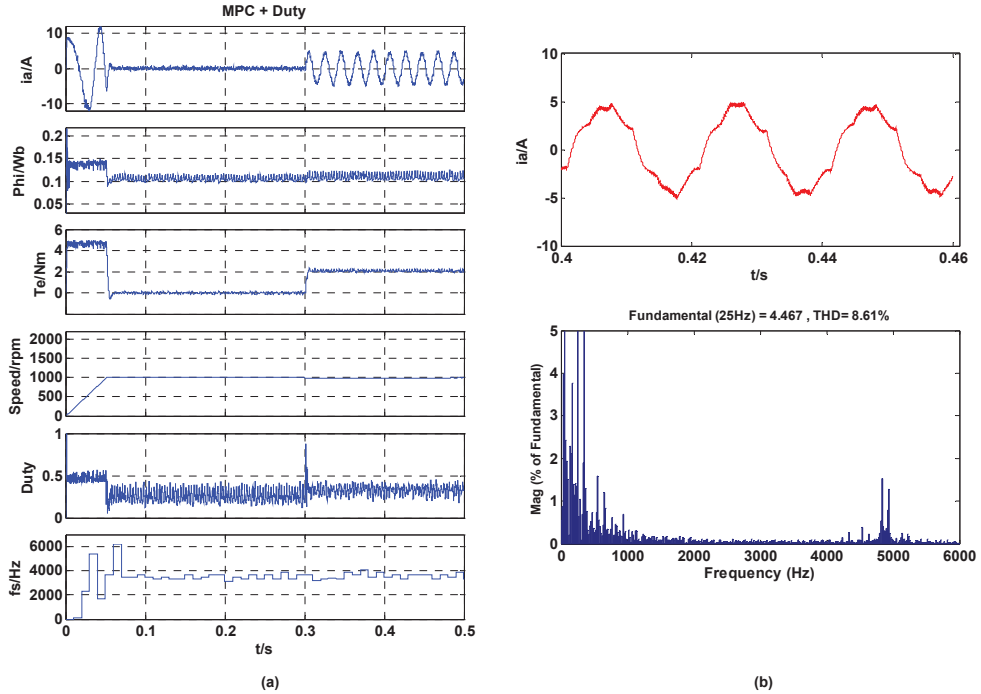

Fig. 4.3 Combined load test for MPC with duty ratio optimization at 1000 rpm: (a) start-up, steady-state and external load test, (b) stator current harmonic spectrum

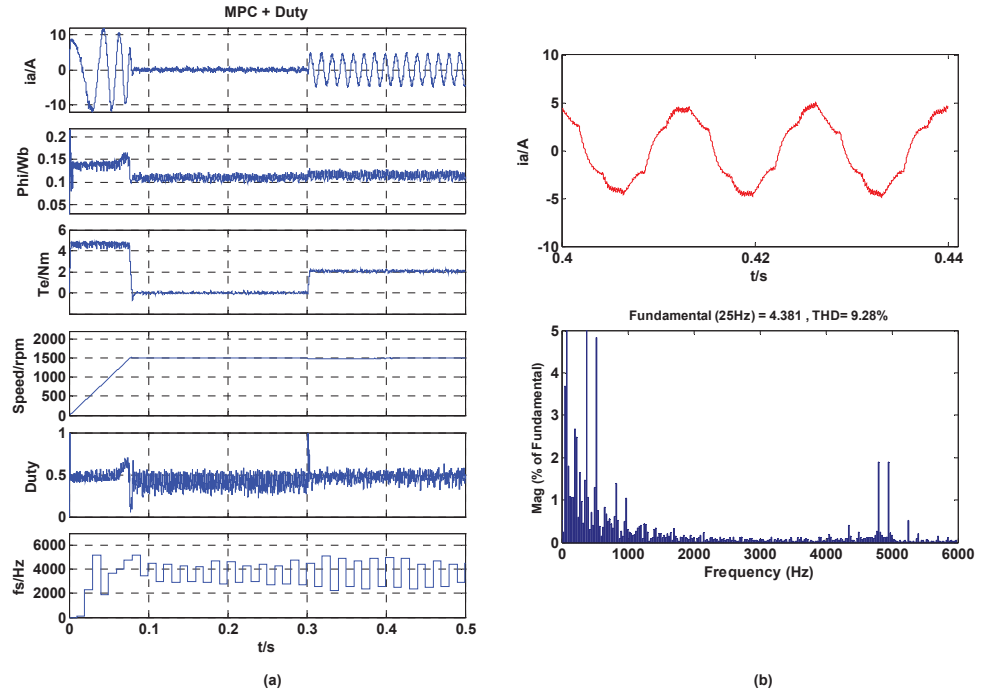

Fig. 4.4 Combined load test for MPC with duty ratio optimization at 1500 rpm: (a) start-up, steady-state and external load test, (b) stator current harmonic spectrum

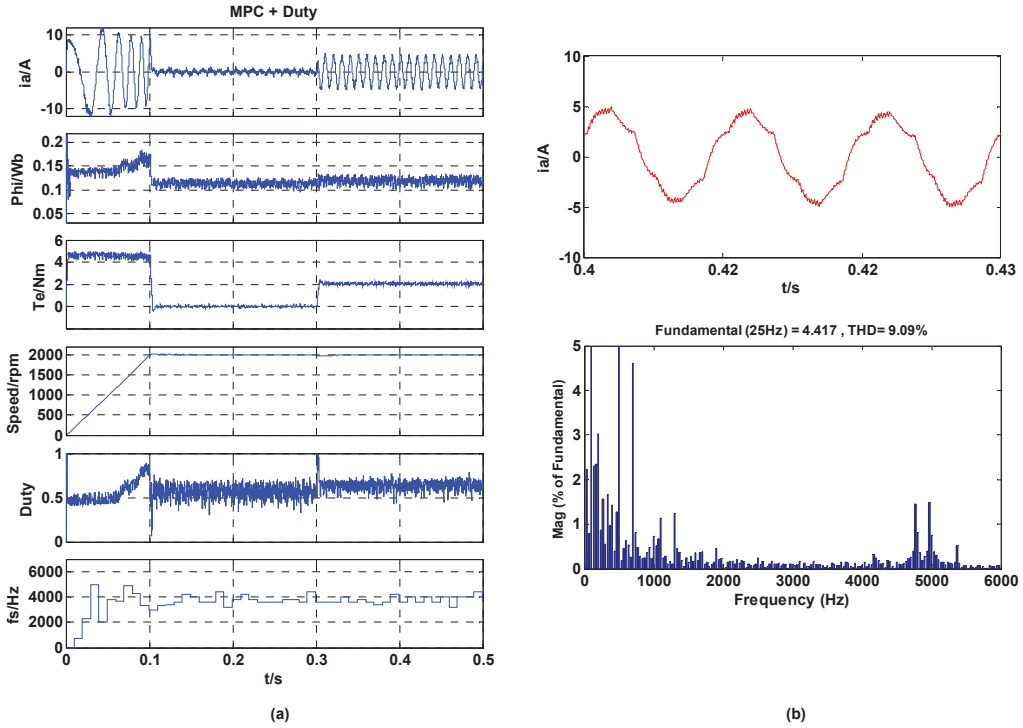

Fig. 4.5 Combined load test for MPC with duty ratio optimization at 2000 rpm: (a) start-up, steady-state and external load test, (b) stator current harmonic spectrum

It can be found that the proposed MPC scheme present very low torque and flux ripples and excellent dynamic response. The proposed MPC scheme also presents very low stator current THDs and narrow harmonic spectrums with the dominant harmonics around 5 kHz.

4.3.2 Reversing test (from 1000rpm to -500 rpm)

In this section, the motor maintain the speed of 1000 rpm from 0s and the reference speed is set to -500 rpm from 0.05s. In Fig. 4-6, from top to bottom, the curves are the stator current, stator flux, torque and motor speed respectively.

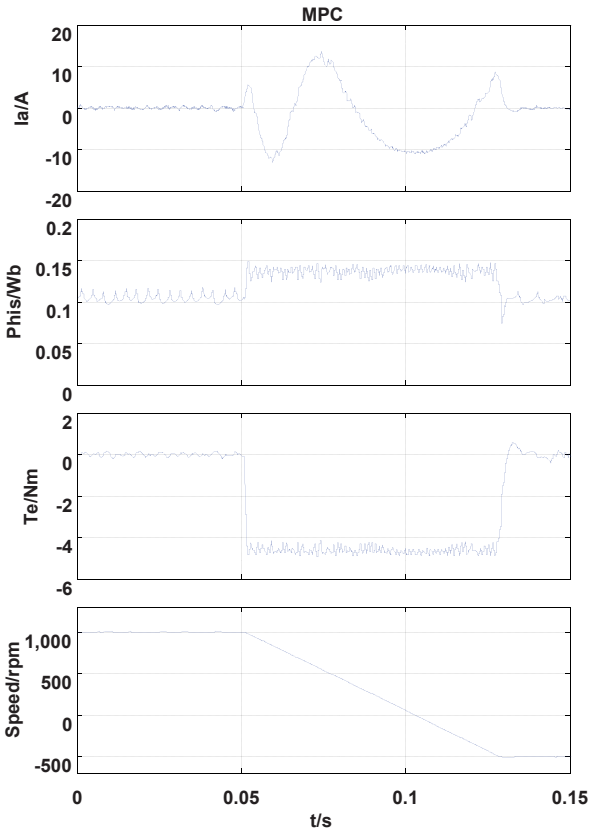

Fig. 4.6 Reversing test for MPC with duty ratio optimization

Fig. 4.6 shows the simulation result of reversing test from +1000 rpm to –500 rpm. As shown, the proposed performed well and the motor speed was reversed within a short time period.

4.4 Experimental Testing of DTC and MPC with Duty Ratio Optimization

The experimental tests are performed on the same testing platform introduced in Chapter 3.

4.4.1 Steady state responses

The steady-state responses at 500 rpm, 1000 rpm, 1500 rpm and 2000 rpm are presented in this section, respectively. In Figs. 4-7 to 4-10, from top to bottom, the curves shown are the torque, stator flux, switching frequency and duty ratio (only for MPC with duty). It is seen that in MPC with duty ratio optimization, the torque and flux ripples are reduced significantly compared to other methods. The duty ratio increases along with the increase in motor speed. The quantitative index of the average switching frequency, stator flux ripple and torque ripple for these tests will be summarized in Section 4.5.

500 rpm

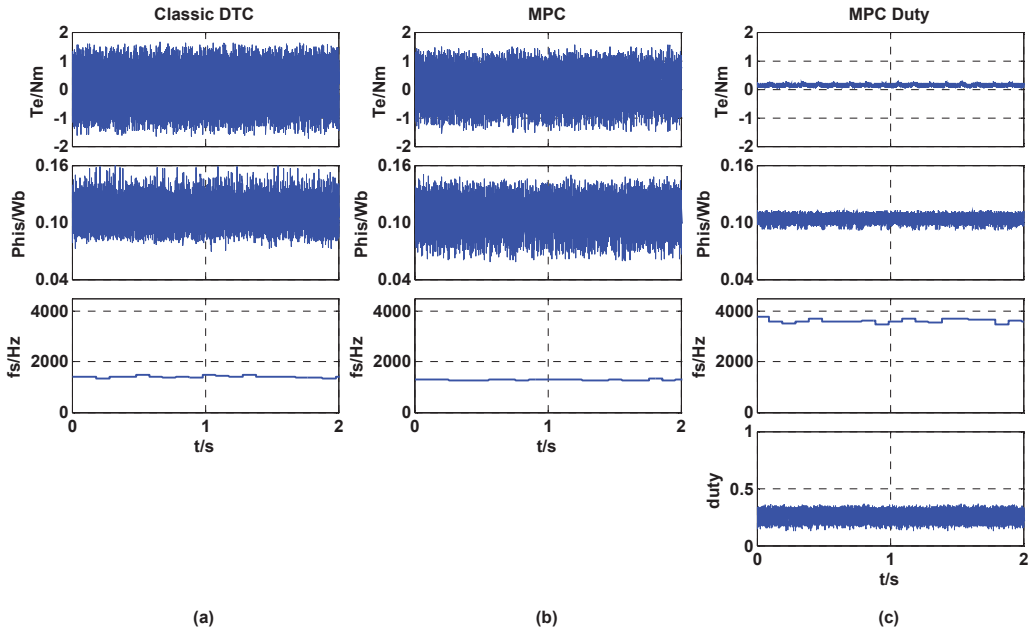

Fig. 4.7 Steady-state response at 500 rpm for: (a) DTC, (b) MPC and (c) MPC with duty ratio optimization

1000 rpm

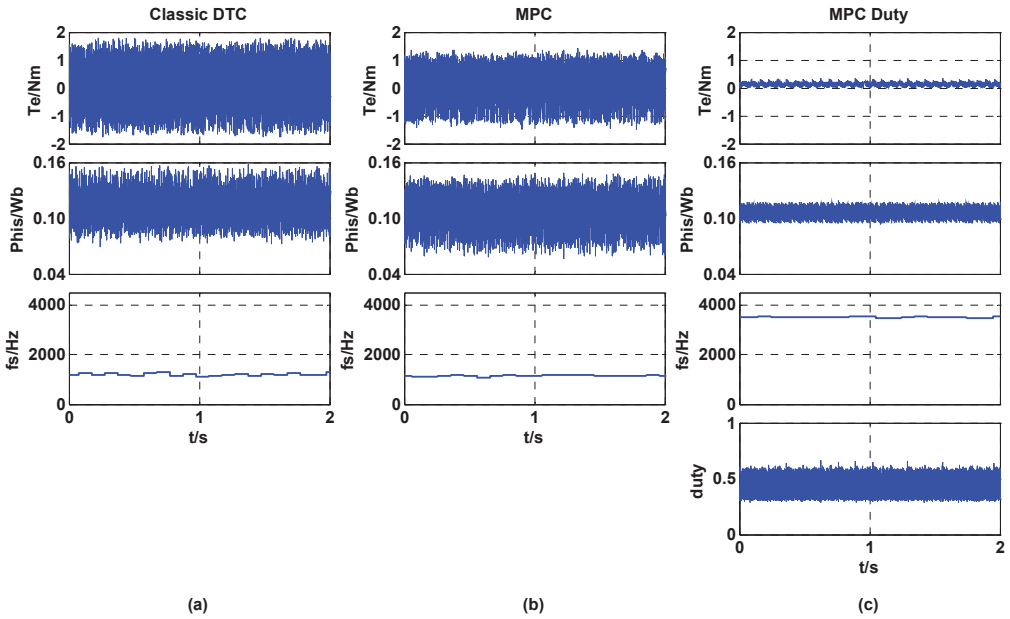

Fig. 4.8 Steady-state response at 1000 rpm for: (a) DTC, (b) MPC and (c) MPC with duty ratio optimization

1500 rpm

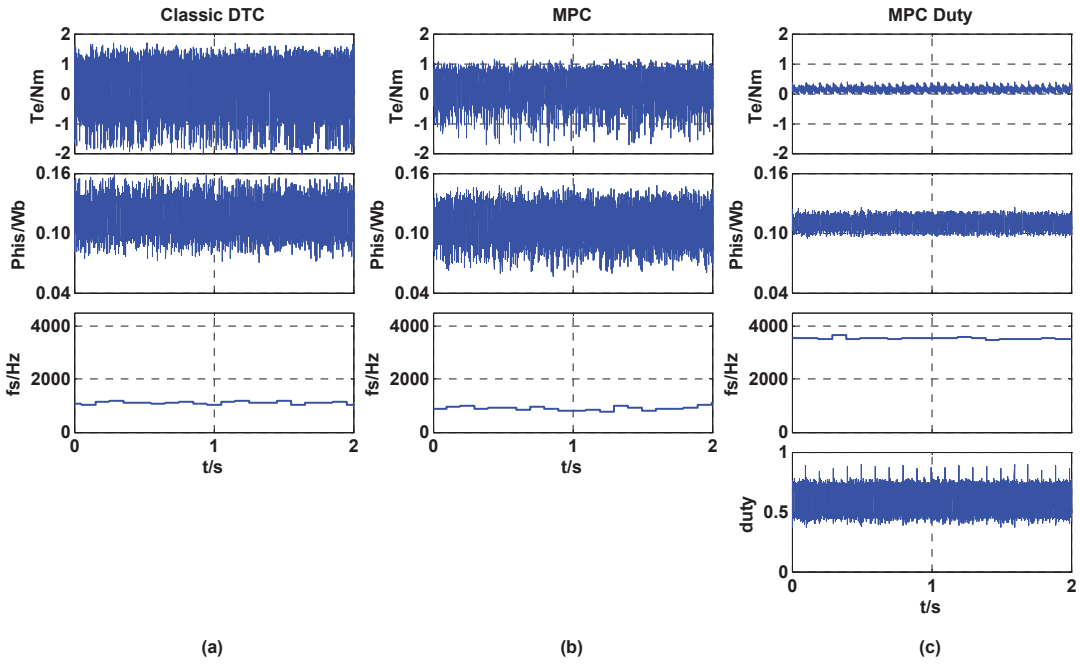

Fig. 4.9 Steady-state response at 1500 rpm for: (a) DTC, (b) MPC and (c) MPC with duty ratio optimization

2000 rpm

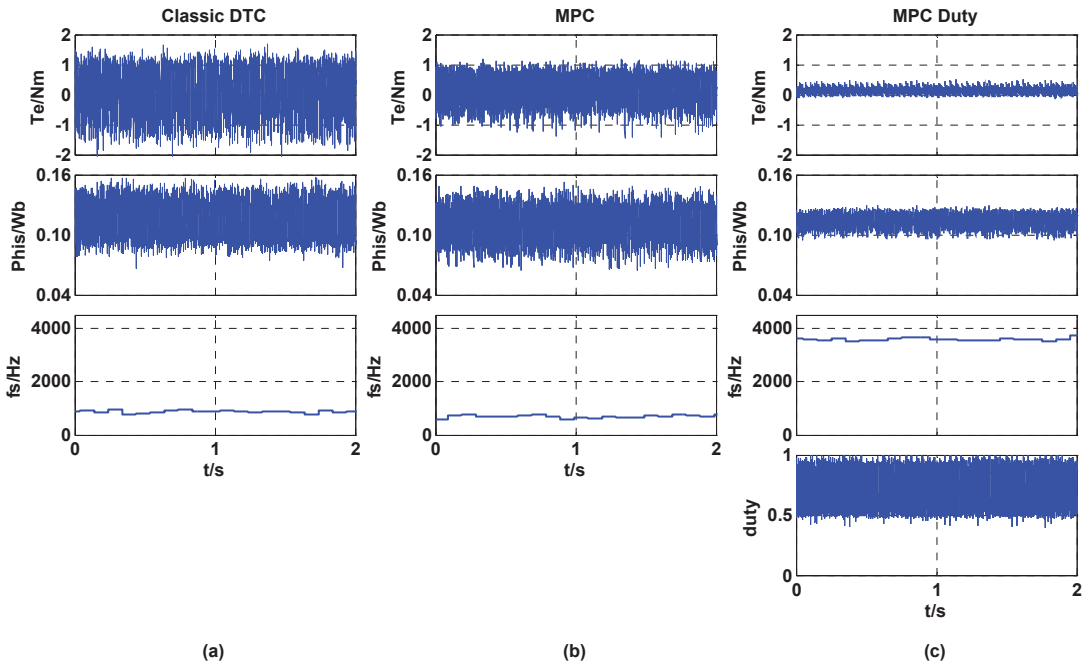

Fig. 4.10 Steady-state response at 2000 rpm for: (a) DTC, (b) MPC and (c) MPC with duty ratio optimization

4.4.2 Dynamic response

In this section, the experimental start-up response is presented in Fig. 4.11. By introducing the ramp-up function in the PI controller, the motor speed accelerates from 0 to 2000 rpm steadily with a small overshoot. From top to bottom, the curves shown are the stator current, stator flux, torque and rotor speed.

The reversing test is presented in Fig. 4.12. The motor maintains the speed of +1000 rpm from 0s and the reference speed is set to –500 rpm at around 0.7s. From top to bottom, the curves are the stator current, stator flux, torque and motor speed respectively. As shown, the proposed method performed well. Within 1.5 s, the motor speed was reversed.

The external load tests are presented in Figs. 4.13 and 4.14. In Fig. 4.13, the motor operates at a steady state of 500 rpm and a 2 Nm load is suddenly applied on the shaft. In Fig. 4.14, the motor operates at a steady state of 1000 rpm and a 1 Nm load is applied.

From these tests it can be found that the motor speed returns to its original value due to the fast response of torque in a very short period.

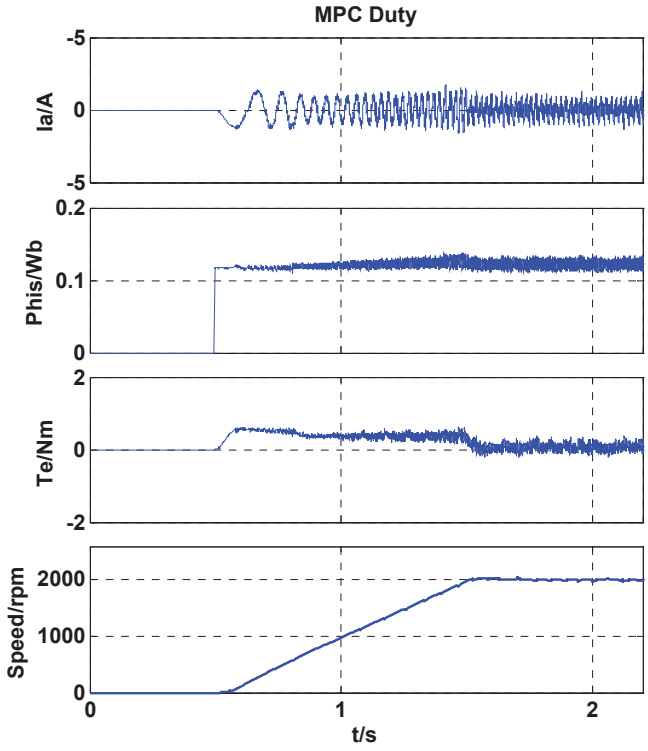

Fig. 4.11 Start-up response from standstill to 2000 rpm for MPC with duty ratio optimization

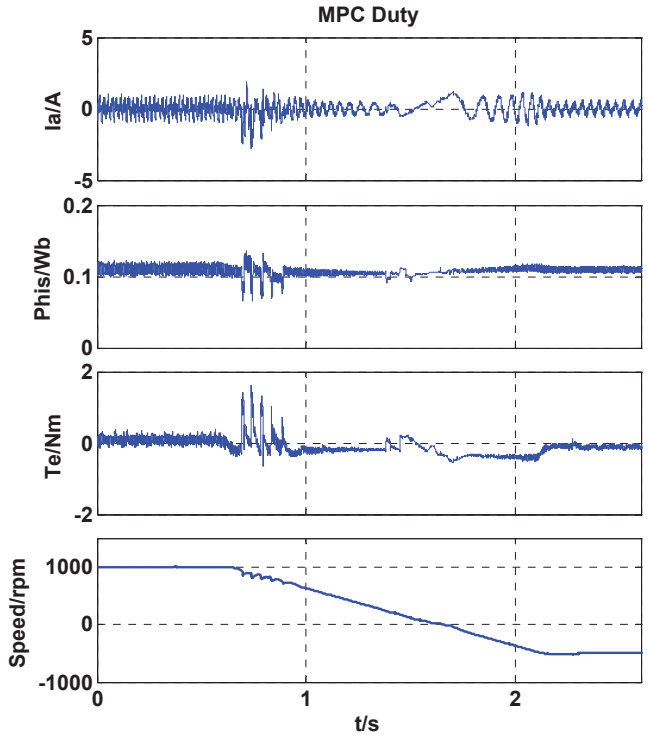

Fig. 4.12 Reversing test for MPC with duty ratio optimization

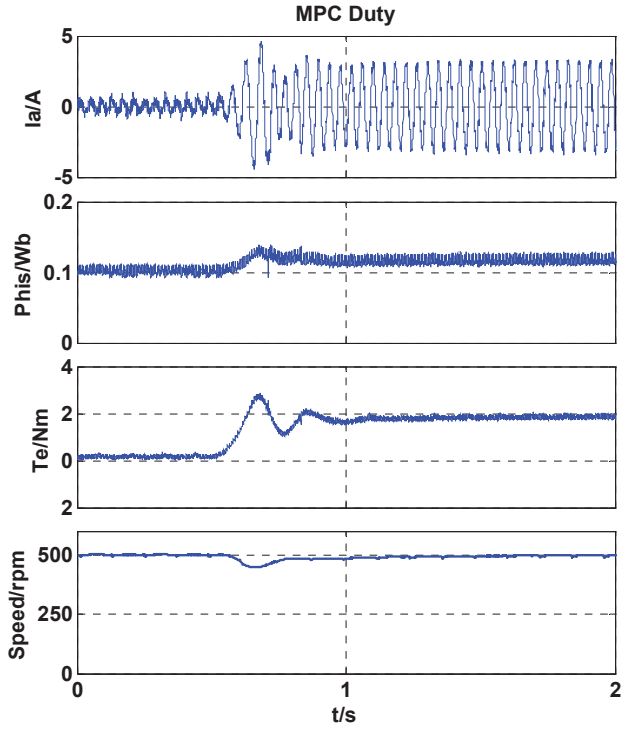

Fig. 4.13 Response to 2 Nm external load at 500 rpm for MPC with duty ratio optimization

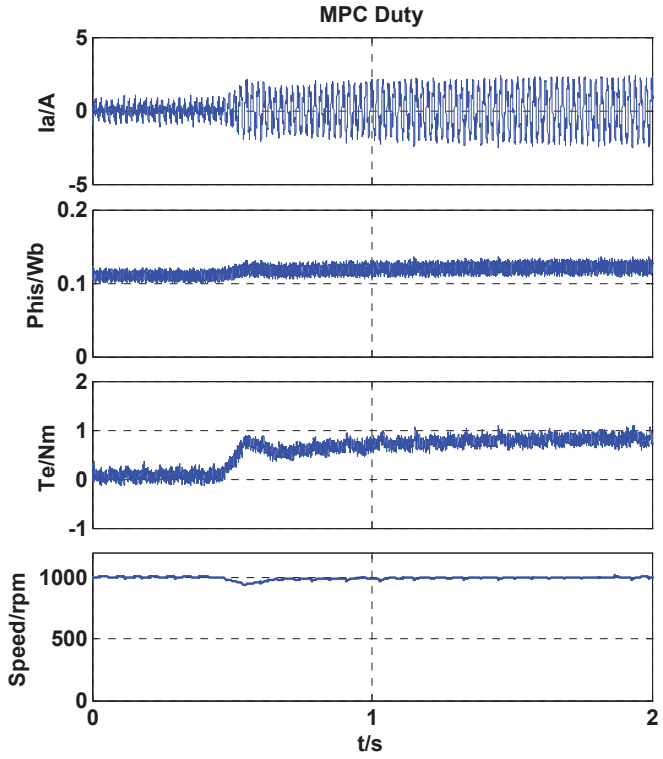

Fig. 4.14 Response to 1 Nm external load at 1000 rpm for MPC with duty ratio optimization

4.5 Comparison of DTC, MPC, and MPC with Duty Ratio Optimization

The results of steady-state simulation and experimental tests are summarized in this section with the results of DTC and MPC copied from Chapter 3.

Group 1

Table 4-2a Steady-state response at 500 rpm (simulation)

Method	THD (%)	f_{av} (Hz)	ψ_{rip} (Wb)	T_{rip} (Nm)
DTC	26.22	1.7411k	0.0151	0.7249
MPC	17.83	1.5200k	0.0150	0.5733
MPC + duty	6.80	3.6534k	0.0020	0.0912

Table 4-2b Steady-state response at 500 rpm (experimental)

Method	f_{av} (Hz)	ψ_{rip} (Wb)	T_{rip} (Nm)
DTC	1.3989k	0.0166	0.7840
MPC	1.2769k	0.0188	0.6780
MPC + duty	3.6107k	0.0046	0.0499

Group 2

Table 4-3a Steady-state response at 1000 rpm (simulation)

Method	THD (%)	f_{av} (Hz)	ψ_{rip} (Wb)	T_{rip} (Nm)
DTC	28.83	1.5972k	0.0155	0.6869
MPC	18.55	1.5692k	0.0138	0.4952
MPC + duty	8.61	3.4989k	0.0047	0.0800

Table 4-3b Steady-state response at 1000 rpm (experimental)

Method	f_{av} (Hz)	ψ_{rip} (Wb)	T_{rip} (Nm)
DTC	1.2129k	0.0167	0.8446
MPC	1.1393k	0.0173	0.6394
MPC + duty	3.5037k	0.0057	0.0649

Group 3

Table 4-4a Steady-state response at 1500 rpm (simulation)

Method	THD (%)	f_{av} (Hz)	ψ_{rip} (Wb)	T_{rip} (Nm)
DTC	20.17	1.2413k	0.0133	0.7191
MPC	17.75	1.4188k	0.0136	0.4432
MPC + duty	9.28	3.6011k	0.0052	0.0671

Table 4-4b Steady-state response at 1500 rpm (experimental)

Method	f_{av} (Hz)	ψ_{rip} (Wb)	T_{rip} (Nm)
DTC	1.0965k	0.0168	0.8020
MPC	0.9126k	0.0162	0.5084
MPC + duty	3.5305k	0.0061	0.0780

Group 4

Table 4-5a Steady-state response at 2000 rpm (simulation)

Method	THD (%)	f_{av} (Hz)	ψ_{rip} (Wb)	T_{rip} (Nm)
DTC	26.80	1.2279k	0.0183	0.9046
MPC	13.13	1.2016k	0.0126	0.5031
MPC + duty	9.09	3.7765k	0.0062	0.0688

Table 4-5b Steady-state response at 2000 rpm (experimental)

Method	f_{av} (Hz)	ψ_{rip} (Wb)	T_{rip} (Nm)
DTC	0.8774k	0.0165	0.6952
MPC	0.7033k	0.0154	0.4642
MPC + duty	3.5791k	0.0070	0.1218

The tests results listed above are discussed in detail:

- **MPC+duty vs. DTC**

From the simulation results, by comparing with DTC, the introduction of duty ratio optimization to MPC can reduce the stator current THD by 74.1% (500 rpm), 70.1% (1000 rpm), 54.0% (1500 rpm) and 66.1% (2000 rpm), reduce the flux ripple by 86.8% (500 rpm), 69.7% (1000 rpm), 60.9 % (1500 rpm) and 66.1% (2000 rpm) and reduce the torque ripple by 87.4% (500 rpm), 88.4% (1000 rpm), 89.4% (1500 rpm) and 92.4% (2000 rpm).

From the experimental tests results, it is seen that the implementation of duty ratio optimization can reduce the flux ripple by 72.3% (500 rpm), 65.9% (1000 rpm), 63.7% (1500 rpm) and 57.6% (2000 rpm) and reduce the torque ripple by 93.6%(500 rpm), 92.3% (1000 rpm), 90.3% (1500 rpm) and 82.5% (2000 rpm).

With the help of duty ratio optimization, a tremendous drop in torque and flux ripples can be seen in both simulation and experimental tests. It also should be noticed that the switching frequency almost increase by three times in most tests.

- **MPC+duty vs. MPC**

From the simulation results, by comparing with MPC, the introduction of duty ratio optimization can reduce the stator current THD by 61.9% (500 rpm), 53.6% (1000 rpm), 47.7% (1500 rpm) and 30.8% (2000 rpm), reduce the flux ripple by 86.7% (500 rpm), 65.9% (1000 rpm), 61.8 % (1500 rpm) and 50.8% (2000 rpm) and reduce the torque ripple by 84.1% (500 rpm), 83.8% (1000 rpm), 84.9% (1500 rpm) and 86.3% (2000 rpm).

From the experimental tests results, it is seen that the implementation of duty ratio optimization can reduce the flux ripple by 75.5% (500 rpm), 67.1% (1000 rpm), 62.3% (1500 rpm) and 54.5% (2000 rpm) and reduce the torque ripple by 92.6%(500 rpm), 89.9% (1000 rpm), 84.7% (1500 rpm) and 73.8% (2000 rpm).

As shown in above tests analysis, a significant decrease in torque and flux ripples can be found as well as a dramatic increase of switching frequency.

Summary

According to the analysis above, it can be concluded that:

- MPC with duty ratio optimization can achieve a better performance than DTC and original MPC in terms of torque and flux ripples reduction;
- Under the same system sampling frequency (5 kHz), the switching frequency of the proposed method is much higher than other methods;
- In DTC and MPC, the switching frequency slightly decreases along with the increase of motor speed. However, the switching frequency is almost stable in the proposed method.

4.6 The Influence of Variable Sampling Frequency on Drive Performance

4.6.1 Simulation test

In this section, the steady-state performance under a wide range of sampling frequency (1.5 kHz – 20 kHz) of the control methods mentioned above is tested numerically in Matlab/Simulink. These simulations are performed at 1000 rpm with no load and the sampling frequencies are set to 1.5 kHz, 2 kHz, 2.5 kHz, 3 kHz, 3.5 kHz, 4 kHz, 4.5 kHz, 5 kHz, 6 kHz, 7 kHz, 8 kHz, 9 kHz, 10 kHz, 12.5 kHz, 15 kHz, 18 kHz and 20 kHz, respectively. The torque ripple is obtained by standard deviations.

In Fig. 4.15, the horizontal axis is the sampling frequency and the vertical axis is the torque ripple. In Fig. 4.16, the horizontal axis is the sampling frequency and the vertical axis is the flux ripple. In the range from 1.5 kHz to 5 kHz, it can be found that the torque and flux ripples reduce rapidly along with the increase of sampling frequency. In the range from 5 kHz to 20 kHz, the trend for the torque and flux ripple reduction is a gradual one.

In Figs. 4.17 and 4.18, the vertical axes are torque ripple and flux ripple, respectively. The horizontal axes in both figures are switching frequency. It can be found that MPC with duty ratio optimization presents smaller torque and flux ripples than the other methods at the same switching frequency.

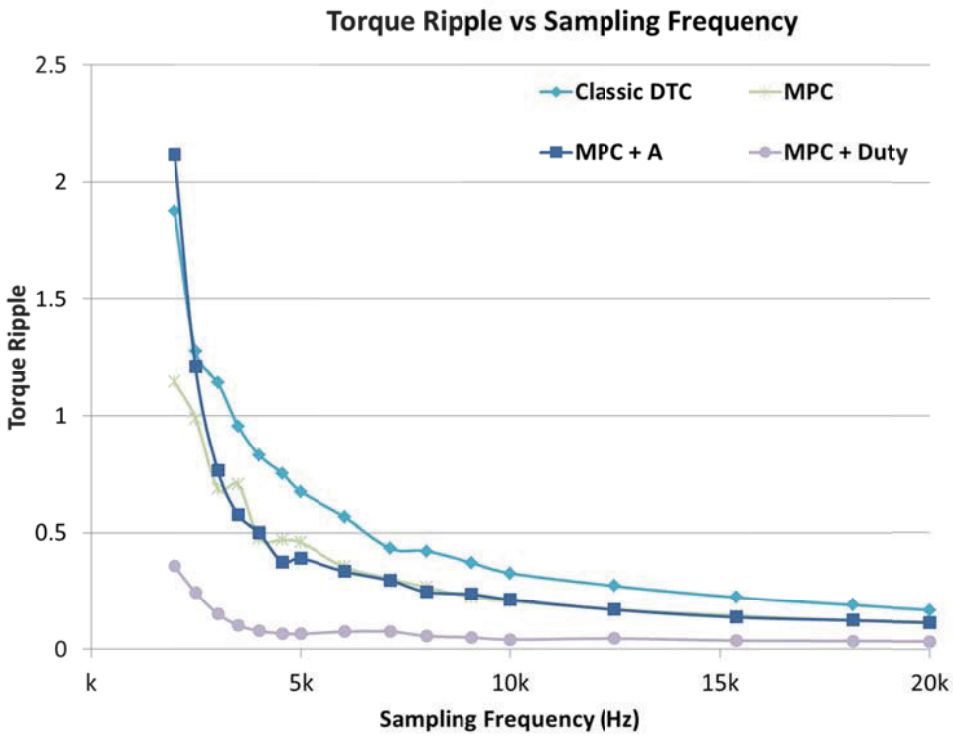

Fig. 4.15 Torque ripple vs. sampling frequency (simulation)

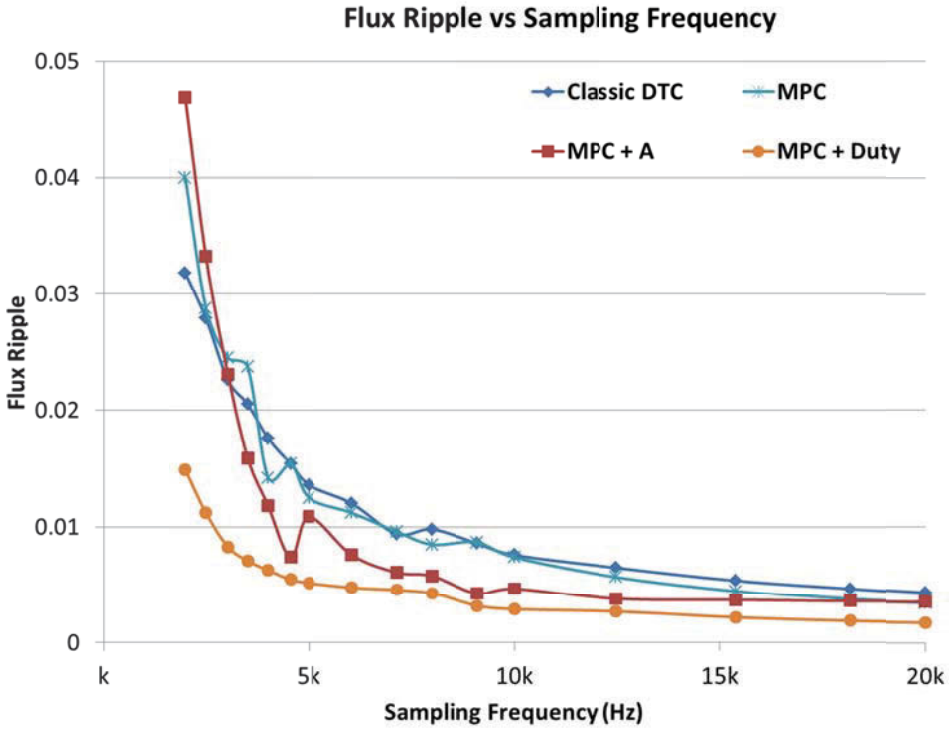

Fig. 4.16 Flux ripple vs. sampling frequency (simulation)

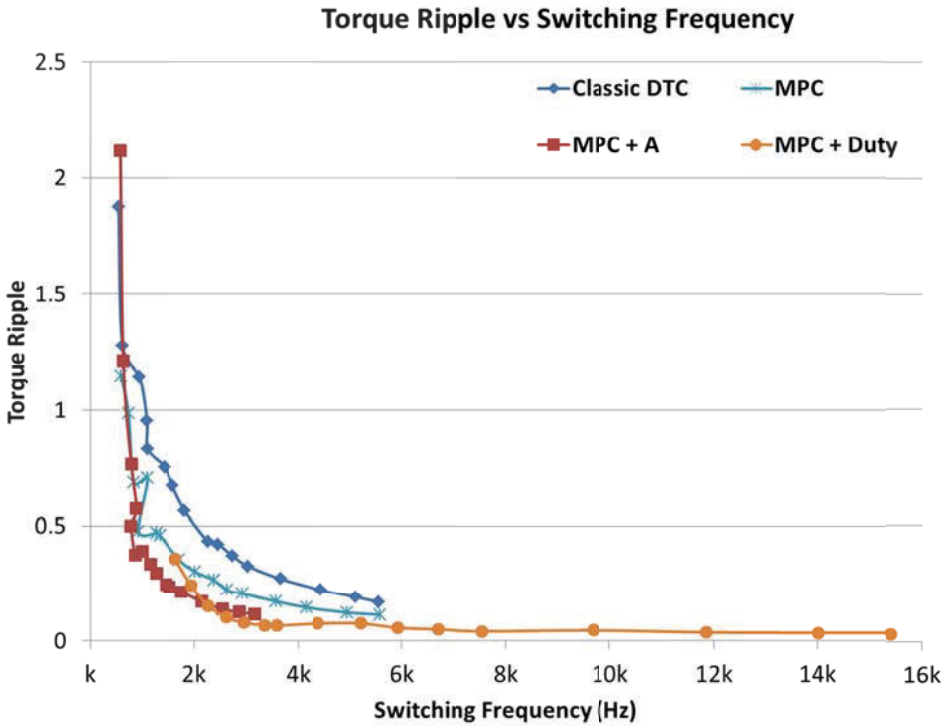

Fig. 4.17 Torque ripple vs. switching frequency (simulation)

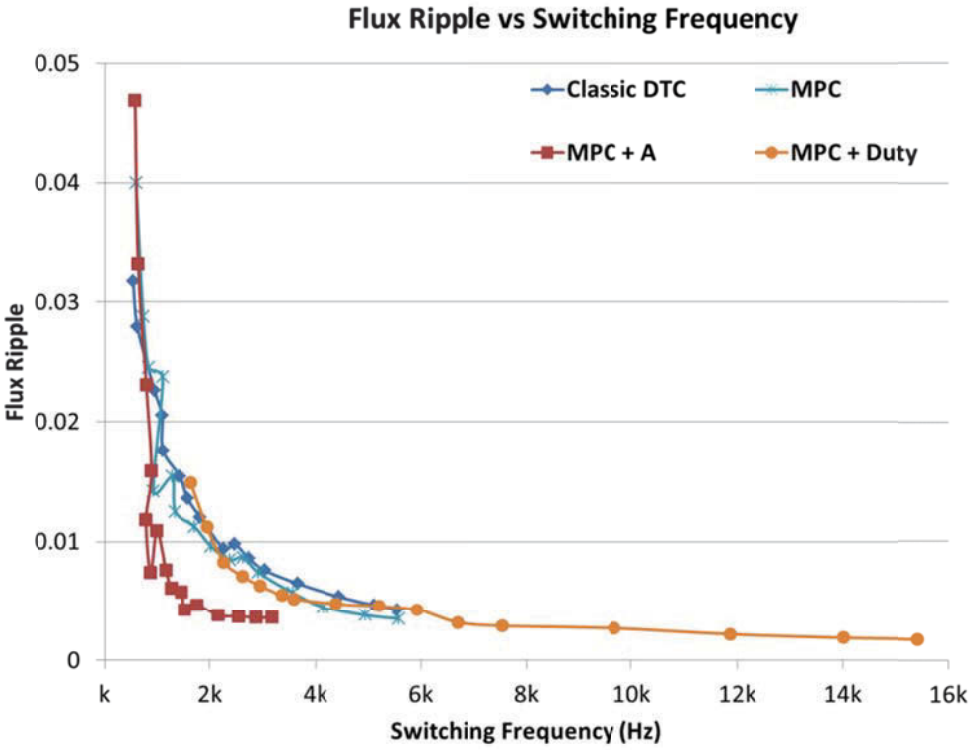

Fig. 4.18 Flux ripple vs. switching frequency (simulation)

4.6.2 Experimental tests

In this section, the steady-state performance under a wide range of sampling frequencies (1.5 kHz – 13 kHz) of the control methods mentioned above is tested in the dSPACE system.

These tests are performed at 1000 rpm with no load and the sampling frequencies are set to 1.5 kHz, 2 kHz, 2.5 kHz, 3 kHz, 3.5 kHz, 4 kHz, 4.5 kHz, 5 kHz, 6 kHz, 7 kHz, 8 kHz, 10 kHz, 11 kHz, 12 kHz and 13 kHz, respectively. Due to the different characteristics of the control methods and limited computational power of the dSPACE system, the actual sampling frequencies that can be achieved by each method are varied. The conventional DTC can work from 1.5 kHz to 13 kHz. For MPC and MPC with duty ratio optimization, the highest frequency that can be achieved is 8 kHz.

In Figs. 4.19 and 4.20, the horizontal axis is the sampling frequency and the vertical axes are the torque ripple and flux ripple, respectively. For DTC and MPC, in the range from 1.5 kHz to 5 kHz, it can be found that the torque and flux ripples reduce rapidly along with the increase of sampling frequency. In the range from 5 kHz to 13 kHz, the trend of the torque and flux ripple reduction is gradual. For MPC with duty ratio optimization, the curve is relatively plain and it lies at the bottom of the figure.

In Figs. 4.21 and 4.22, the horizontal axis is the switching frequency and the vertical axes are the torque ripple and flux ripple, respectively. These figures are more informative than Figs. 4.19 and 4.20 in some extent because the actual switching efficiency is used as the variable. It can be observed that the torque ripples of DTC and MPC decrease dramatically along with the increase of switching frequency. In contrast, the torque ripple reduction of the proposed method seems quite limited.

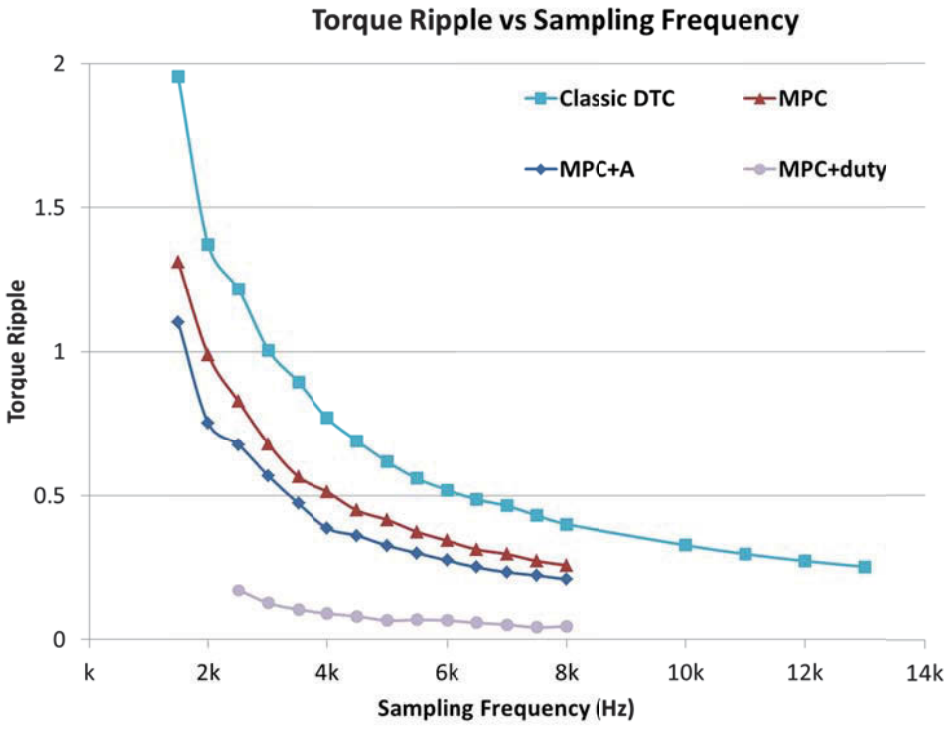

Fig. 4.19 Torque ripple vs. sampling frequency (exprimental)

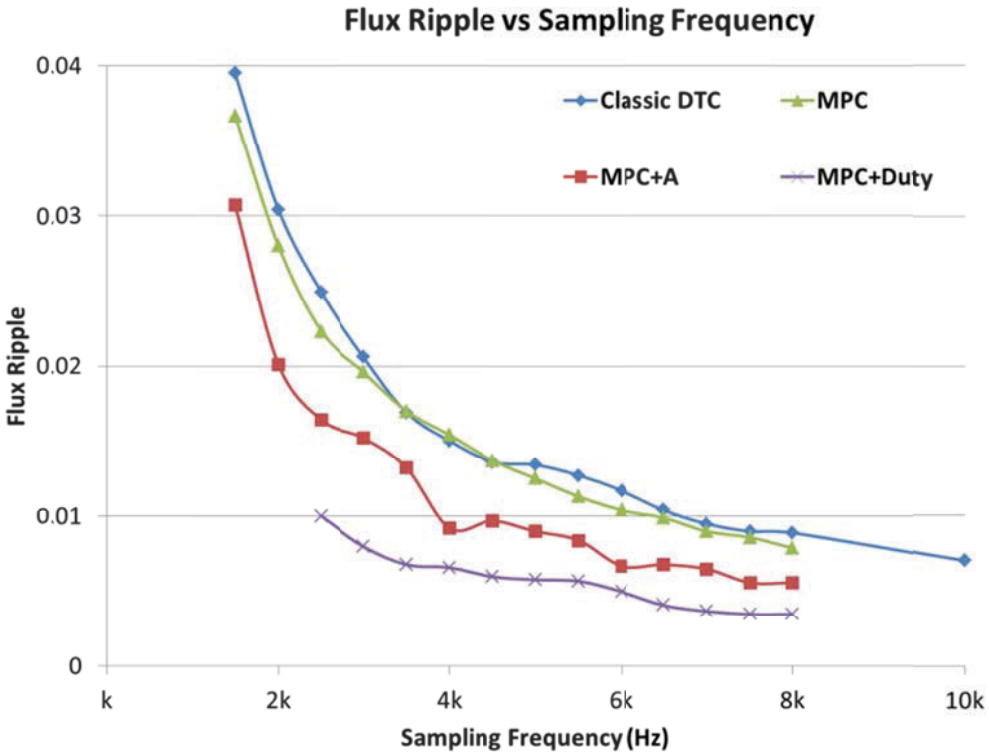

Fig. 4.20 Flux ripple vs. sampling frequency (exprimental)

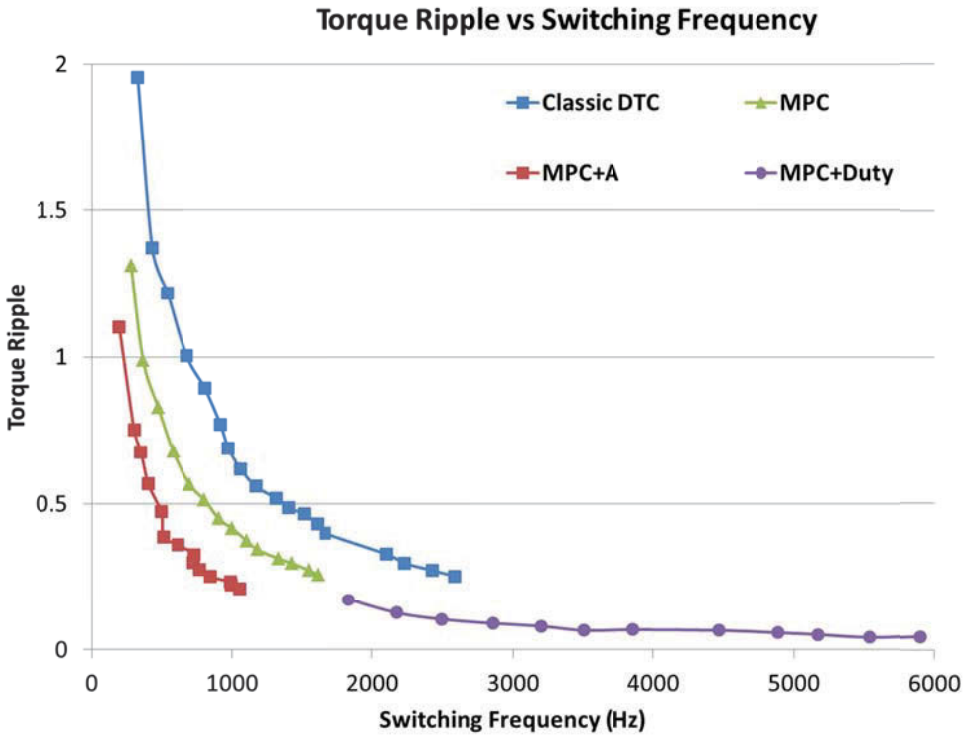

Fig. 4.21 Torque ripple vs. switching frequency (exprimental)

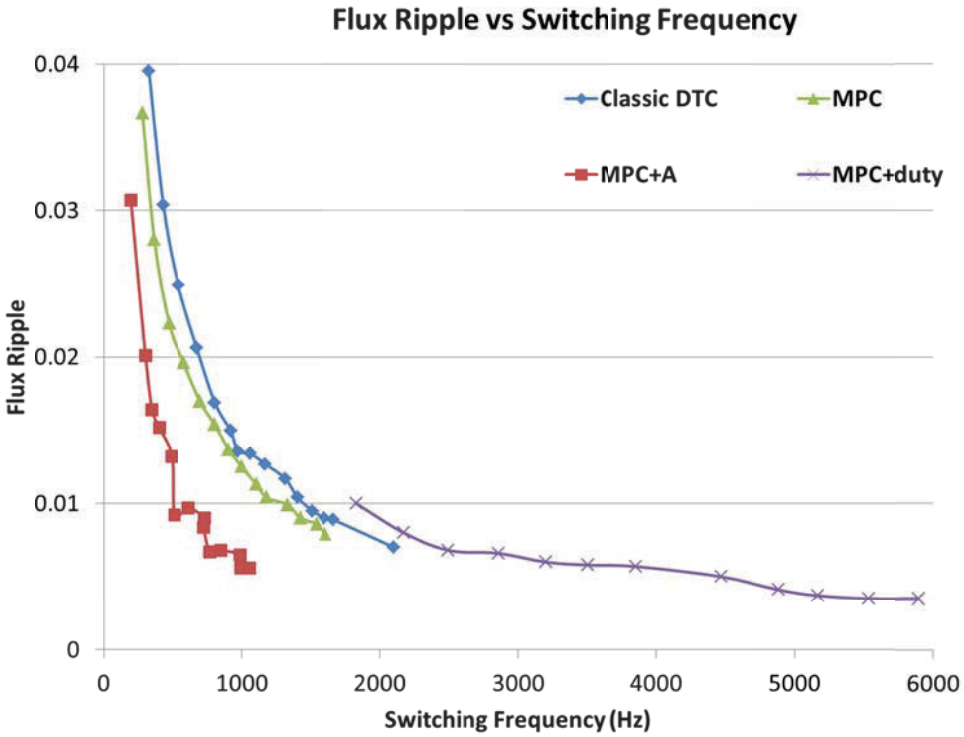

Fig. 4.22 Flux ripple vs. switching frequency (exprimental)

4.7 Conclusion

A model-based predictive control with duty ratio optimization method is proposed in this chapter, in order to reduce both torque and flux ripples. It is achieved by adjusting the duty ratio of the active voltage vector and null voltage vector. As a development of the method introduced in [4.17], the proposed method can achieve a better performance than its predecessor in terms of stator current THD and torque and flux ripples. The effectiveness of the proposed method is confirmed by a comparative study with prior arts using simulation and experimental verification on a PMSM drive.

In addition, the influence of system sampling frequency on the steady-state performance is investigated. The new method even with low sampling frequencies can achieve much smaller torque ripple than DTC and MPC. Its steady-state performance is also much less sensitive to the variation of system sampling frequency.

REFERENCES

[4.1] J. Lee, J. Hong, K. Nam, R. Ortega, L. Praly, and A. Astolfi, "Sensorless control of surface-mount permanent-magnet synchronous motors based on a nonlinear observer," *IEEE Trans. Power Electron.*, vol. 25, no. 2, pp. 290–297, Feb. 2010.

[4.2] S. Y. Kim, W. Lee, M. S. Rho, and S. Y. Park, "Effective dead-time compensation using a simple vectorial disturbance estimator in PMSM drives," *IEEE Trans. Ind. Electron.*, vol. 57, no. 5, pp. 1609–1614, May 2010.

[4.3] F. Genduso, R. Miceli, C. Rando, and G. R. Galluzzo, "Back EMF sensorless-control algorithm for high-dynamic performance PMSM," *IEEE Trans. Ind. Electron.*, vol. 57, no. 6, pp. 2092–2100, Jun. 2010.

[4.4] I. Takahashi and T. Noguchi, "A new quick-response and high-efficiency control strategy of an induction motor," *IEEE Trans. Ind. Appl.*, vol. IA- 22, no. 5, pp. 820–827, Sep. 1986.

[4.5] M. Depenbrock, "Direct self-control (DSC) of inverter-fed induction machine," *IEEE Trans. Power Electron.*, vol. 3, no. 4, pp. 420–429, Oct. 1988.

[4.6] G. S. Buja and M. P. Kazmierkowski, "Direct torque control of PWM inverter-fed AC motors—A survey," *IEEE Trans. Ind. Electron.*, vol. 51, no. 4, pp. 744–757, Aug. 2004.

[4.7] Y.-S. Lai and J.-H. Chen, "A new approach to direct torque control of induction motor drives for constant inverter switching frequency and torque ripple reduction," *IEEE Trans. Energy Convers.*, vol. 16, no. 3, pp. 220– 227, Sep. 2001.

[4.8] C. Lascu and A. Trzynadlowski, "Combining the principles of sliding mode, direct torque control, and space-vector modulation in a high-performance

sensorless ac drive," *IEEE Trans. Ind. Appl.* vol. 40, no. 1, pp. 170–177, Jan./Feb. 2004.

[4.9] Y. Zhang, J. Zhu, W. Xu, J. Hu, D. G. Dorrell, and Z. Zhao, "Speed sensorless stator flux oriented control of three-level inverter-fed induction motor drive based on fuzzy logic and sliding mode control," in *Proc. 36th IEEE IECON*, 2010, pp. 2926–2931.

[4.10] J. K. Kang and S. K. Sul, "New direct torque control of induction motor for minimum torque ripple and constant switching frequency," *IEEE Trans. Ind. Appl.*, vol. 35, no. 5, pp. 1076–1082, Sep./Oct. 1999.

[4.11] K. B. Lee, J. H. Song, I. Choy, and J. Y. Yoo, "Torque ripple reduction in DTC of induction motor driven by three-level inverter with low switching frequency," *IEEE Trans. Power Electron*, vol. 17, no. 2, pp. 255–264, Mar. 2002.

[4.12] K.-K. Shyu, J.-K. Lin, V.-T. Pham, M.-J. Yang, and T.-W. Wang, "Global minimum torque ripple design for direct torque control of induction motor drives," *IEEE Trans. Ind. Electron.*, vol. 57, no. 9, pp. 3148–3156, Sep. 2010.

[4.13] M. Pacas and J. Weber, "Predictive direct torque control for the PM synchronous machine," *IEEE Trans. Ind. Electron.*, vol. 52, no. 5, pp. 1350–1356, Oct. 2005.

[4.14] E. Flach, R. Hoffmann, and P. Mutschler, "Direct mean torque control of an induction motor," in *Proc. EPE*, 1997, vol. 3, pp. 672–677.

[4.15] L. Romeral, A. Arias, E. Aldabas, and M. Jayne, "Novel direct torque control (DTC) scheme with fuzzy adaptive torque-ripple reduction," *IEEE Trans. Ind. Electron.*, vol. 50, no. 3, pp. 487–492, Jun. 2003.

[4.16] G. Abad,M. A. Rodriguez, and J. Poza, "Two-level VSC based predictive direct torque control of the doubly fed induction machine with reduced torque and flux ripples at low constant switching frequency," *IEEE Trans. Power Electron.*,

vol. 23, no. 3, pp. 1050–1061, May 2008.

[4.17] Y. Zhang and J. Zhu, “Direct torque control of permanent magnet synchronous motor with reduced torque ripple and commutation frequency,” IEEE Trans. Power Electron., vol. 26, no. 1, pp. 235–248, Jan. 2011.

[4.18] Tianshi Wang; Jianguo Zhu; Yongchang Zhang; , "Model predictive torque control for PMSM with duty ratio optimization," Electrical Machines and Systems (ICEMS), 2011 International Conference on , vol., no., pp.1-5, 20-23 Aug. 2011

[4.19] H. Miranda, P. Cortes, J. Yuz, and J. Rodriguez, “Predictive torque control of induction machines based on state-space models,” *IEEE Trans. Ind. Electron.*, vol. 56, no. 6, pp. 1916–1924, Jun. 2009.

[4.20] T. Geyer, G. Papafotiou, and M. Morari, “Model predictive direct torque control—Part I: Concept, algorithm, and analysis,” *IEEE Trans. Ind. Electron.*, vol. 56, no. 6, pp. 1894–1905, Jun. 2009.

[4.21] S. Kouro, P. Cortes, R. Vargas, U. Ammann, and J. Rodriguez, “Model predictive control—a simple and powerful method to control power converters,” *IEEE Trans. Ind. Electron.*, vol. 56, no. 6, pp. 1826–1838, Jun. 2009.

[4.22] F. Morel, J.-M. Retif, X. Lin-Shi, and C. Valentin, “Permanent magnet synchronous machine hybrid torque control,” *IEEE Trans. Ind. Electron.*, vol. 55, no. 2, pp. 501–511, Feb. 2008.

[4.23] K. Drobnic, M. Nemec, D. Nedeljkovic, and V. Ambrozic, “Predictive direct control applied to AC drives and active power filter,” *IEEE Trans. Ind. Electron.*, vol. 56, no. 6, pp. 1884–1893, Jun. 2009.

[4.24] Y. Zhang, J. Zhu, and W. Xu, “Predictive torque control of permanent magnet synchronous motor drive with reduced switching frequency,” in *Proc. Int. Conf. Electr. Mach. Syst.*, 2010, pp. 798–803.

CHAPTER 5

CONCLUSIONS AND FUTURE WORK

5.1 Conclusions

The main achievements of this thesis are summarized below:

- A comprehensive literature review was presented for PMSM machine structural topologies and control strategies. The principles, implementations and improvements of various control methods, such as the six-step control, field oriented control (FOC), direct torque control (DTC) and model predictive control (MPC), were discussed in details.
- A comparative study was carried out on PMSM control methods, including numerical simulations and experimental tests. A detailed data analysis based on the results of the simulation and experimental results was presented showing the merits and drawbacks of these control methods.
- An improved MPC method with duty ratio optimization was proposed for PMSMs to minimize the torque and flux ripples. This proposed method is most beneficial when the system is working at a low sampling frequency because in a low frequency range, the proposed MPC drive system can achieve much smaller torque and flux ripples than the original MPC and DTC. Both simulation and experimental results were presented to verify its effectiveness.
- The influence of system sampling frequency on steady-state performance of the classical DTC, original MPC, and improved MPCs were investigated by performing a set of numerical simulations and experimental tests. The torque and flux ripples decrease concurrently with the increase of sampling frequency. However, the trend of this decrease is non-linear. In the low frequency range, the torque and flux ripples drop rapidly. In the high frequency range, the trend for the torque and flux ripple reduction is a gradual decrease.

5.2 Future Work

The possible future work following this project is listed below:

- For the MPC introduced in this thesis, it needs to calculate the predicted value eight times in each sampling period. This is unnecessary because some of the voltage vectors obviously do not meet the requirements, such as torque decrease/increase and stator flux decrease/increase. A simplified MPC can be developed, which may include a voltage vector "filter" in its algorithm, in order to rule out some vectors before they are calculated. In this way, the total calculation time can be greatly reduced, which would be very beneficial when the level of the inverter increases to a three or higher level inverter.
- The one-step delay compensation scheme can be extended to other control methods such as DTC and FOC, in order to improve the performance.
- A flux weakening scheme can be developed for MPC, which is necessary for wide speed range applications, such as electric vehicles.

APPENDIX A. LIST OF PUBLICATIONS FROM THIS WORK

[1] **Tianshi Wang**, Yongchang Zhang and Jianguo Zhu, "Model Predictive Control of PMSMs with Duty Ratio Optimization for Torque Ripple Reduction, *Ind. Electron., IEEE Transactions on*, (Under peer review)

[2] **Tianshi Wang**, Jianguo Zhu and Yongchang Zhang, "Model Predictive Torque Control for PMSM with Duty Ratio Optimization", *Electrical Machines and Systems (ICEMS), 2011 International Conference on* , vol., no., pp.1-5, 20-23 Aug. 2011. **URL:** http://ieeexplore.ieee.org/xpls/abs_all.jsp?arnumber=6073501

[3] **Tianshi Wang**, Jianguo Zhu, Yongchang Zhang, Youguang Guo and Gang Lei, "Simulation and Experimental Studies of Permanent Magnet Synchronous Motor Control Methods", *Applied Superconductivity and Electromagnetic Devices (ASEMD), 2011 International Conference on*, (In press). **URL:** http://ieeexplore.ieee.org/xpls/abs_all.jsp?arnumber=6145113

[4] **Tianshi Wang**, Yongchang Zhang, Youguang Guo and Jianguo Zhu, "An Assessment of The Influence of Sampling Frequency on Steady-State Performance of PMSM Drive System", *Australasian Universities Power Engineering Conference (AUPEC) 2012*, (Accepted)

[5] Gang Lei, Yonguang Guo, Jianguo Zhu, **Tianshi Wang**, "System Level Six Sigma Robust Optimization of a Drive System With PM Transverse Flux Machine," *Magnetics, IEEE Transactions on* , vol.48, no.2, pp.923-926, Feb. 2012. **URL:** http://ieeexplore.ieee.org/xpls/abs_all.jsp?arnumber=6136727

[6] Yongchang Zhang, Zhengxi Li, **Tianshi Wang** and Jianguo Zhu, "Predictive direct torque and flux control of doubly fed induction generator with switching frequency reduction for wind energy applications", *Electrical Machines and Systems (ICEMS), 2011 International Conference on* , vol., no., pp.1-6, 20-23 Aug. 2011. **URL:** http://ieeexplore.ieee.org/xpls/abs_all.jsp?arnumber=4153107

[7] Yongchang Zhang, Zhengxi Li, **Tianshi Wang** and Jianguo Zhu, "Evaluation of a class of improved DTC method applied in DFIG for wind energy applications", *Electrical Machines and Systems (ICEMS), 2011 International Conference on* , vol., no., pp.1-6, 20-23 Aug. 2011. **URL:**

http://ieeexplore.ieee.org/xpls/abs_all.jsp?arnumber=6073720

[8] Wei Xu, Jianguo Zhu, Yongchang Zhang and **Tianshi Wang**, "Electromagnetic design and performance evaluation on 75 kW axially laminated flux switching permanent magnet machine", *Electrical Machines and Systems (ICEMS), 2011 International Conference on* , vol., no., pp.1-6, 20-23 Aug. 2011. **URL:** http://ieeexplore.ieee.org/xpls/abs_all.jsp?arnumber=6073716